Progress Report No 21

THEORETICAL PARACHUTE INVESTIGATIONS

Aeronautical Systems Division Contract No. AF 33(616)-8310; Project No 6065; Task No 60252

1 March 1962 to 31 May 1962

Department of Aeronautics and Engineering Mechanics, No 5007

University of Minnesota

Dr. H. G. Heinrich, Professor, Department of Aeronautics and Engineering Mechanics
Dr. T. Riabokin, Research Associate, Department of Aeronautics and Engineering Mechanics
Prof. S. K. Ibrahim, Research Fellow, Department of Aeronautics and Engineering Mechanics
Mr. E. L. Haak, Senior Engineer, Department of Aeronautics and Engineering Mechanics
Mr. R. J. Niccum, Senior Engineer, Department of Aeronautics and Engineering Mechanics
and graduate and undergraduate students of the Department of Aeronautics and Engineering Mechanics (see Appendix)

TABLE OF CONTENTS

THEORETICAL PARACHUTE INVESTIGATIONS

Progress Report No 21

INTRODUCTION

1.0 This is the twenty-first quarterly report covering the time from 1 March 1962 to 31 May 1962 on the study program on basic information of Aerodynamic Deceleration.

1.1 As in preceding reporting periods, work during this reporting period has been pursued in accordance with the technical program, and is described in the following sections of this report.

2.0 Investigation of Wake Effects on the Behavior of Parachutes and Other Retardation Devices Behind Large Bodies at Subsonic and Supersonic Speeds

2.1 Width of Wake Behind Basic Bodies of Revolution in Subsonic Flow

2.1.1 Introduction

Progress Report No 20 presented initial results of an attempt to determine experimentally the wake width close behind ten bodies of revolution in subsonic flow. It was postulated that a functional dependence of wake width on distance downstream could be expressed in the form

$$\frac{b}{R} = k\left(\frac{X}{D}\right)^n , \qquad (1.1)$$

where b = radial width of wake
R = radius of primary body = $D/2$
n,k = constants
X = distance behind body.

The constants in this empirical relationship were determined for each body from experimental data presented initially in Progress Report No 17.

In this report, the experimental velocity distributions for the ten bodies are presented more accurately, and the details of the derivation of the empirical constants are presented. In addition, similar information is presented for an ogive cylinder with no afterbody, based on experimental data obtained from Progress Report No 17, and also for a circular disk based on experimental data from Ref 1.

2.1.2 Analysis

Tables 1-1 through 1-12 present experimental velocity distributions in the wakes of the twelve bodies of revolution shown in Fig 1-1 for X/D positions of 2, 4, 6, 8, 10, 12, 16, and 20. These ratios of velocity in the wake to velocity in free stream were extracted from pressure coefficient measurements which were presented in Progress Report No 17 and in Ref 1. These same velocity distributions are presented on geometrically accurate graphs in Figs 1-2 through 1-13.

For purposes of this analysis, the wake boundary is defined by the points where the velocity defect is ten per cent of the velocity defect at the centerline, i.e., $(V_\infty - V_b)/(V_\infty - V_{CL}) = 0.10$. Using this definition, experimental wake widths were measured for each X/D position for the twelve bodies above. These experimental wake widths are indicated in Figs 1-2 through 1-13, and are tabulated in Table 1-13.

If the relationship of Eqn (1.1) is to be an accurate representation of the wake width, it is necessary that the experimental wake widths plot as straight lines on log-log coordinate paper. Such plots are presented in Figs 1-14 through 1-25 for the twelve bodies under consideration. It is seen that for the more or less streamlined bodies, in particular, Models F through L, the experimental wake widths plot as a straight line within the limits of experimental error. This is also true for Model A, the hollow hemisphere open to the flow. For the bluff bodies, Models B through E, the experimental wake widths are found to lie on one straight line in the region $2 \leqslant X/D \leqslant 8$, and on a second straight line in the region $8 \leqslant X/D \leqslant 20$.

For the twelve bodies above, an approximate representation of wake width in the region $2 \leqslant X/D \leqslant 20$ can be obtained by assuming a straight line through the experimental wake widths

as shown in Figs 1-14 through 1-25, and determining the empirical constants of Eqn (1.1) from this straight line. As stated above, the accuracy of this assumption will be best for Model A and the streamlined bodies, Models F through L, although Models I through L show some large deviations, particularly at $X/D = 4$. It is felt that this deviation is caused by the movement of the turbulent boundary layer separation point downstream to some position on the afterbody of these models, giving an initially narrower wake. Using this one-line approximation of the experimental wake widths, the empirical constants were determined for each body, and are presented in Table 1-14. Using these constants, the empirical wake widths were calculated and are shown superimposed on the velocity distributions in Figs 1-2 through 1-13. It is seen that this one line approximation is indeed very accurate for Model A and Models F through L.

Since the region $2 \leq X/D \leq 8$ is of particular interest in problems of aerodynamic retardation, a better representation of wake width behind each of the bluff bodies (Models B through E) can be obtained by assuming one straight line approximation in the region $2 \leq X/D \leq 8$ and a second in the region $8 \leq X/D \leq 20$. These two-line approximations are shown in Figs 1-15 through 1-18, and the constants thus determined are given in Table 1-14. The empirical wake widths then calculated are superimposed on the lower halves of Figs 1-3 through 1-6; it is seen that such a two-line approximation is very accurate for these bodies.

When the one-line approximations for all bodies are plotted together as in Fig 1-26, it is seen that three general groupings of wake width according to the body shape (or C_D) are indicated. As shown in Fig 1-28 A, wakes close behind bluff bodies similar to Models A through E can be represented in a first approximation by a single straight line giving the empirical constants

$$\frac{b}{R} = 1.25 \left(\frac{X}{D} \right)^{0.46} . \qquad (1.1a)$$

Figure 1-28 B shows the single approximating line for intermediate body shapes similar to Models F through H, with the corresponding wake width given by

$$\frac{b}{R} = 0.90\left(\frac{X}{D}\right)^{0.50} . \qquad (1.1b)$$

Similarly, Fig 1-28 C shows the single approximating line for streamlined bodies similar to Models I through L, with the corresponding wake width given by

$$\frac{b}{R} = 0.60\left(\frac{X}{D}\right)^{0.47} . \qquad (1.1c)$$

It is seen that in these general approximations the exponent n is nearly the same for the three body groups. The effect of increased streamlining of the bodies or of a decreasing drag coefficient is a decreasing multiplier k.

When the two-line approximations shown in Figs 1-15 through 1-18 are plotted together as in Fig 1-27, it is seen that the single approximating curve shown will quite accurately represent the wake widths of Models B through E. Determining the constants for this general approximation yields for the region $2 \leq X/D \leq 8$,

$$\frac{b}{R} = 1.30\left(\frac{X}{D}\right)^{0.38} , \qquad (1.1d)$$

and for the region $8 \leq X/D \leq 20$,

$$\frac{b}{R} = 0.78\left(\frac{X}{D}\right)^{0.63} . \qquad (1.1e)$$

2.1.3 Summary

The wake widths behind twelve bodies of revolution

in subsonic flow have been measured experimentally. It has been found possible to represent these wake widths for all bodies over the range $2 \leq X/D \leq 20$ by Eqn (1.1), with the appropriate constants for each body presented in Table 1-14. For the bluff bodies (Models B through E) a better representation of wake width is obtained by considering separately the regions $2 \leq X/D \leq 8$ and $8 \leq X/D \leq 20$; the appropriate constants are also given in Table 1-14.

A more general representation of wake width is obtained by dividing the above bodies into groups of bluff, intermediate, and streamlined bodies, with Eqns (1.1a), (1.1b), and (1.1c) giving the appropriate empirical constants. These general empirical formulas should be sufficiently accurate for most wake problems.

2.1.4 Proposed Work

As stated in Progress Report No 17, Sec 2.1.5, it has not been possible to obtain good agreement between the theoretical pressure distributions in the wake as predicted by Ref 2 and experimental data, in the region close behind a body. The theory uses the classical assumption that the wake width, b, increases with the 1/3 power of X/D. From the above analysis it is seen that this assumption is not correct in the region $2 \leq X/D \leq 20$ behind bodies of revolution. Therefore, during the next reporting period the theory of Ref 2 will be modified using the above results in an attempt to obtain closer agreement between theoretical and experimental pressure distributions in the wake close behind bodies of revolution.

2.2 Theoretical Analysis of Turbulent Wake in Supersonic Flow

2.2.1 Introduction

Progress Report No 19 presented a set of linearized partial differential equations describing the velocity, pressure, and the temperature in the wake of an axially symmetric body. During the last reporting period, solutions for the set of equations were obtained and presented. The solutions are:

$$u^* = K_1 h(x^*) e^{-h(x^*)r^{*2}},$$

$$v^* = 2BK_1^2 f(x^*) h^3(x^*) r^* e^{-h(x^*)r^{*2}},$$

$$p^* = 4B^2 K_1^3 \gamma M_\infty^2 h^4(x^*) f^2(x^*) \left[h(x^*)r^{*2} + \right.$$

$$\left. + \frac{f'(x^*)}{4BK_1 h^2(x^*) f^2(x^*)} - 2 \right] e^{-h(x^*)r^{*2}},$$

$$T^* = K_4 h_1(x^*) e^{-h_1(x^*)r^{*2}},$$

Where $$h(x^*) = \left[8BK_1 \int f(x^*)dx^* + K_2 \right]^{-1/2},$$

$$h_1(x^*) = \left[\frac{4\gamma x^*}{RePr} + K_3 \right]^{-1},$$

with terms defined as in Section 2.4, Progress Report No 19.

During this reporting period an attempt was made to determine the integration constants, K_1, K_2, K_3, and K_4. The results of this attempt are to date inconclusive.

Since the solutions of the equations are valid for relatively large distances downstream of the body, expanded experimental data for the larger downstream distances is necessary for a comparison between theory and experiment. Without this wider range of data, the correlation of theory with experiment is difficult to obtain.

2.2.2 Proposed Work

Experimental data presently available for shorter distances downstream of various bodies will be used in further attempts to compare theory with experimental results. In addition, consideration will be given to conducting a limited number of wake study experiments at larger distances downstream of the body than are provided for by present data.

REFERENCES

1. Rubbert, Paul E.: Investigation of the Velocity Distribution in the Wake of an Axially Symmetric Body, Master's Thesis submitted to the Graduate School of the University of Minnesota, July, 1960.

2. Heinrich, H. G. and Riabokin, T.: Analytical and Experimental Considerations of the Velocity Distribution in the Wake of a Body of Revolution, WADC TR No. 60-257, December, 1959.

r/R	X/D							
	2	4	6	8	10	12	16	20
7.67	1.00	1.00	1.00	1.00	1.00	1.00	1.00	1.00
5.67	1.00	1.00	1.00	1.00	1.00	1.00	0.99	0.99
4.67	1.00	1.00	1.00	1.00	1.00	1.00	0.98	0.99
4.00	1.00	1.00	1.00	0.99	0.99	0.99	0.98	0.98
3.33	1.00	1.00	0.99	0.98	0.98	0.98	0.97	0.97
2.67	1.00	0.97	0.96	0.96	0.96	0.96	0.96	0.96
2.00	0.94	0.94	0.93	0.94	0.95	0.94	0.95	0.96
1.33	0.78	0.84	0.88	0.92	0.94	0.93	0.95	0.96
1.07	0.40	0.80	0.88	0.90	0.93	0.93	0.95	0.96
0.80	0.26	0.79	0.87	0.91	0.93	0.93	0.94	0.95
0.53	0.14	0.77	0.87	0.91	0.94	0.93	0.94	0.95
0.27	—	0.75	0.87	0.91	0.92	0.93	0.94	0.95
0	—	0.75	0.87	0.91	0.92	0.93	0.94	0.95
0.27	—	0.75	0.87	0.91	0.92	0.93	0.94	0.95
0.53	0.14	0.77	0.87	0.91	0.94	0.93	0.94	0.95
0.80	0.26	0.79	0.87	0.91	0.93	0.93	0.94	0.95
1.07	0.40	0.80	0.88	0.90	0.93	0.93	0.94	0.96
1.33	0.78	0.84	0.88	0.92	0.94	0.93	0.94	0.96
2.00	0.94	0.94	0.93	0.94	0.95	0.94	0.95	0.96
2.67	1.00	0.97	0.96	0.96	0.96	0.96	0.96	0.96
3.33	1.00	1.00	0.99	0.98	0.98	0.98	0.97	0.97
4.00	1.00	1.00	1.00	0.99	0.99	0.99	0.98	0.98
4.67	1.00	1.00	1.00	1.00	1.00	1.00	0.98	0.99
5.67	1.00	1.00	1.00	1.00	1.00	1.00	0.99	0.99
7.67	1.00	1.00	1.00	1.00	1.00	1.00	1.00	1.00

V/V_∞

TABLE 1-1. EXPERIMENTAL VELOCITY DISTRIBUTION IN WAKE OF MODEL A

r/R	x/D							
	2	4	6	8	10	12	16	20
4.70	1.00	1.00	1.00	1.00	1.00	1.00	1.00	0.99
3.90	1.00	1.00	1.00	0.99	0.99	0.98	0.99	0.98
3.10	1.00	1.00	1.00	0.99	0.98	0.98	0.98	0.98
2.70	1.00	1.00	0.99	0.98	0.97	0.97	0.97	0.97
2.30	1.00	0.98	0.97	0.96	0.96	0.96	0.96	0.97
1.90	0.91	0.90	0.94	0.94	0.94	0.95	0.95	0.96
1.50	0.55	0.84	0.89	0.92	0.92	0.94	0.95	0.95
1.10	0	0.79	0.88	0.90	0.91	0.93	0.95	0.95
0.90	0	0.75	0.86	0.90	0.91	0.93	0.94	0.95
0.70	0	0.74	0.85	0.90	0.91	0.92	0.94	0.95
0.50	0	0.78	0.85	0.89	0.91	0.92	0.94	0.95
0.30	0	0.70	0.85	0.89	0.91	0.92	0.94	0.94
0.10	0	0.69	0.84	0.89	0.91	0.92	0.94	0.95
0.30	0	0.70	0.85	0.89	0.91	0.92	0.94	0.94
0.50	0	0.78	0.85	0.89	0.91	0.92	0.94	0.95
0.70	0	0.74	0.85	0.90	0.91	0.92	0.94	0.95
0.90	0	0.75	0.86	0.90	0.91	0.93	0.94	0.95
1.10	0	0.79	0.88	0.90	0.91	0.93	0.95	0.95
1.50	0.55	0.84	0.89	0.92	0.92	0.94	0.95	0.95
1.90	0.91	0.90	0.94	0.94	0.94	0.95	0.95	0.96
2.30	1.00	0.98	0.97	0.96	0.96	0.96	0.96	0.97
2.70	1.00	1.00	0.99	0.98	0.97	0.97	0.97	0.97
3.10	1.00	1.00	1.00	0.99	0.98	0.98	0.98	0.98
3.90	1.00	1.00	1.00	0.99	0.99	0.98	0.99	0.98
4.70	1.00	1.00	1.00	1.00	1.00	1.00	1.00	0.99

V/V_∞

TABLE 1-2. EXPERIMENTAL VELOCITY DISTRIBUTION IN WAKE OF MODEL B

V/V_∞	r/R	X/D							
		2	4	6	8	10	12	16	20
	7.67	1.00	1.00	1.00	1.00	1.00	1.00	1.00	1.00
	5.67	1.00	1.00	1.00	1.00	1.00	1.00	1.00	1.00
	4.67	1.00	1.00	1.00	1.00	1.00	1.00	1.00	0.99
	4.00	1.00	1.00	1.00	1.00	1.00	1.00	0.99	0.98
	3.33	1.00	1.00	1.00	1.00	0.99	0.98	0.95	0.97
	2.67	1.00	0.98	0.99	0.98	0.97	0.97	0.96	0.96
	2.00	1.00	0.95	0.95	0.95	0.95	0.95	0.95	0.96
	1.33	0.41	0.82	0.88	0.91	0.92	0.94	0.94	0.95
	1.07	0.14	0.77	0.87	0.90	0.92	0.93	0.94	0.95
	0.80		0.72	0.85	0.90	0.90	0.93	0.94	0.95
	0.53		0.69	0.85	0.90	0.90	0.93	0.94	0.95
	0.27		0.67	0.85	0.89	0.91	0.93	0.94	0.95
	0		0.66	0.85	0.89	0.91	0.92	0.93	0.94
	0.27		0.67	0.85	0.89	0.91	0.93	0.94	0.95
	0.53		0.69	0.85	0.90	0.90	0.93	0.94	0.95
	0.80		0.72	0.85	0.90	0.90	0.93	0.94	0.95
	1.07	0.14	0.77	0.87	0.90	0.92	0.93	0.94	0.95
	1.33	0.41	0.82	0.88	0.91	0.92	0.94	0.94	0.95
	2.00	1.00	0.95	0.95	0.95	0.95	0.95	0.95	0.96
	2.67	1.00	0.98	0.99	0.98	0.97	0.97	0.96	0.96
	3.33	1.00	1.00	1.00	1.00	0.99	0.98	0.95	0.97
	4.00	1.00	1.00	1.00	1.00	1.00	1.00	0.99	0.98
	4.67	1.00	1.00	1.00	1.00	1.00	1.00	1.00	0.99
	5.67	1.00	1.00	1.00	1.00	1.00	1.00	1.00	1.00
	7.67	1.00	1.00	1.00	1.00	1.00	1.00	1.00	1.00

TABLE 1-3. EXPERIMENTAL VELOCITY DISTRIBUTION IN WAKE OF MODEL C

V/V_o	r/R	X/D							
		2	4	6	8	10	12	16	20
	7.67	1.00	1.00	1.00	1.00	1.00	1.00	1.00	1.00
	5.67	1.00	1.00	1.00	1.00	1.00	1.00	1.00	1.00
	4.67	1.00	1.00	1.00	1.00	1.00	1.00	1.00	1.00
	4.00	1.00	0.99	1.00	1.00	1.00	1.00	0.99	0.99
	3.33	1.00	0.99	0.99	1.00	0.99	0.99	0.98	0.98
	2.67	1.00	0.99	0.99	0.99	0.98	0.98	0.98	0.98
	2.00	1.00	0.96	0.96	0.96	0.96	0.96	0.96	0.96
	1.33	0.66	0.85	0.90	0.92	0.93	0.94	0.95	0.96
	1.07	0.41	0.82	0.89	0.92	0.92	0.93	0.94	0.96
	0.80	0.17	0.79	0.88	0.90	0.92	0.93	0.94	0.96
	0.53	0.17	0.77	0.87	0.90	0.92	0.93	0.94	0.96
	0.27	0.14	0.75	0.86	0.90	0.92	0.93	0.93	0.96
	0	0.14	0.75	0.86	0.90	0.92	0.93	0.93	0.96
	0.27	0.14	0.75	0.86	0.90	0.92	0.93	0.93	0.96
	0.53	0.17	0.77	0.87	0.90	0.92	0.93	0.94	0.96
	0.80	0.17	0.79	0.88	0.90	0.92	0.93	0.94	0.96
	1.07	0.41	0.82	0.89	0.92	0.92	0.93	0.94	0.96
	1.33	0.66	0.85	0.90	0.92	0.93	0.94	0.95	0.96
	2.00	1.00	0.96	0.96	0.96	0.96	0.96	0.96	0.96
	2.67	1.00	0.99	0.99	0.98	0.98	0.98	0.98	0.98
	3.33	1.00	0.99	0.99	1.00	0.99	0.99	0.98	0.98
	4.00	1.00	0.99	1.00	1.00	1.00	1.00	0.99	0.99
	4.67	1.00	1.00	1.00	1.00	1.00	1.00	1.00	1.00
	5.67	1.00	1.00	1.00	1.00	1.00	1.00	1.00	1.00
	7.67	1.00	1.00	1.00	1.00	1.00	1.00	1.00	1.00

TABLE 1-4. EXPERIMENTAL VELOCITY DISTRIBUTION IN WAKE OF MODEL D

V/V_∞	r/R	x/D							
		2	4	6	8	10	12	16	20
	7.67	1.00	1.00	1.00	1.00	1.00	1.00	1.00	1.00
	5.67	1.00	1.00	1.00	1.00	1.00	1.00	1.00	1.00
	4.67	1.00	1.00	1.00	1.00	1.00	1.00	1.00	0.99
	4.00	1.00	1.00	1.00	1.00	0.99	0.99	0.99	0.98
	3.33	1.00	1.00	1.00	1.00	0.99	0.99	0.99	0.98
	2.67	0.94	0.99	0.99	0.98	0.98	0.98	0.97	0.97
	2.00	0.94	0.97	0.97	0.96	0.96	0.96	0.95	0.96
	1.33	0.68	0.87	0.90	0.92	0.93	0.94	0.95	0.95
	1.07	0.40	0.82	0.88	0.90	0.92	0.94	0.94	0.95
	0.80	0.17	0.77	0.87	0.90	0.92	0.94	0.95	0.95
	0.53	0.00	0.73	0.87	0.90	0.92	0.94	0.95	0.95
	0.27	0.00	0.71	0.86	0.90	0.92	0.94	0.95	0.95
	0	0.00	0.71	0.86	0.90	0.91	0.93	0.94	0.95
	0.27	0.00	0.71	0.86	0.90	0.92	0.94	0.95	0.95
	0.53	0.00	0.73	0.87	0.90	0.92	0.94	0.95	0.95
	0.80	0.17	0.77	0.87	0.90	0.92	0.94	0.95	0.95
	1.07	0.40	0.82	0.88	0.90	0.92	0.94	0.94	0.95
	1.33	0.68	0.87	0.90	0.92	0.93	0.94	0.95	0.95
	2.00	0.94	0.97	0.97	0.96	0.96	0.96	0.96	0.96
	2.67	0.94	0.99	0.99	0.98	0.98	0.98	0.97	0.97
	3.33	1.00	1.00	1.00	1.00	0.99	0.99	0.98	0.98
	4.00	1.00	1.00	1.00	1.00	0.99	0.99	0.99	0.98
	4.67	1.00	1.00	1.00	1.00	1.00	1.00	1.00	0.99
	5.67	1.00	1.00	1.00	1.00	1.00	1.00	1.00	1.00
	7.67	1.00	1.00	1.00	1.00	1.00	1.00	1.00	1.00

TABLE 1-5. EXPERIMENTAL VELOCITY DISTRIBUTION IN WAKE OF MODEL E

V/V_∞	r/R	X/D							
		2	4	6	8	10	12	16	20
	7.67	1.00	1.00	1.00	1.00	1.00	1.00	1.00	1.00
	5.67	1.00	1.00	1.00	1.00	1.00	1.00	1.00	1.00
	4.67	1.00	1.00	1.00	1.00	1.00	1.00	1.00	1.00
	4.00	1.00	1.00	1.00	1.00	1.00	1.00	1.00	1.00
	3.33	1.00	1.00	1.00	1.00	0.99	1.00	0.99	0.99
	2.67	1.00	1.00	1.00	1.00	0.99	0.99	0.98	0.98
	2.00	1.00	0.99	0.98	0.97	0.97	0.97	0.97	0.97
	1.33	0.92	0.93	0.94	0.94	0.94	0.95	0.96	0.96
	1.07	0.73	0.87	0.91	0.93	0.94	0.94	0.96	0.96
	0.80	0.47	0.84	0.90	0.92	0.93	0.94	0.96	0.96
	0.53	0.20	0.81	0.90	0.92	0.93	0.94	0.96	0.96
	0.27	0.00	0.80	0.88	0.92	0.93	0.94	0.95	0.96
	0	0.00	0.80	0.88	0.91	0.93	0.94	0.95	0.96
	0.27	0.00	0.80	0.88	0.92	0.93	0.94	0.95	0.96
	0.53	0.20	0.81	0.90	0.92	0.93	0.94	0.96	0.96
	0.80	0.47	0.84	0.90	0.92	0.93	0.94	0.96	0.96
	1.07	0.73	0.87	0.91	0.93	0.94	0.94	0.96	0.96
	1.33	0.92	0.91	0.94	0.94	0.94	0.94	0.96	0.96
	2.00	1.00	0.99	0.98	0.97	0.97	0.97	0.97	0.97
	2.67	1.00	1.00	1.00	1.00	0.99	0.99	0.98	0.98
	3.33	1.00	1.00	1.00	1.00	0.99	1.00	0.99	0.99
	4.00	1.00	1.00	1.00	1.00	1.00	1.00	1.00	1.00
	4.67	1.00	1.00	1.00	1.00	1.00	1.00	1.00	1.00
	5.67	1.00	1.00	1.00	1.00	1.00	1.00	1.00	1.00
	7.67	1.00	1.00	1.00	1.00	1.00	1.00	1.00	1.00

TABLE 1-6. EXPERIMENTAL VELOCITY DISTRIBUTION IN WAKE OF MODEL F

r/R	X/D							
	2	4	6	8	10	12	16	20
7.67	1.00	1.00	1.00	1.00	1.00	1.00	1.00	1.00
5.67	1.00	1.00	1.00	1.00	1.00	1.00	1.00	1.00
4.67	1.00	1.00	1.00	1.00	1.00	1.00	1.00	1.00
4.00	1.00	1.00	1.00	1.00	1.00	1.00	1.00	1.00
3.33	1.00	1.00	1.00	1.00	0.99	1.00	1.00	1.00
2.67	1.00	1.00	1.00	1.00	0.98	1.00	0.99	0.99
2.00	1.00	1.00	0.98	0.99	0.95	0.98	0.98	0.98
1.33	0.93	0.95	0.95	0.95	0.94	0.95	0.96	0.97
1.07	0.82	0.90	0.93	0.94	0.94	0.95	0.96	0.96
0.80	0.68	0.88	0.90	0.93	0.93	0.95	0.95	0.96
0.53	0.50	0.82	0.88	0.92	0.93	0.95	0.95	0.96
0.27	0.33	0.81	0.88	0.90	0.92	0.94	0.95	0.95
0	0.29	0.80	0.87	0.90	0.93	0.93	0.94	0.95
0.27	0.33	0.81	0.88	0.90	0.93	0.94	0.95	0.95
0.53	0.50	0.82	0.88	0.92	0.94	0.95	0.95	0.96
0.80	0.68	0.88	0.90	0.93	0.94	0.95	0.95	0.96
1.07	0.82	0.90	0.93	0.94	0.95	0.95	0.96	0.96
1.33	0.93	0.95	0.95	0.95	0.98	0.95	0.96	0.97
2.00	1.00	1.00	0.98	0.99	0.99	0.98	0.98	0.98
2.67	1.00	1.00	1.00	1.00	1.00	1.00	0.99	0.99
3.33	1.00	1.00	1.00	1.00	1.00	1.00	1.00	1.00
4.00	1.00	1.00	1.00	1.00	1.00	1.00	1.00	1.00
4.67	1.00	1.00	1.00	1.00	1.00	1.00	1.00	1.00
5.67	1.00	1.00	1.00	1.00	1.00	1.00	1.00	1.00
7.67	1.00	1.00	1.00	1.00	1.00	1.00	1.00	1.00

V/V_∞

TABLE 1-7. EXPERIMENTAL VELOCITY DISTRIBUTION IN WAKE OF MODEL G

V/V_o	r/R	X/D							
		2	4	6	8	10	12	16	20
	7.67	1.00	1.00	1.00	1.00	1.00	1.00	1.00	1.00
	5.67	1.00	1.00	1.00	1.00	1.00	1.00	1.00	1.00
	4.67	1.00	1.00	1.00	1.00	1.00	1.00	0.99	0.99
	4.00	0.99	1.00	0.99	0.99	0.99	0.99	0.99	0.98
	3.33	0.99	0.99	0.99	0.99	0.99	0.99	0.99	0.98
	2.67	0.99	0.99	0.99	0.99	0.99	0.98	0.98	0.98
	2.00	0.99	0.99	0.99	0.99	0.98	0.98	0.98	0.97
	1.33	0.98	0.98	0.98	0.97	0.97	0.97	0.98	0.97
	1.07	0.97	0.97	0.97	0.96	0.96	0.96	0.97	0.96
	0.80	0.96	0.95	0.95	0.95	0.95	0.96	0.96	0.96
	0.53	0.89	0.92	0.93	0.95	0.94	0.94	0.95	0.95
	0.27	0.79	0.90	0.91	0.92	0.93	0.94	0.95	0.95
	0	0.74	0.88	0.90	0.93	0.93	0.94	0.95	0.95
	0.27	0.79	0.90	0.91	0.92	0.93	0.94	0.95	0.95
	0.53	0.89	0.92	0.93	0.95	0.94	0.94	0.95	0.95
	0.80	0.96	0.95	0.95	0.95	0.95	0.96	0.96	0.96
	1.07	0.97	0.97	0.97	0.96	0.96	0.96	0.97	0.96
	1.33	0.91	0.98	0.98	0.97	0.97	0.97	0.98	0.97
	2.00	0.99	0.99	0.99	0.99	0.98	0.98	0.98	0.97
	2.67	0.99	0.99	0.99	0.99	0.99	0.98	0.98	0.98
	3.33	0.99	0.99	0.99	0.99	0.99	0.99	0.99	0.98
	4.00	0.99	1.00	0.99	0.99	0.99	0.99	0.99	0.98
	4.67	1.00	1.00	1.00	1.00	1.00	1.00	0.99	0.99
	5.67	1.00	1.00	1.00	1.00	1.00	1.00	1.00	1.00
	7.67	1.00	1.00	1.00	1.00	1.00	1.00	1.00	1.00

TABLE 1-8. EXPERIMENTAL VELOCITY DISTRIBUTION IN WAKE OF MODEL H

r/R	x/D							
	2	4	6	8	10	12	16	20
7.67	1.00	1.00	1.00	1.00	1.00	1.00	1.00	1.00
5.67	1.00	1.00	1.00	1.00	1.00	1.00	1.00	1.00
4.67	1.00	1.00	1.00	1.00	1.00	1.00	1.00	1.00
4.00	1.00	1.00	1.00	1.00	1.00	1.00	1.00	1.00
3.33	1.00	1.00	1.00	1.00	1.00	1.00	1.00	1.00
2.67	1.00	1.00	1.00	1.00	1.00	1.00	1.00	1.00
2.00	1.00	1.00	1.00	1.00	0.99	0.99	0.99	0.99
1.33	0.99	0.99	0.97	0.96	0.97	0.96	0.96	0.96
1.07	0.98	0.97	0.95	0.95	0.95	0.96	0.95	0.96
0.80	0.93	0.93	0.93	0.94	0.94	0.94	0.95	0.96
0.53	0.84	0.88	0.90	0.92	0.93	0.93	0.94	0.96
0.27	0.75	0.84	0.88	0.92	0.92	0.92	0.93	0.95
0	0.74	0.81	0.86	0.90	0.90	0.92	0.93	0.95
0.27	0.75	0.84	0.88	0.92	0.92	0.92	0.93	0.95
0.53	0.84	0.88	0.90	0.92	0.93	0.93	0.94	0.96
0.80	0.93	0.93	0.93	0.94	0.94	0.94	0.95	0.96
1.07	0.98	0.97	0.95	0.95	0.95	0.96	0.95	0.96
1.33	0.99	0.99	0.97	0.96	0.97	0.96	0.96	0.96
2.00	1.00	1.00	1.00	1.00	0.99	0.99	0.99	0.99
2.67	1.00	1.00	1.00	1.00	1.00	1.00	1.00	1.00
3.33	1.00	1.00	1.00	1.00	1.00	1.00	1.00	1.00
4.00	1.00	1.00	1.00	1.00	1.00	1.00	1.00	1.00
4.67	1.00	1.00	1.00	1.00	1.00	1.00	1.00	1.00
5.67	1.00	1.00	1.00	1.00	1.00	1.00	1.00	1.00
7.67	1.00	1.00	1.00	1.00	1.00	1.00	1.00	1.00

V/V_o

TABLE 1-9. EXPERIMENTAL VELOCITY DISTRIBUTION IN WAKE OF MODEL I

r/R	X/D							
	2	4	6	8	10	12	16	20
7.67	1.00	1.00	1.00	1.00	1.00	1.00	1.00	1.00
5.67	1.00	1.00	1.00	1.00	1.00	1.00	1.00	1.00
4.67	1.00	1.00	1.00	1.00	1.00	1.00	1.00	1.00
4.00	1.00	1.00	1.00	1.00	1.00	1.00	1.00	1.00
3.33	1.00	1.00	1.00	1.00	1.00	1.00	1.00	1.00
2.67	1.00	1.00	1.00	1.00	1.00	1.00	1.00	0.99
2.00	1.00	1.00	1.00	1.00	1.00	1.00	0.99	0.98
1.33	0.99	1.00	0.97	0.97	0.97	0.97	0.96	0.96
1.07	0.99	0.99	0.94	0.95	0.95	0.95	0.95	0.95
0.80	0.98	0.95	0.90	0.93	0.93	0.93	0.95	0.96
0.53	0.84	0.86	0.90	0.90	0.91	0.91	0.94	0.95
0.27	0.71	0.79	0.89	0.86	0.90	0.90	0.93	0.95
0	0.66	0.75	0.88	0.85	0.89	0.90	0.92	0.94
0.27	0.71	0.79	0.89	0.86	0.90	0.90	0.93	0.95
0.53	0.84	0.86	0.90	0.90	0.91	0.91	0.94	0.95
0.80	0.98	0.95	0.90	0.93	0.93	0.93	0.95	0.96
1.07	0.99	0.99	0.94	0.95	0.95	0.95	0.95	0.95
1.33	0.99	1.00	0.97	0.97	0.97	0.97	0.96	0.96
2.00	1.00	1.00	1.00	1.00	1.00	1.00	0.99	0.98
2.67	1.00	1.00	1.00	1.00	1.00	1.00	1.00	0.99
3.33	1.00	1.00	1.00	1.00	1.00	1.00	1.00	1.00
4.00	1.00	1.00	1.00	1.00	1.00	1.00	1.00	1.00
4.67	1.00	1.00	1.00	1.00	1.00	1.00	1.00	1.00
5.67	1.00	1.00	1.00	1.00	1.00	1.00	1.00	1.00
7.67	1.00	1.00	1.00	1.00	1.00	1.00	1.00	1.00

V/V_∞

TABLE 1-10. EXPERIMENTAL VELOCITY DISTRIBUTION IN WAKE OF MODEL J

r/R	x/D							
	2	4	6	8	10	12	16	20
7.67	1.00	1.00	1.00	1.00	1.00	1.00	1.00	1.00
5.67	1.00	1.00	1.00	1.00	1.00	1.00	1.00	1.00
4.67	1.00	1.00	1.00	1.00	1.00	1.00	1.00	1.00
4.00	1.00	1.00	1.00	1.00	1.00	1.00	1.00	1.00
3.33	1.00	1.00	1.00	1.00	1.00	1.00	1.00	1.00
2.67	1.00	1.00	1.00	1.00	1.00	1.00	1.00	1.00
2.00	0.99	1.00	1.00	1.00	0.99	1.00	0.99	0.99
1.33	0.99	0.99	0.99	0.98	0.98	0.97	0.96	0.97
1.07	0.99	0.99	0.97	0.95	0.96	0.95	0.95	0.95
0.80	0.98	0.96	0.93	0.92	0.93	0.93	0.94	0.94
0.53	0.87	0.85	0.88	0.91	0.90	0.92	0.93	0.94
0.27	0.72	0.76	0.83	0.86	0.85	0.90	0.93	0.93
0	0.64	0.71	0.83	0.86	0.85	0.88	0.92	0.92
0.27	0.72	0.76	0.83	0.86	0.86	0.90	0.93	0.93
0.53	0.87	0.85	0.88	0.91	0.90	0.92	0.93	0.94
0.80	0.98	0.96	0.93	0.92	0.93	0.93	0.94	0.94
1.07	0.99	0.99	0.97	0.95	0.96	0.95	0.95	0.95
1.33	0.99	0.99	0.99	0.98	0.98	0.97	0.96	0.97
2.00	0.99	1.00	1.00	1.00	0.99	1.00	0.99	0.99
2.67	1.00	1.00	1.00	1.00	1.00	1.00	1.00	1.00
3.33	1.00	1.00	1.00	1.00	1.00	1.00	1.00	1.00
4.00	1.00	1.00	1.00	1.00	1.00	1.00	1.00	1.00
4.67	1.00	1.00	1.00	1.00	1.00	1.00	1.00	1.00
5.67	1.00	1.00	1.00	1.00	1.00	1.00	1.00	1.00
7.67	1.00	1.00	1.00	1.00	1.00	1.00	1.00	1.00

V/V_∞

TABLE 1-11. EXPERIMENTAL VELOCITY DISTRIBUTION IN WAKE OF MODEL K

$\frac{V}{V_\infty}$	r/R	X/D							
		2	4	6	8	10	12	16	20
	7.67	1.00	1.00	1.00	1.00	1.00	1.00	1.00	1.00
	5.67	1.00	1.00	1.00	1.00	1.00	1.00	1.00	1.00
	4.67	1.00	1.00	1.00	1.00	1.00	1.00	1.00	1.00
	4.00	1.00	1.00	1.00	1.00	1.00	1.00	1.00	1.00
	3.33	1.00	1.00	1.00	1.00	1.00	1.00	1.00	1.00
	2.67	1.00	1.00	1.00	1.00	1.00	1.00	1.00	1.00
	2.00	1.00	1.00	1.00	1.00	1.00	0.99	0.99	0.99
	1.33	0.99	0.99	0.98	0.97	0.98	0.98	0.95	0.96
	1.07	0.99	0.99	0.95	0.94	0.96	0.95	0.94	0.95
	0.80	0.97	0.96	0.90	0.91	0.93	0.93	0.94	0.95
	0.53	0.88	0.90	0.90	0.89	0.90	0.91	0.94	0.94
	0.27	0.72	0.77	0.87	0.88	0.86	0.90	0.93	0.93
	0	0.66	0.71	0.88	0.89	0.83	0.90	0.93	0.93
	0.27	0.72	0.77	0.87	0.88	0.86	0.90	0.93	0.93
	0.53	0.88	0.90	0.90	0.89	0.90	0.91	0.94	0.94
	0.80	0.97	0.96	0.90	0.91	0.93	0.93	0.94	0.95
	1.07	0.99	0.99	0.95	0.94	0.96	0.95	0.94	0.95
	1.33	0.99	0.99	0.98	0.97	0.98	0.98	0.95	0.96
	2.00	1.00	1.00	1.00	1.00	1.00	0.99	0.99	0.99
	2.67	1.00	1.00	1.00	1.00	1.00	1.00	1.00	1.00
	3.33	1.00	1.00	1.00	1.00	1.00	1.00	1.00	1.00
	4.00	1.00	1.00	1.00	1.00	1.00	1.00	1.00	1.00
	4.67	1.00	1.00	1.00	1.00	1.00	1.00	1.00	1.00
	5.67	1.00	1.00	1.00	1.00	1.00	1.00	1.00	1.00
	7.67	1.00	1.00	1.00	1.00	1.00	1.00	1.00	1.00

TABLE 112 EXPERIMENTAL VELOCITY DISTRIBUTION IN WAKE OF MODEL L

MODEL		X/D=2	4	6	8	10	12	16	20
A	b/R	1.70	2.55	3.50	3.70	4.00	4.50	6.00	6.30
B	b/R	1.88	2.20	2.60	3.05	3.70	4.10	4.60	5.40
C	b/R	1.75	2.25	2.55	2.90	3.40	4.00	4.50	5.00
D	b/R	1.70	2.30	2.60	2.80	3.40	3.80	4.20	4.80
E	b/R	1.70	2.15	2.50	2.80	3.10	3.80	4.60	5.00
F	b/R	1.30	1.85	2.25	2.50	2.80	2.90	3.50	4.20
G	b/R	1.35	1.75	2.25	2.25	2.70	2.90	2.90	3.40
H	b/R	1.10	1.70	2.20	3.00	3.30	3.60	4.30	5.00
I	b/R	1.03	1.20	1.75	1.95	2.00	2.00	2.30	2.50
J	b/R	0.80	0.98	1.65	1.55	1.75	1.85	2.40	2.80
K	b/R	0.72	0.85	1.20	1.40	1.60	1.90	2.20	2.30
L	b/R	0.82	0.90	1.50	1.75	1.70	1.70	2.20	2.50

TABLE 1-13. EXPERIMENTAL WAKE WIDTHS

MODEL	C_{D_0}	$2 \leq X/D \leq 20$		$2 \leq X/D \leq 8$		$8 \leq X/D \leq 20$	
		k	n	k	n	k	n
A	1.40	1.14	0.582				
B	1.11	1.26	0.454	1.39	0.368	0.788	0.642
C	1.03	1.33	0.394	1.36	0.365	0.734	0.660
D	0.836	1.34	0.384	1.30	0.384	0.879	0.574
E	0.743	1.32	0.393	1.33	0.358	0.684	0.678
F	0.577	0.927	0.488				
G	0.425	0.985	0.397				
H	0.350	0.693	0.665				
I	0.230	0.810	0.376				
J	0.206	0.541	0.522				
K	0.197	0.493	0.531				
L	0.194	0.565	0.491				

TABLE 1-14. EMPIRICAL WAKE WIDTH CONSTANTS

NOTE: ALL BODIES HAVE DIAMETER = 1.50"

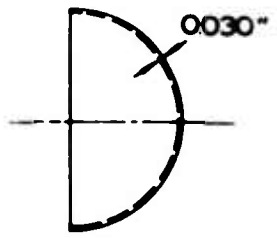

MODEL A
HOLLOW HEMISPHERE
(OPEN TO FLOW)
C_o = 1.40

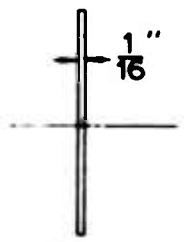

MODEL B
DISK
C_o = 1.11

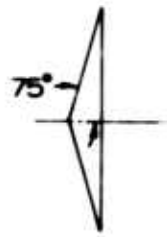

MODEL C
CONE
C_o = 1.03

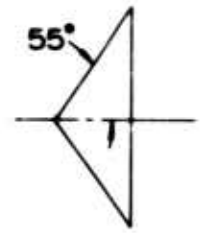

MODEL D
CONE
C_o = 0.836

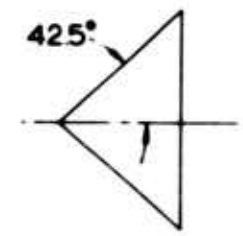

MODEL E
CONE
C_o = 0.743

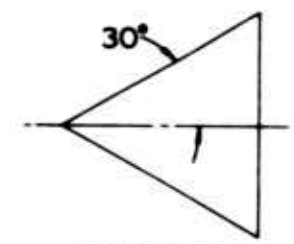

MODEL F
CONE
C_o = 0.577

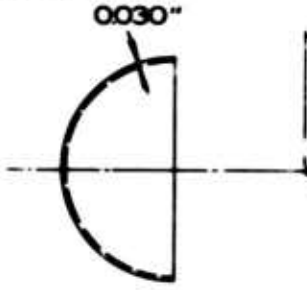

MODEL G
HOLLOW HEMISPHERE
(CLOSED TO FLOW)
C_o = 0.425

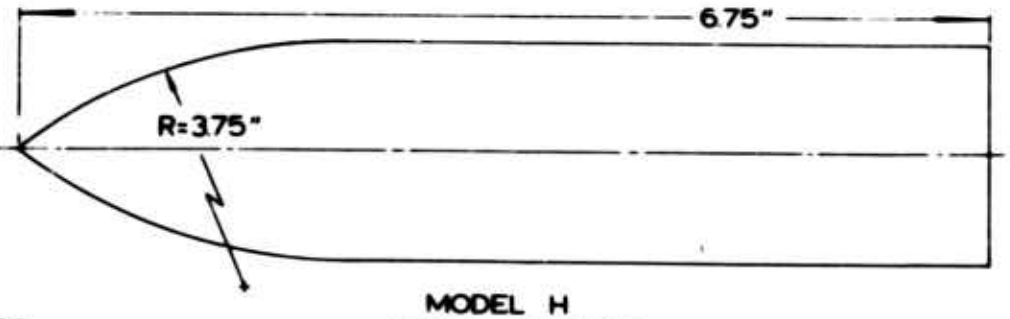

MODEL H
OGIVE CYLINDER
C_o = 0.350

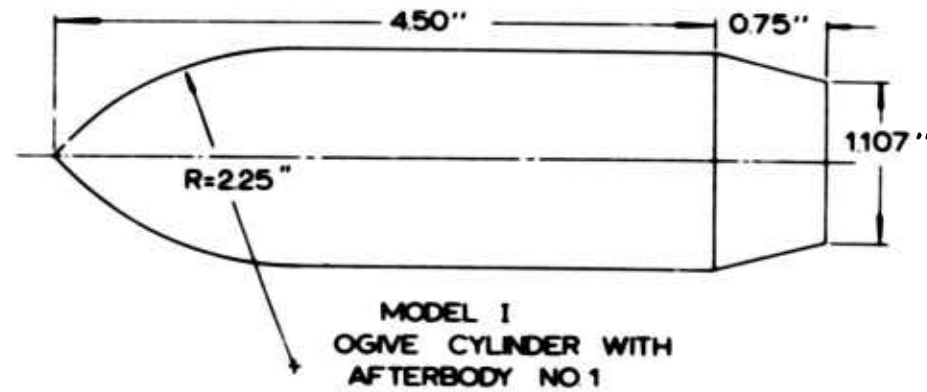

MODEL I
OGIVE CYLINDER WITH
AFTERBODY NO 1
C_o = 0.230

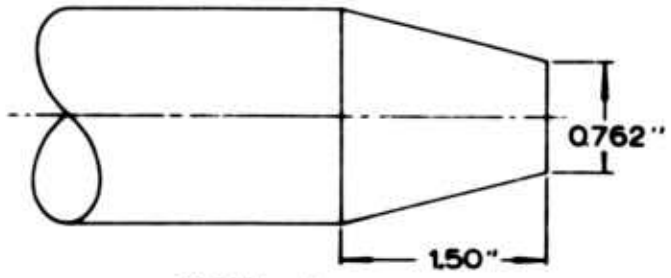

MODEL J
OGIVE CYLINDER WITH
AFTERBODY NO 2
C_o = 0.206

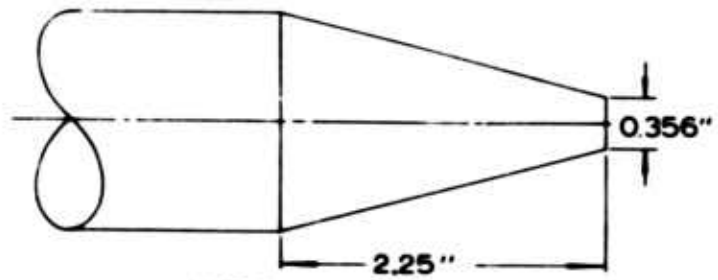

MODEL K
OGIVE CYLINDER WITH
AFTERBODY NO 3
C_o = 0.197

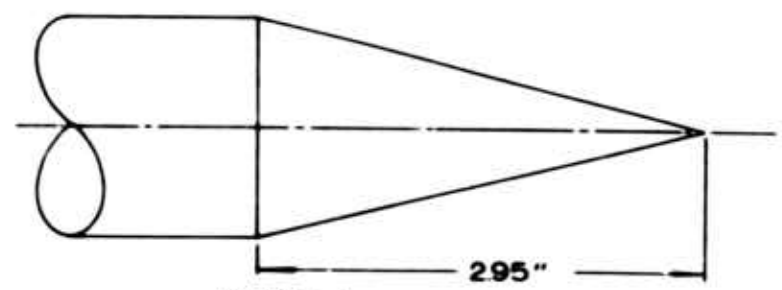

MODEL L
OGIVE CYLINDER WITH
AFTERBODY NO 4
C_o = 0.194

FIG 1-1. BODIES OF REVOLUTION

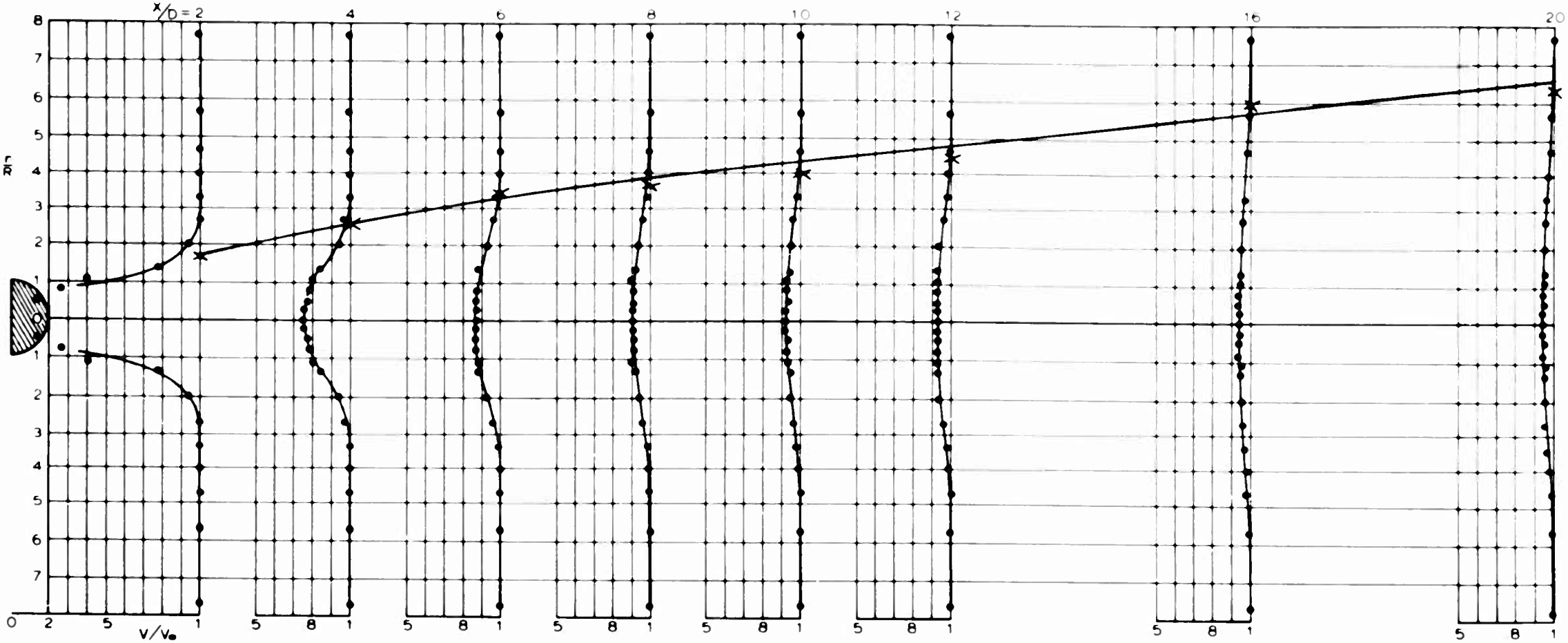

FIG 1-2. EXPERIMENTAL VELOCITY DISTRIBUTION IN WAKE OF HOLLOW HEMISPHERE (CUP FORWARD)——MODEL A

WAKE WIDTH { EXPERIMENTAL X
EMPIRICAL, ONE LINE APPROXIMATION ——

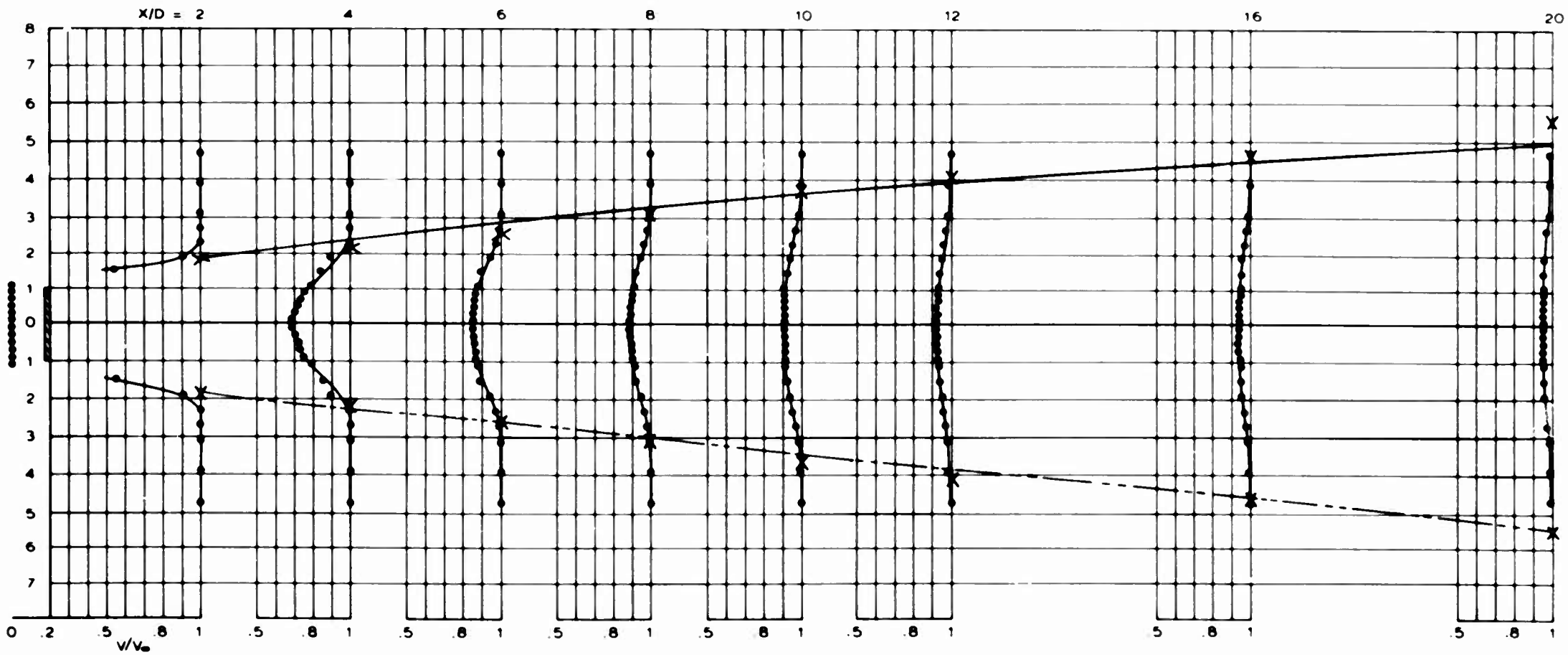

FIG 1-3. EXPERIMENTAL VELOCITY DISTRIBUTION IN WAKE OF DISK—MODEL B

WAKE WIDTH { EXPERIMENTAL X
EMPIRICAL, ONE LINE APPROXIMATION ——
EMPIRICAL, TWO LINE APPROXIMATION — - - —

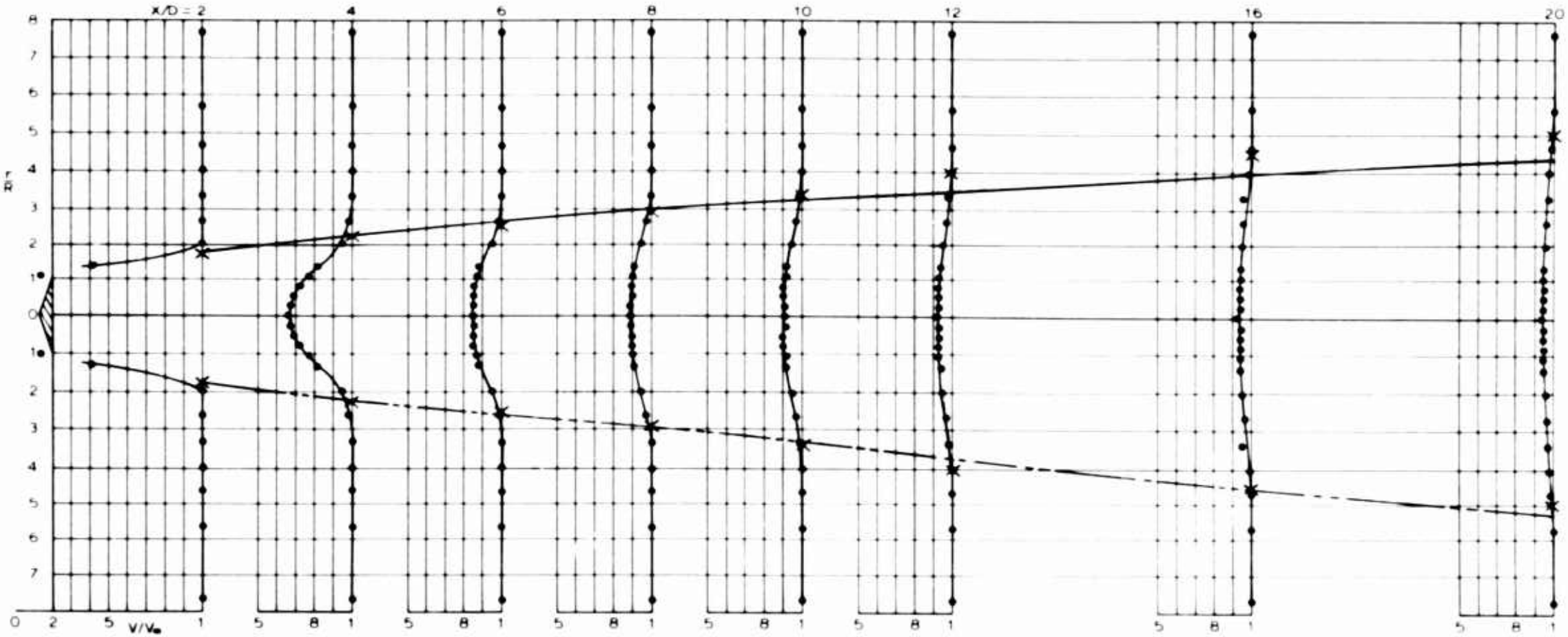

FIG 1-4. EXPERIMENTAL VELOCITY DISTRIBUTION IN WAKE OF CONE (OC = 75°)——MODEL C

WAKE WIDTH { EXPERIMENTAL X
EMPIRICAL, ONE LINE APPROXIMATION ———
EMPIRICAL, TWO LINE APPROXIMATION — - —

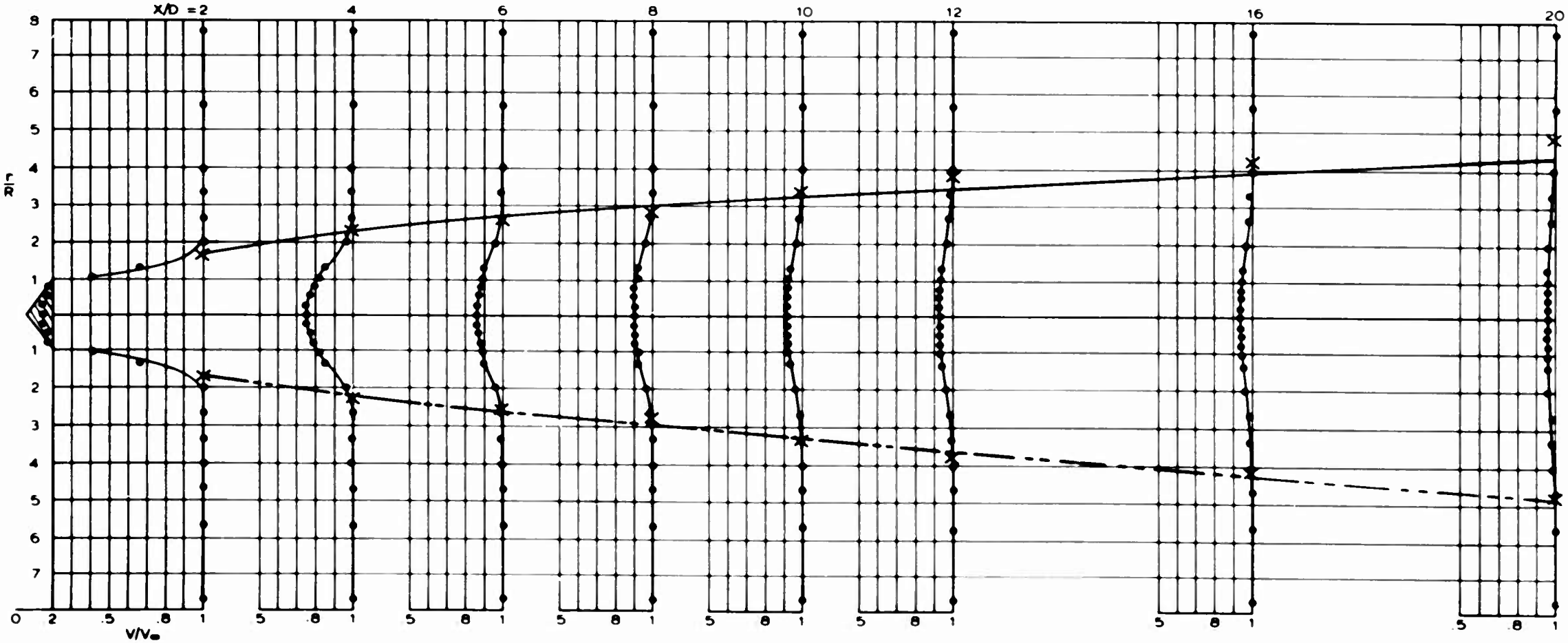

FIG 1-5. EXPERIMENTAL VELOCITY DISTRIBUTION IN WAKE OF CONE ($\alpha = 55°$)——MODEL D

WAKE WIDTH { EXPERIMENTAL ×
EMPIRICAL, ONE LINE APPROXIMATION ———
EMPIRICAL, TWO LINE APPROXIMATION — · · —

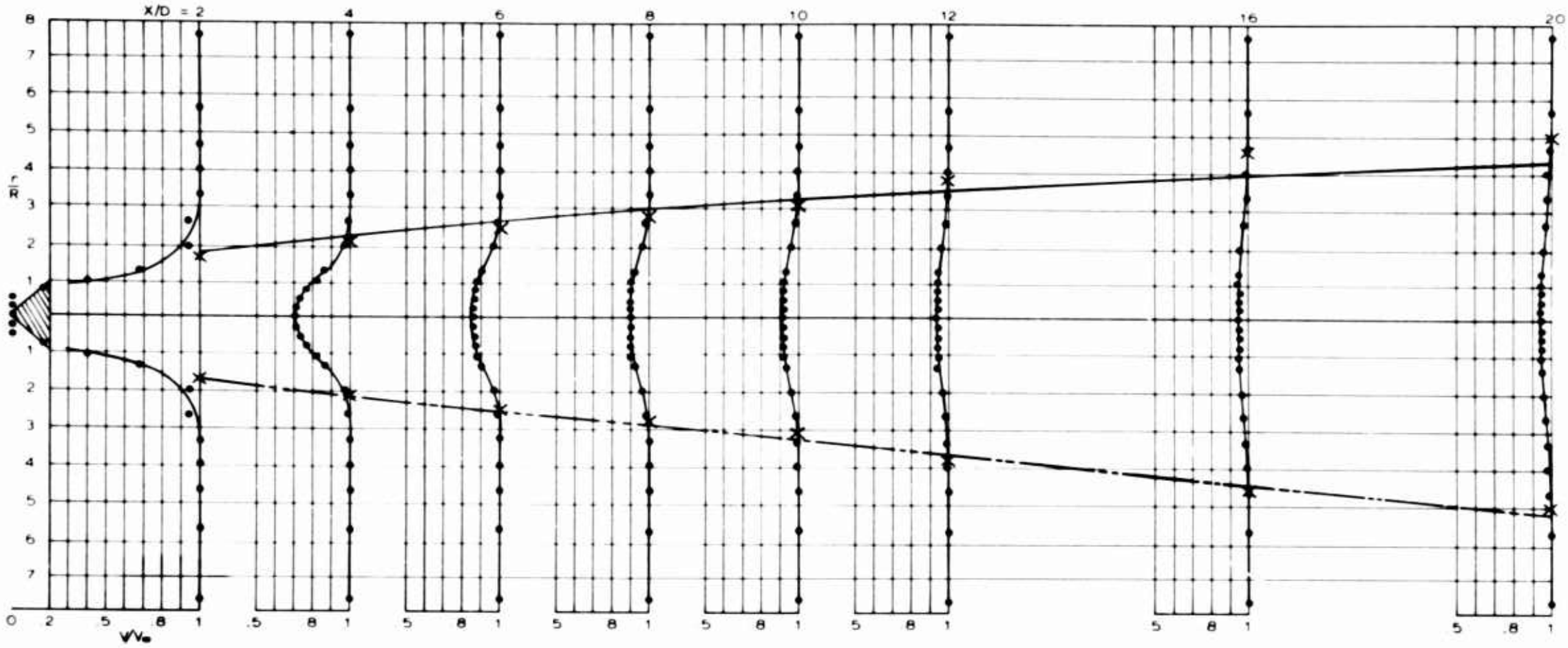

FIG 16. EXPERIMENTAL VELOCITY DISTRIBUTION IN WAKE OF CONE (α = 42.5°)——MODEL E

WAKE WIDTH { EXPERIMENTAL ×
EMPIRICAL, ONE LINE APPROXIMATION ——
EMPIRICAL, TWO LINE APPROXIMATION ——·——

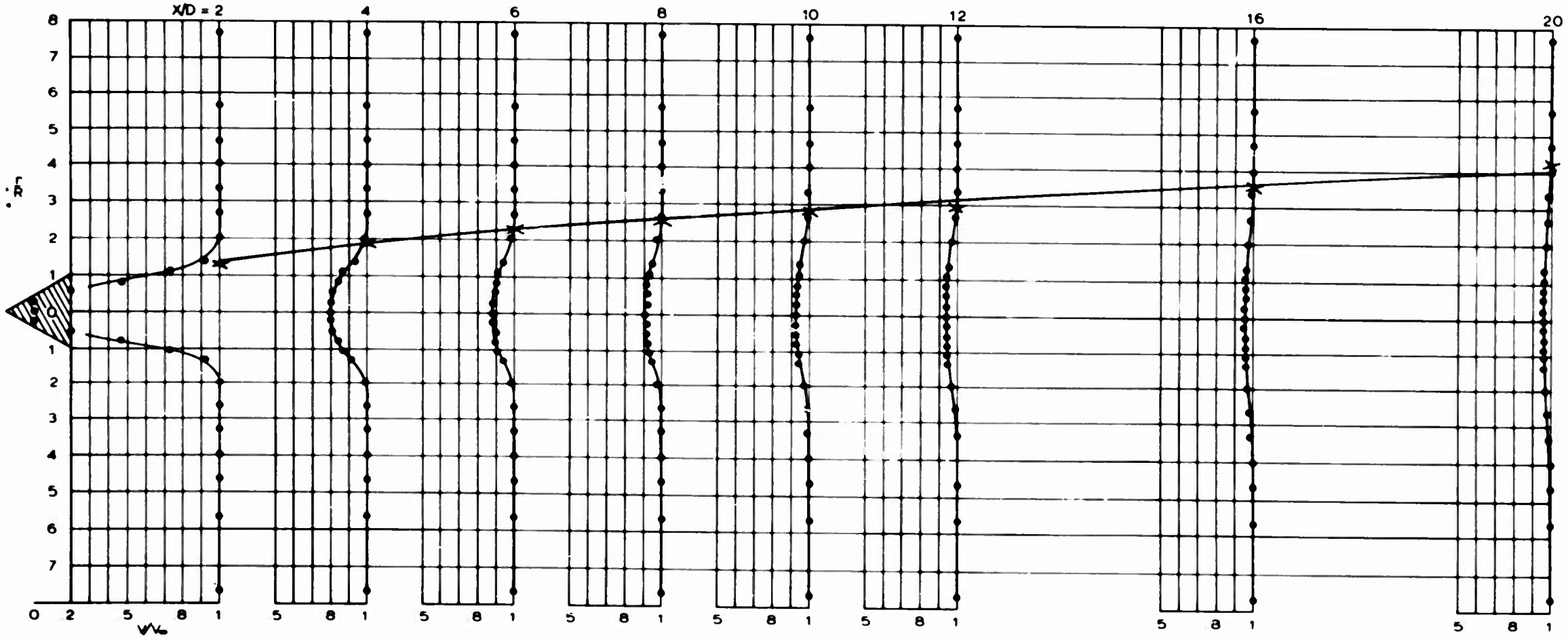

FIG 1-7. EXPERIMENTAL VELOCITY DISTRIBUTION IN WAKE OF CONE ($\alpha_c = 30°$)——MODEL F

WAKE WIDTH { EXPERIMENTAL ×
EMPIRICAL, ONE LINE APPROXIMATION ———

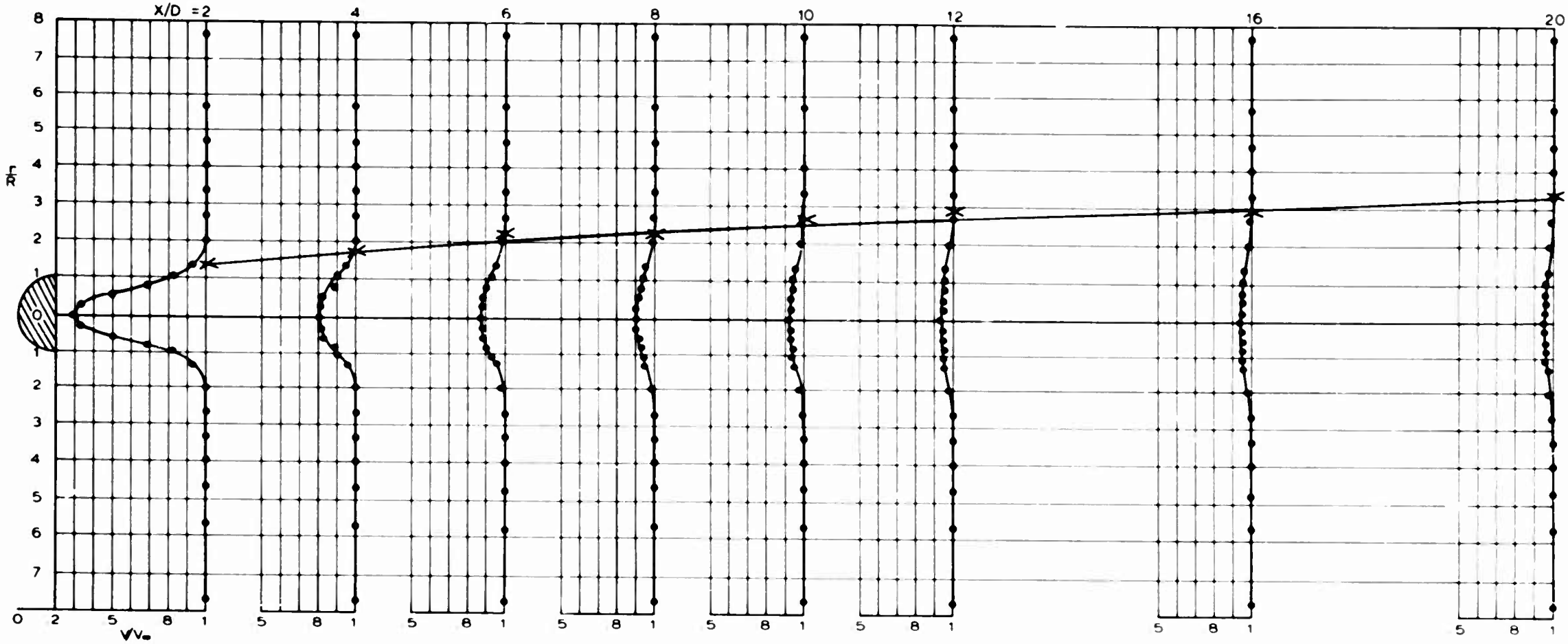

FIG 1-8. EXPERIMENTAL VELOCITY DISTRIBUTION IN WAKE OF HOLLOW HEMISPHERE (CUP BACKWARD)——MODEL G

WAKE WIDTH { EXPERIMENTAL ×
EMPIRICAL, ONE LINE APPROXIMATION ———

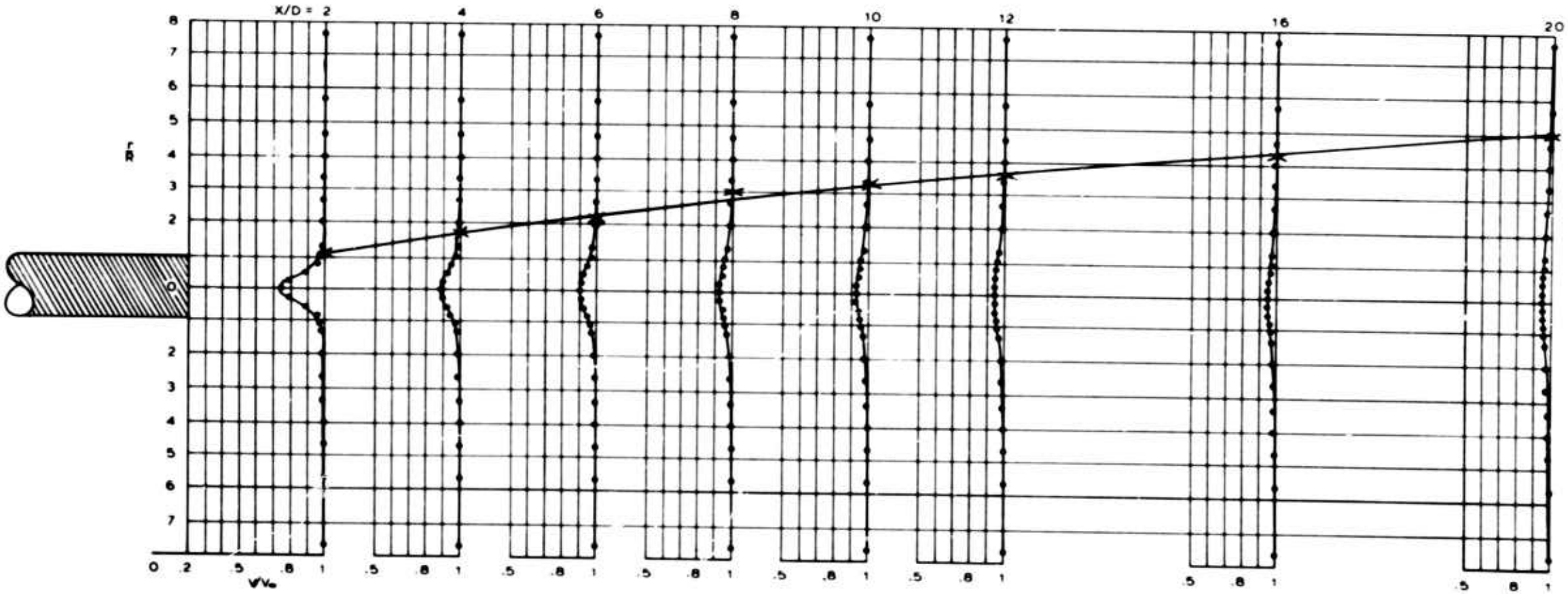

FIG 1-9. EXPERIMENTAL VELOCITY DISTRIBUTION IN WAKE OF OGIVE CYLINDER——MODEL H

WAKE WIDTH { EXPERIMENTAL X
EMPIRICAL, ONE LINE APPROXIMATION ——

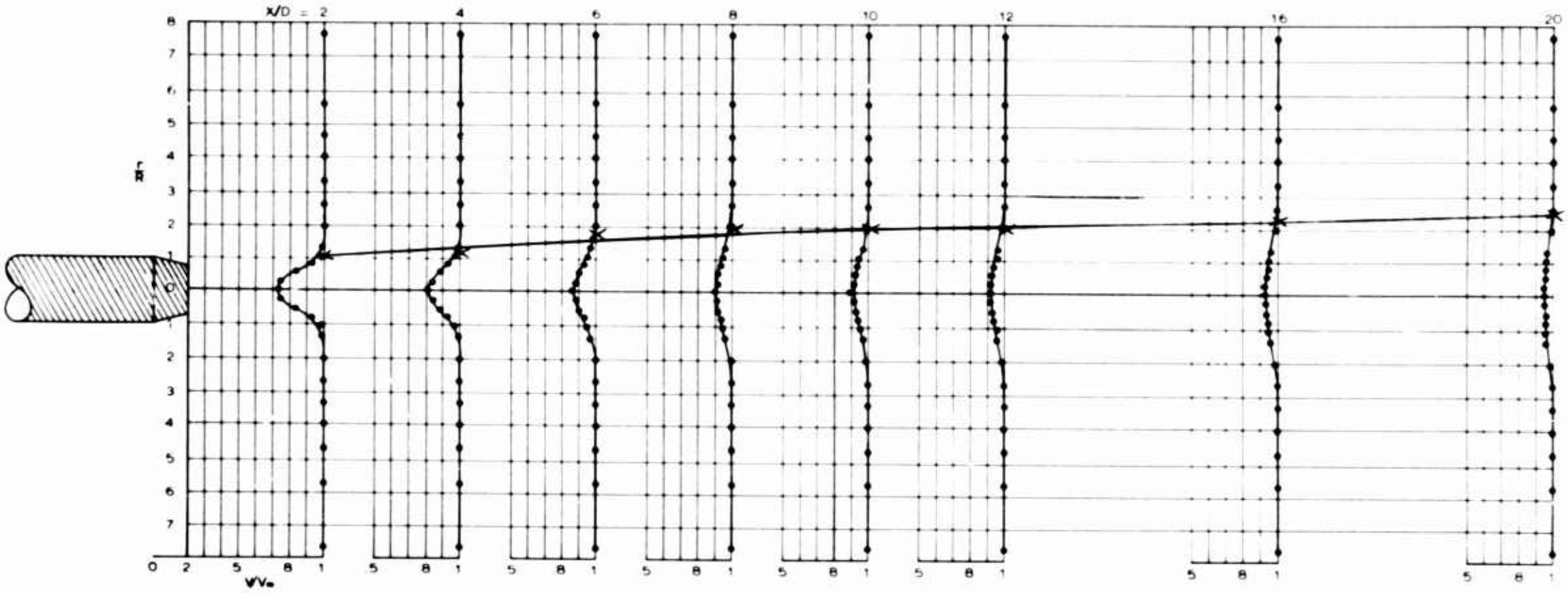

FIG 1-10. EXPERIMENTAL VELOCITY DISTRIBUTION IN WAKE OF OGME CYLINDER WITH AFTERBODY NO. 1——MODEL I

WAKE WIDTH { EXPERIMENTAL ×
EMPIRICAL, ONE LINE APPROXIMATION ———

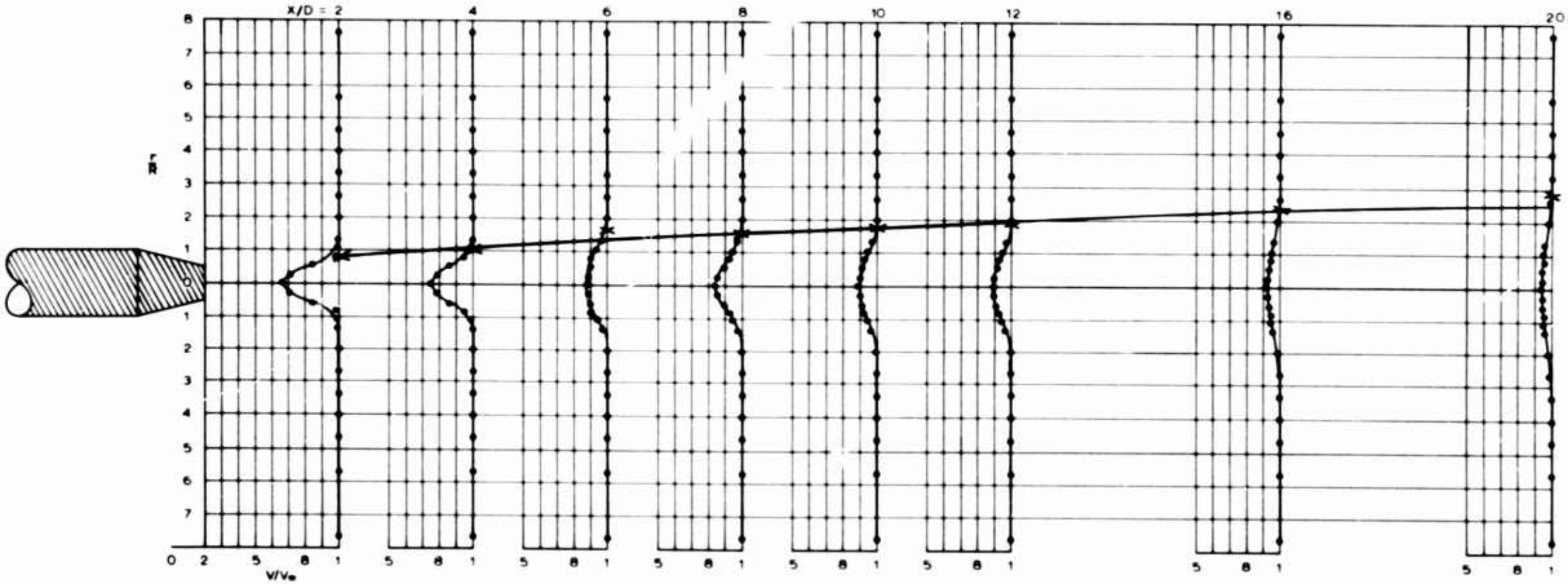

FIG 111. EXPERIMENTAL VELOCITY DISTRIBUTION IN WAKE OF OGIVE CYLINDER WITH AFTERBODY NO. 2—MODEL J

WAKE WIDTH { EXPERIMENTAL ×
EMPIRICAL, ONE LINE APPROXIMATION ———

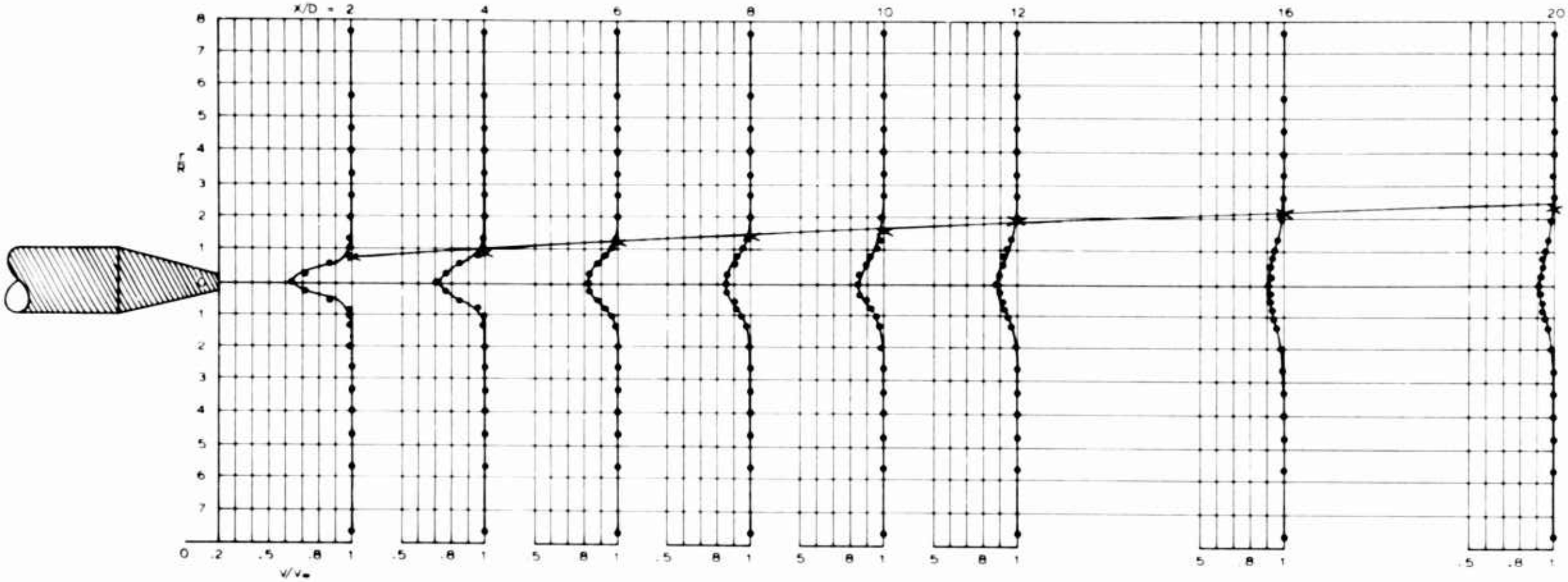

FIG 1-12. EXPERIMENTAL VELOCITY DISTRIBUTION IN WAKE OF OGIVE CYLINDER WITH AFTERBODY NO. 3—MODEL K

WAKE WIDTH { EXPERIMENTAL X
EMPIRICAL, ONE LINE APPROXIMATION ———

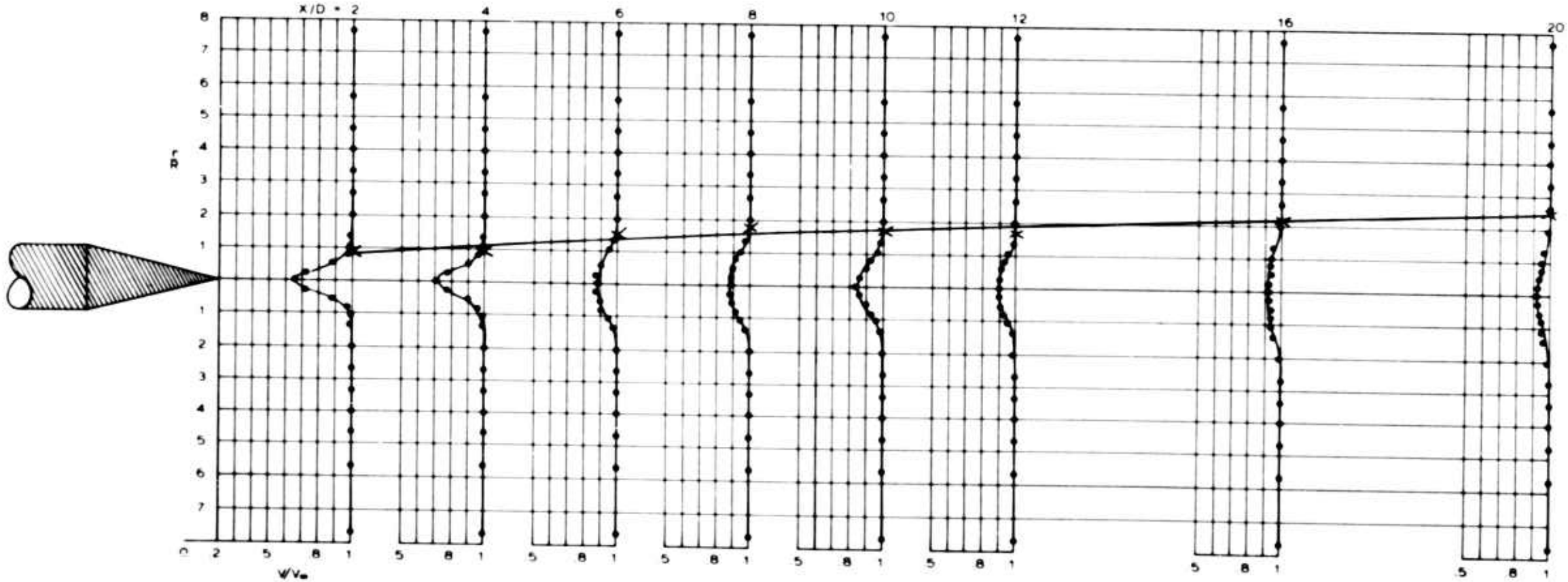

FIG 113. EXPERIMENTAL VELOCITY DISTRIBUTION IN WAKE OF OGIVE CYLINDER WITH AFTERBODY NO. 4——MODEL L

WAKE WIDTH {EXPERIMENTAL X
{EMPIRICAL, ONE LINE APPROXIMATION ——

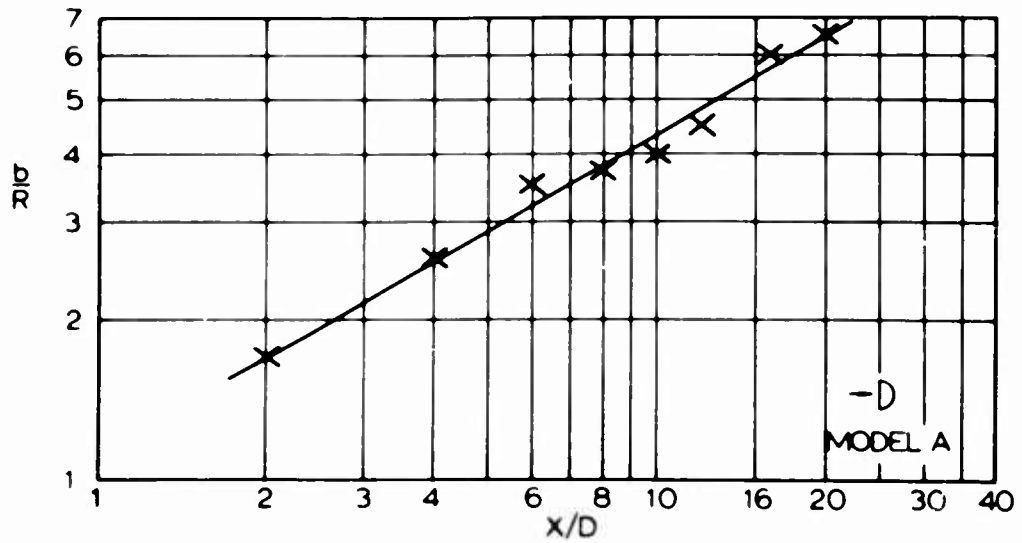

FIG 1-14. EXPERIMENTAL WAKE WIDTH OF MODEL A

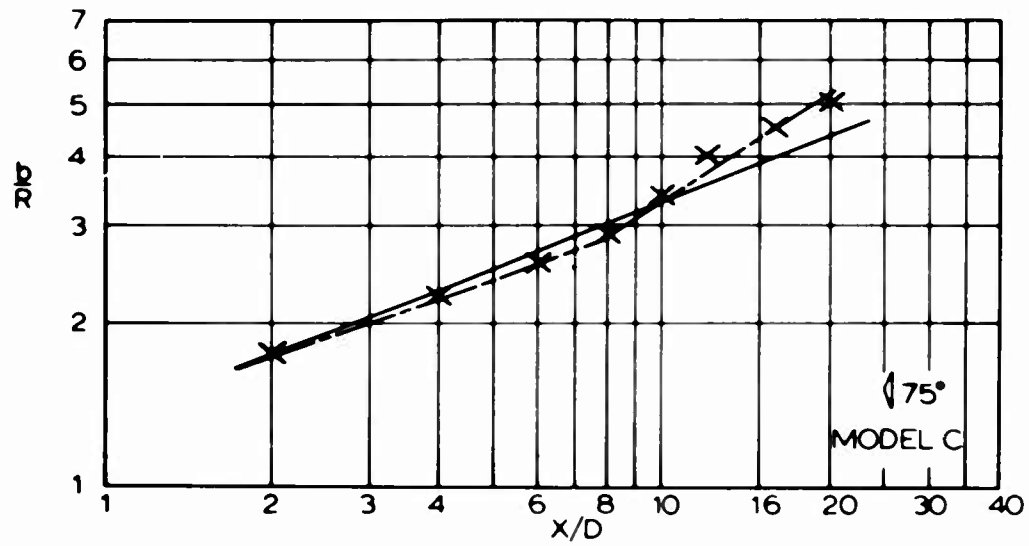

FIG 1-16. EXPERIMENTAL WAKE WIDTH OF MODEL C

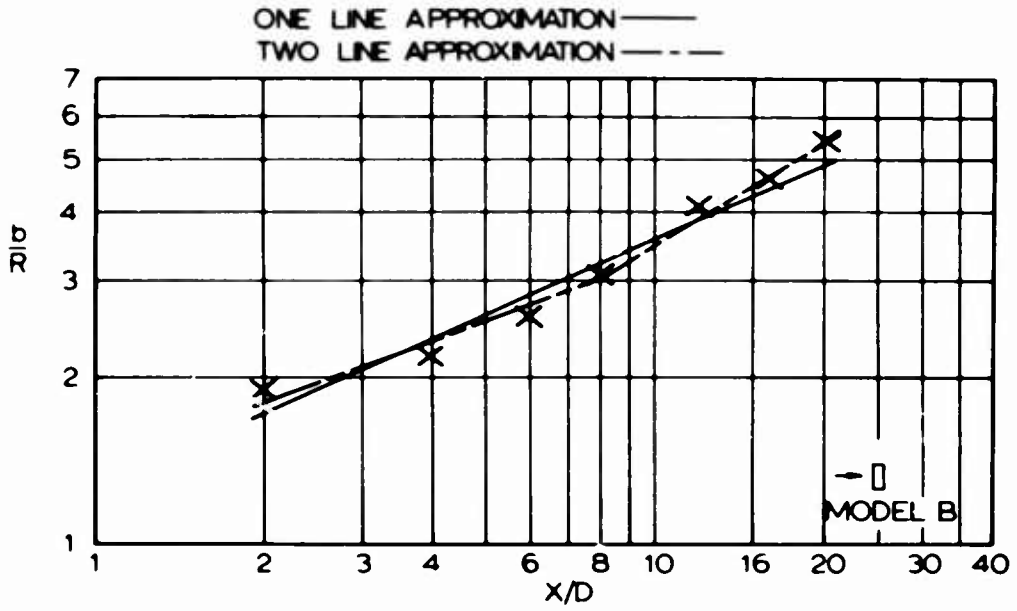

FIG 1-15. EXPERIMENTAL WAKE WIDTH OF MODEL B

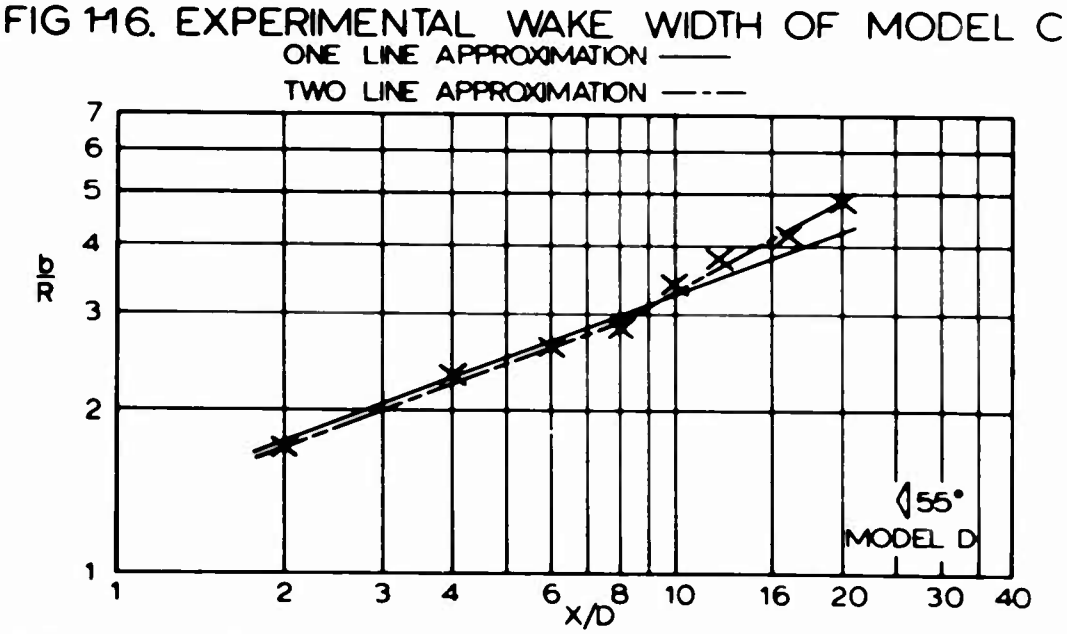

FIG 1-17. EXPERIMENTAL WAKE WIDTH OF MODEL D

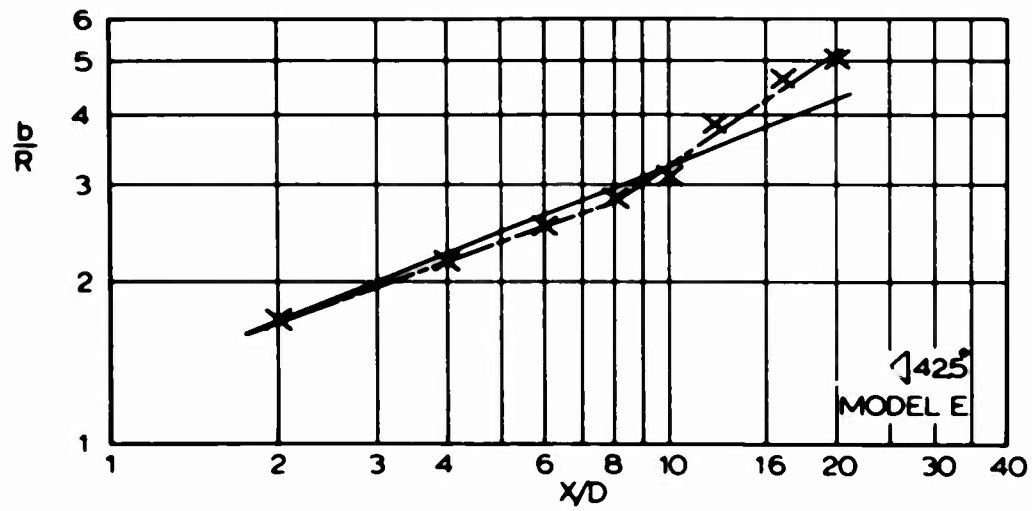

FIG 1-18. EXPERIMENTAL WAKE WIDTH OF MODEL E

ONE LINE APPROXIMATION ———

TWO LINE APPROXIMATION — · —

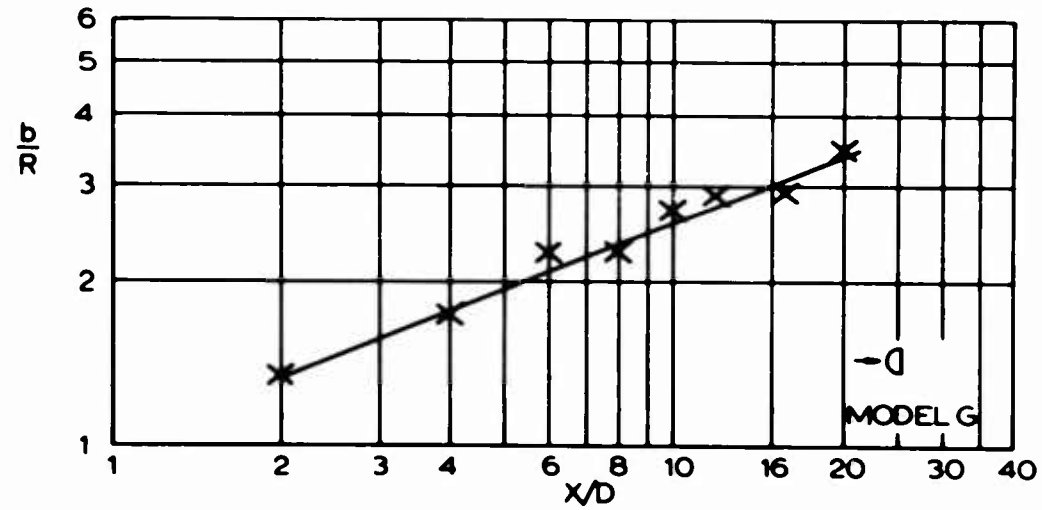

FIG 1-20. EXPERIMENTAL WAKE WIDTH OF MODEL G

ONE LINE APPROXIMATION ———

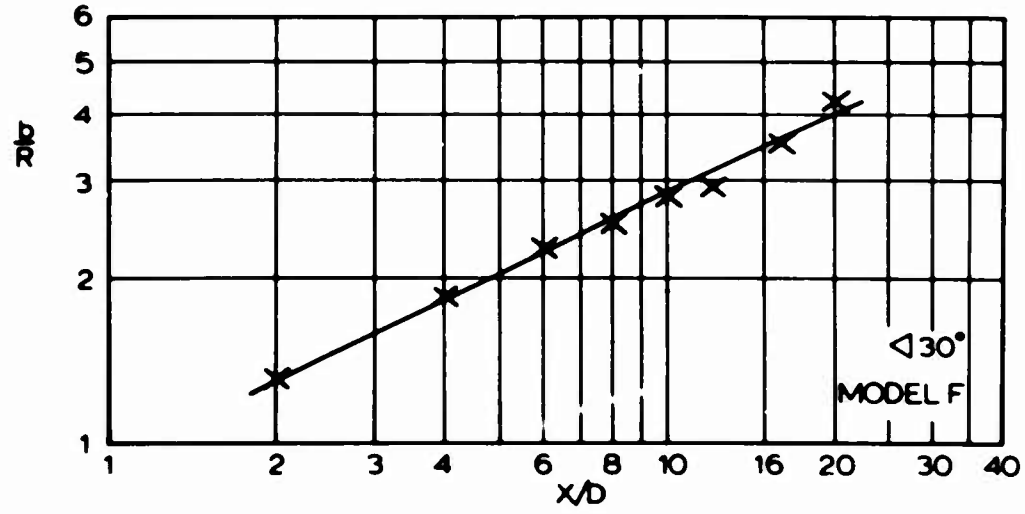

FIG 1-19. EXPERIMENTAL WAKE WIDTH OF MODEL F

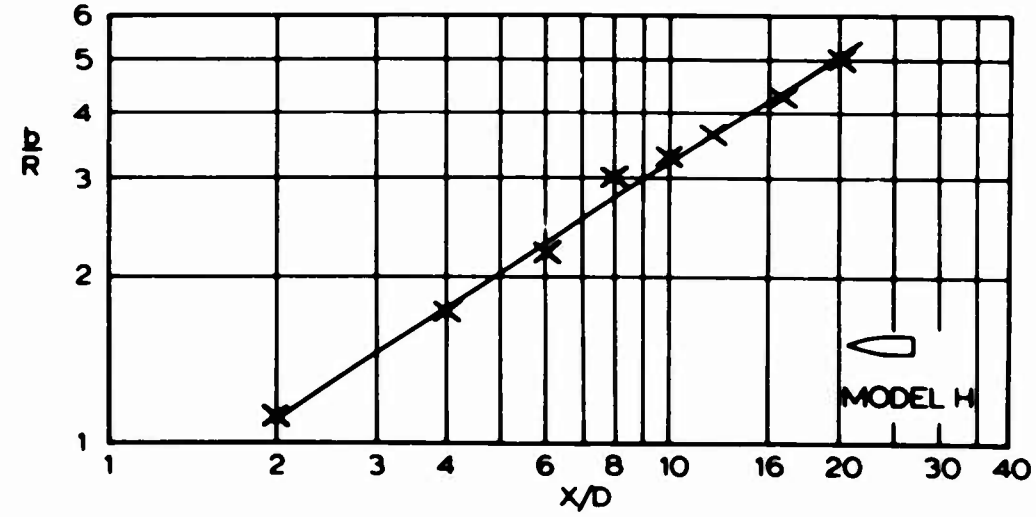

FIG 1-21. EXPERIMENTAL WAKE WIDTH OF MODEL H

FIG 1-22. EXPERIMENTAL WAKE WIDTH OF MODEL I

ONE LINE APPROXIMATION ——

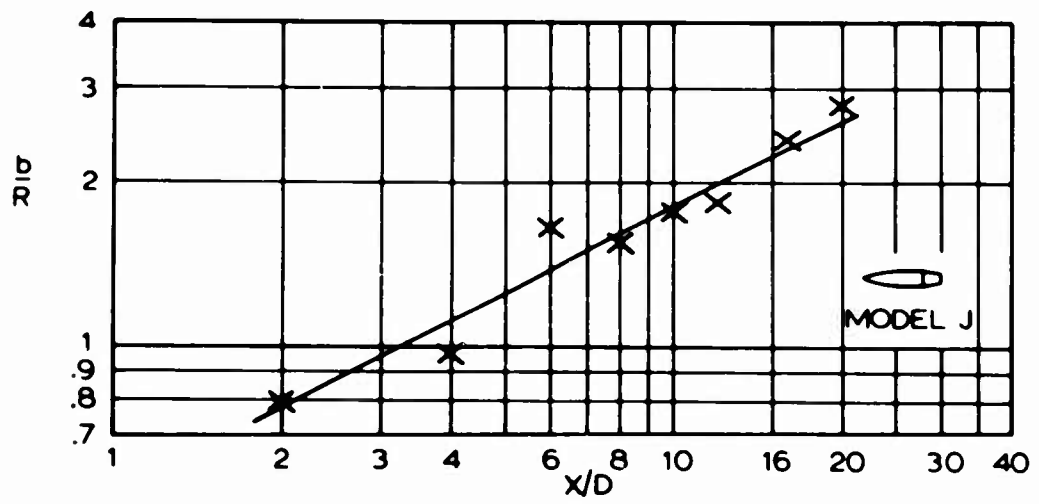

FIG 1-23. EXPERIMENTAL WAKE WIDTH OF MODEL J

FIG 1-24. EXPERIMENTAL WAKE WIDTH OF MODEL K

ONE LINE APPROXIMATION ——

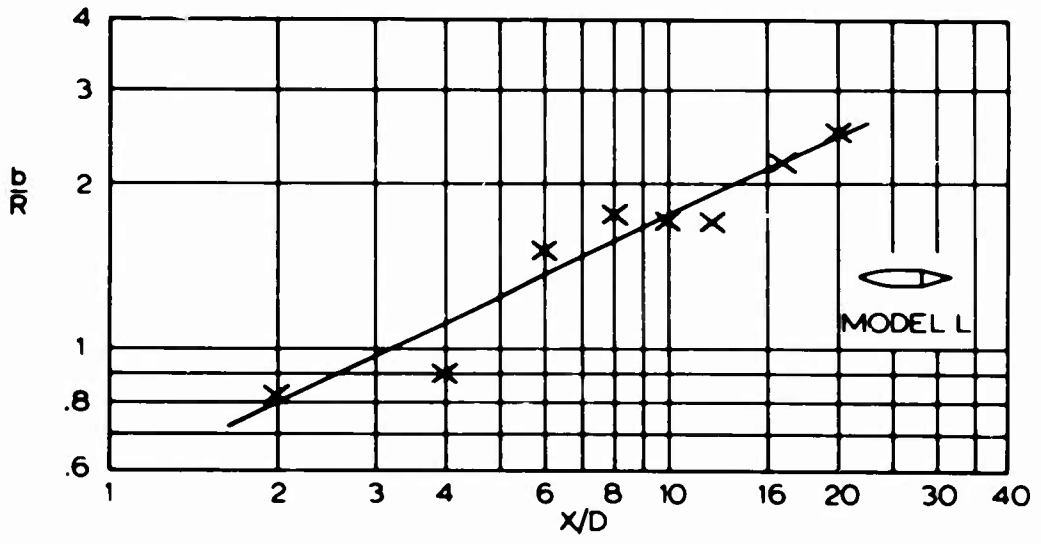

FIG 1-25. EXPERIMENTAL WAKE WIDTH OF MODEL L

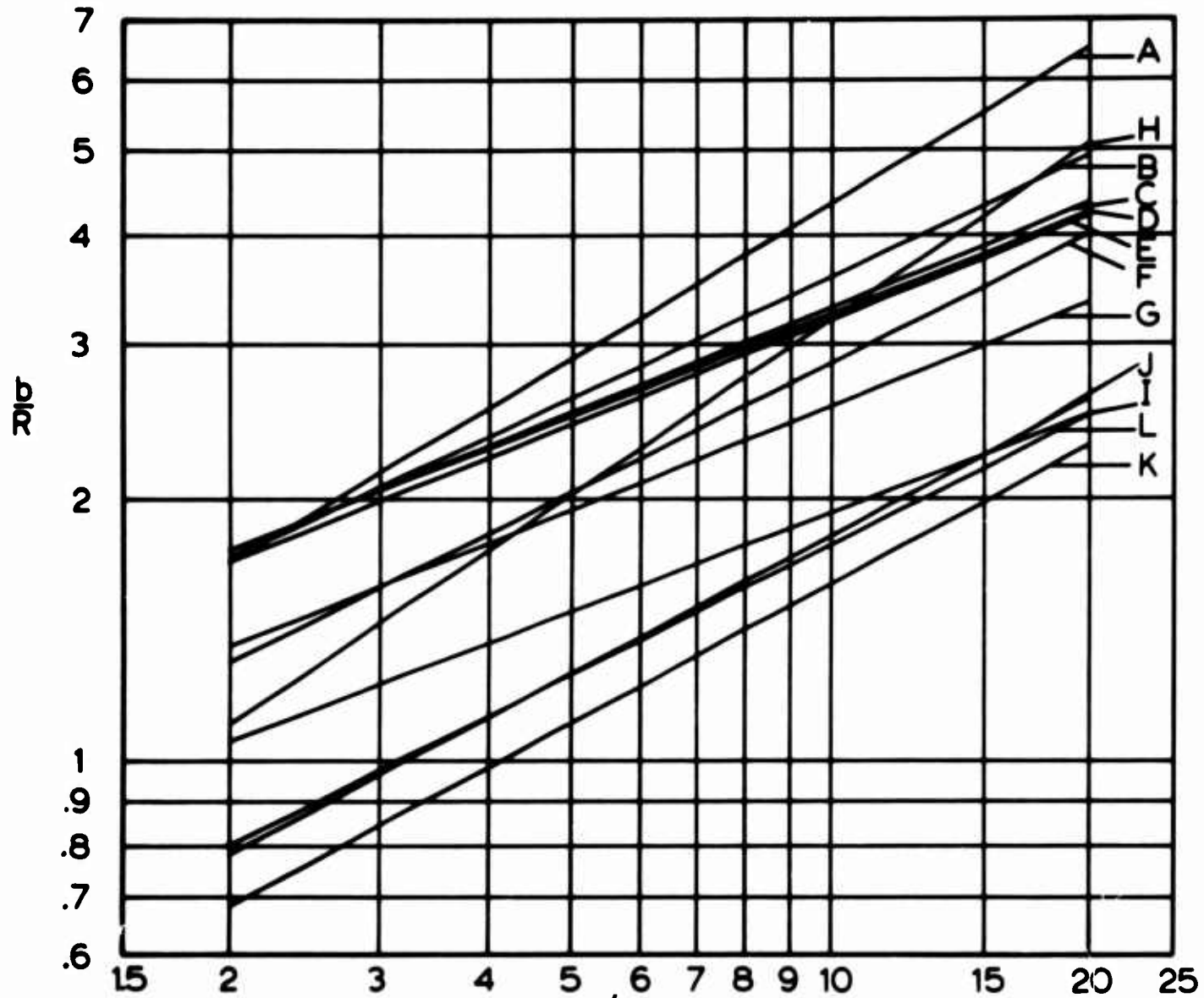

FIG 1-26. ONE LINE APPROX. OF EXPERIMENTAL WAKE WIDTH

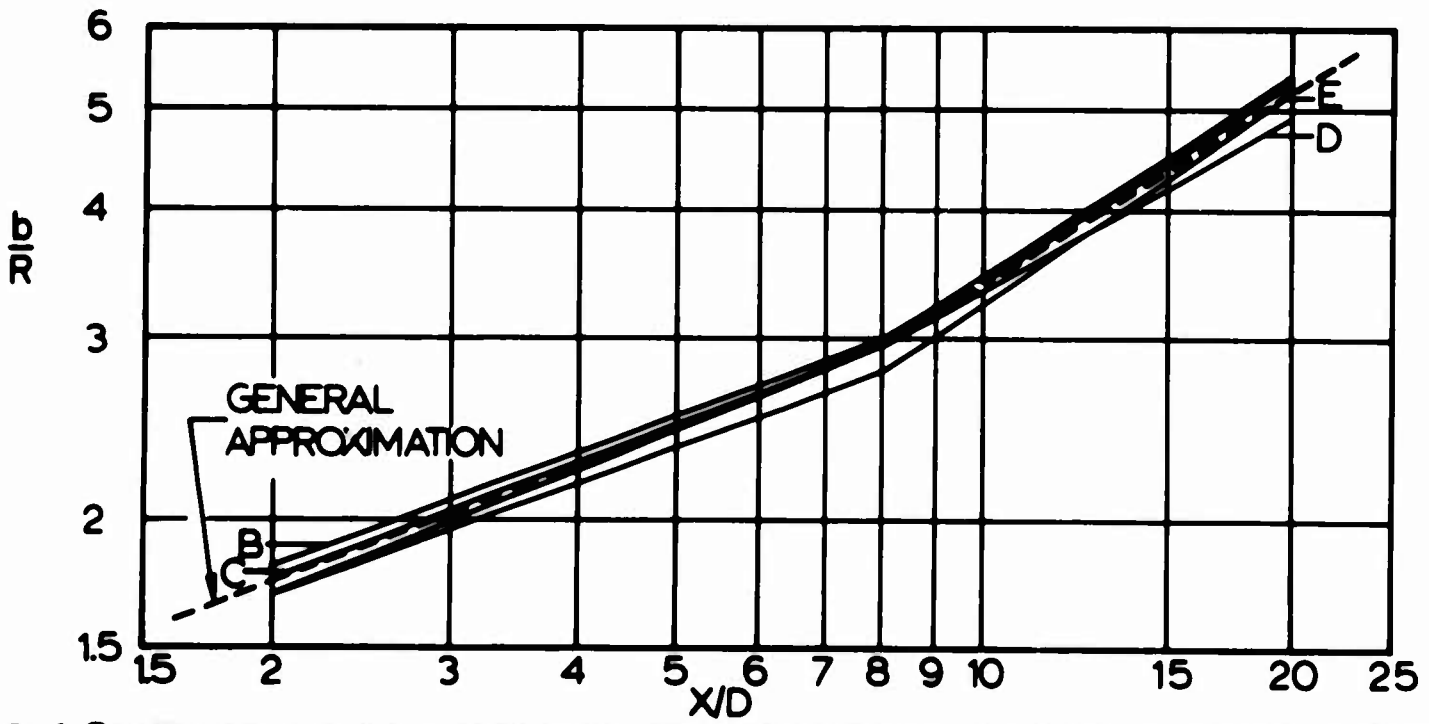

FIG 1-27. TWO LINE APPROX. OF EXPERIMENTAL WAKE WIDTH

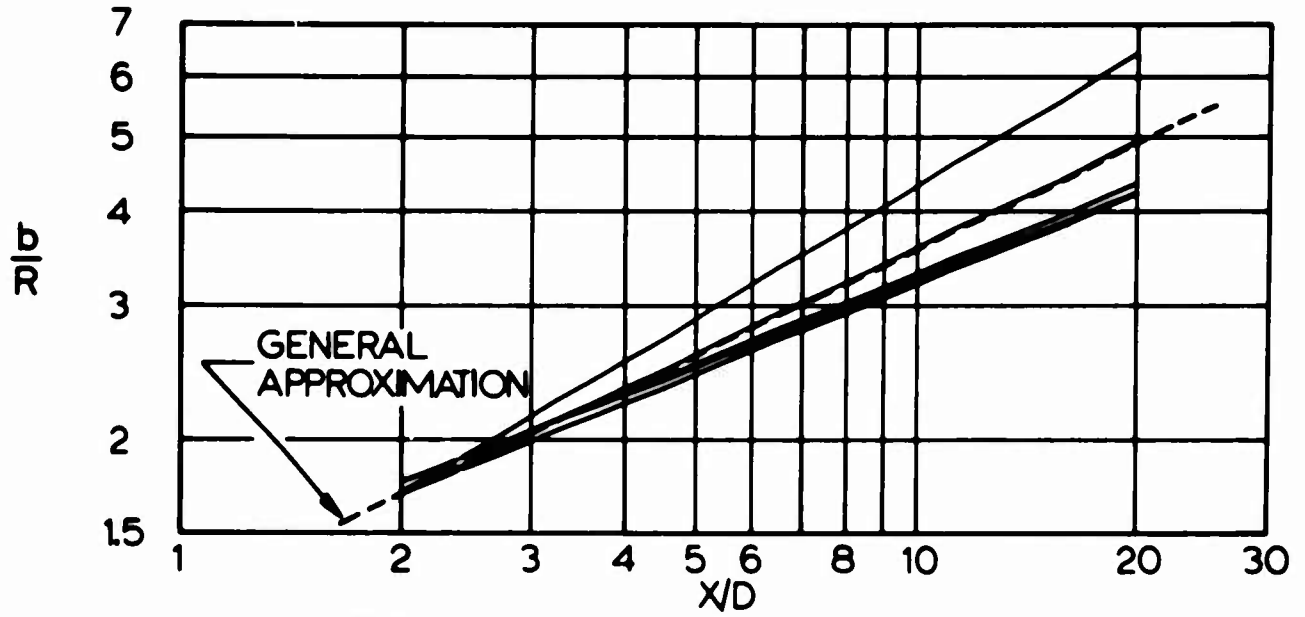

A. BLUFF BODIES, MODELS A-E

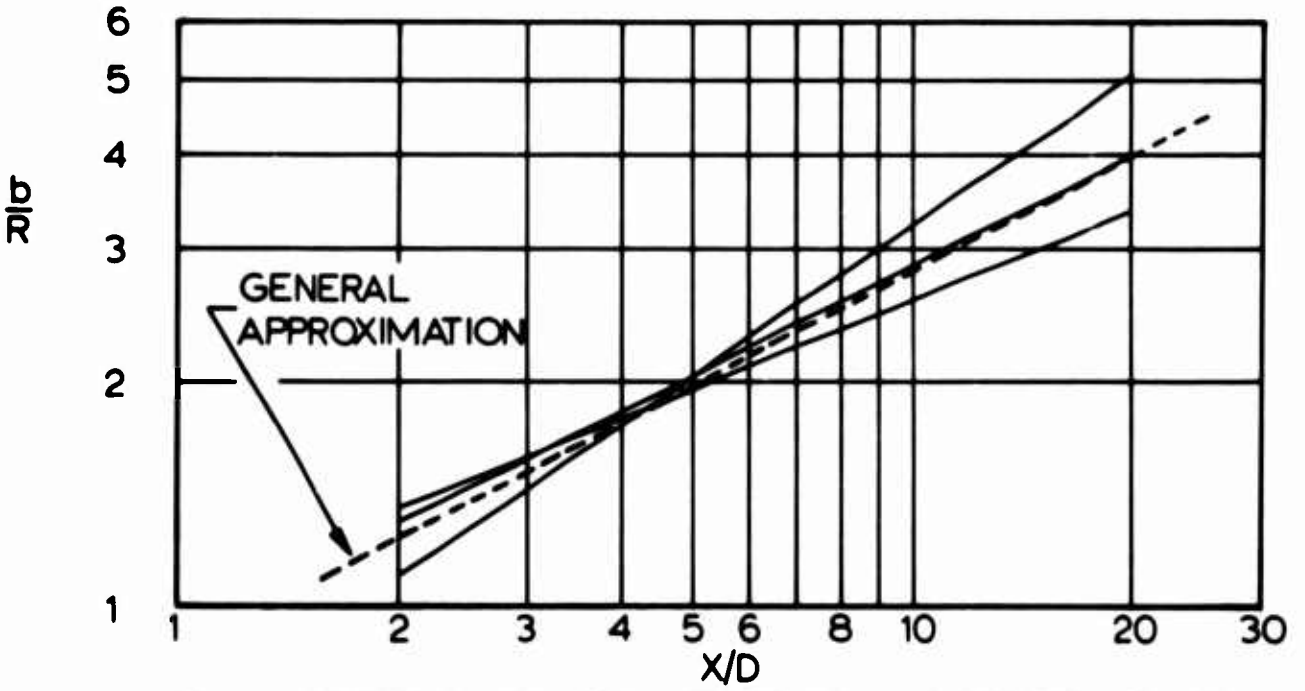

B. INTERMEDIATE BODIES, MODELS F-H

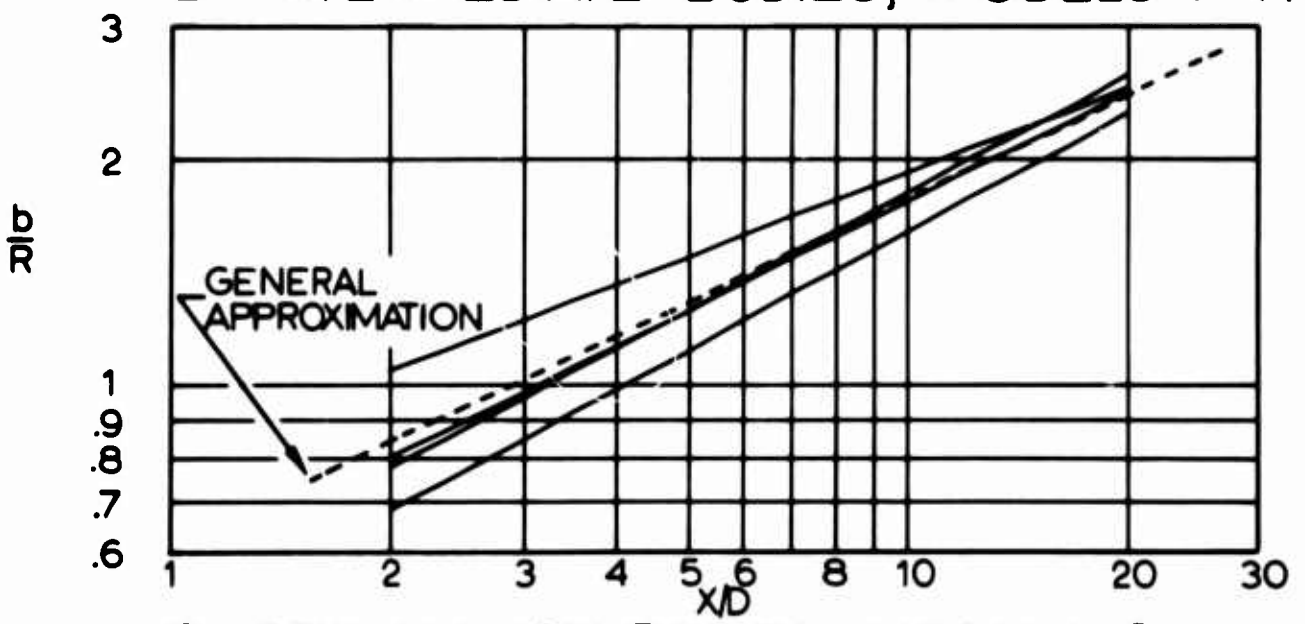

C. STREAMLINED BODIES, MODELS I-L

FIG 1-28 GENERAL APPROXIMATIONS OF WAKE WIDTH

3.0 Investigation of Basic Stability Parameters of Conventional Parachutes

3.1 Experimental Determination of the Apparent Moment of Inertia of Parachutes

3.1.1 Introduction

In Progress Report No 20, an experimental method to determine the apparent moment of inertia was presented. The theory and supporting references were also presented in the same report.

During the present reporting period, tests were conducted with simple geometric bodies. The results obtained were compared with those of the references to check the validity of the experimental procedure used and the accuracy of the test results.

3.1.2 Test Apparatus Modifications

It was found during the initial tests that the mounting of the "Shaevitz" transducer was not rigid enough. Since the allowable tolerance in the setting of the core and the coil of the transducer is very small, the core was attached to a more rigid mounting. With this modification, the system performs satisfactorily.

By attaching a pulley to the test frame, it was possible to use static loading (Fig 4-1) as a means of determining the spring constant.

3.1.3 Models

In the preliminary experiments conducted during this reporting period, the models used were similar to those used in Refs 1 and 2. These models were used to enable comparison of recent experimental results obtained with the modified apparatus with the values obtained by previous experimenters and by theoretical methods. The three bodies used in the experiments consisted of a sphere, a cube, and a circular disk. Reference 2 provides experimental data for cubes and spheres and cites further references for theoretical calculations dealing with spheres. Reference 1 contains experimental data for several disks and cites theoretical references for the purpose of comparing theoretical and experimental results.

It was discovered in earlier tests that the size of the models had to be relatively large so as to reduce the relative effects of the system friction. The optimum sized model for the system used has a mass comparable to or greater than a one inch diameter brass sphere.

3.1.4 Experimental Procedure

The test models are mounted on the apparatus as shown in Fig 4-2 to insure symmetry and to optimize the amplitude of oscillation.

Progress Report No 20, Sec 3.1.3, presented a detailed description of the basic apparatus used. During testing of the models, the oscillator frequency is constantly checked for accuracy by feeding the signals into a y-axis amplifier of an oscilloscope and feeding 60 cycle line current into the x-amplifier. By observing the Lissajous figure appearing on the oscilloscope screen, any whole number or simple fraction multiple of 60 cycles per second can be set on the oscilloscope.

In these tests, a frequency of 15 cycles per second was used as the time base, corresponding to a 4 to 1 Lissajous figure on the screen. This time base frequency is fed into one channel of a Brush Recorder. Into the other channel is fed the output of the strain analyzer which in turn is excited by the transducer mounted on the torsion rod system.

The determination of the spring constant can be accomplished by means of a static or a dynamic test. In the static test, the system was set up as shown in Fig 4-1, with the angle of deflection determined by the small angle formula

$$\Theta = \Delta Y / \ell \quad . \tag{4.1}$$

Since the moment arm used in this experiment seemed to bend appreciably, thereby adding its own deflection, another test was conducted to correct for the additional deflection of the moment arm. The moment arm was secured in a rigid vice and reloaded in the same manner as before. The deflection for any given load measured in this experiment was subtracted from the deflection for the corresponding load on the torsion system. The angles were plotted as a function of the applied torque, with the slope of the line determining the spring constant.

In the dynamic test, the moment of inertia of the system was calculated and the period in air measured. From these values the spring constant was calculated using Eqn 4.2 of Progress Report No 20;

$$K \cong 4\pi^2 \frac{I}{T^2} \tag{4.2}$$

where K is the spring constant.

The calculated moment of inertia included Systems 1 and 2 shown in Fig 4-2. System 3 gave negligible values as compared to Systems 1 and 2. System 1, which included the

models and the members used to attach the models to the torsion rod, had a calculated moment of inertia of 60.8×10^3 gm-cm^2. System 2, which included the fastener and the rods supporting the detection core, had a calculated moment of inertia of 0.331×10^3 gm-cm^2. The torsion rod itself, which had a moment of inertia of 0.00049×10^3 gm-cm^2, constituted System 3.

The spring constant determined in this manner compared very well with the constant determined by the static test. The average value of the spring constant obtained by the static test is 45.8×10^6 dyne-cm. The spring constant determined by dynamic tests is being used in this report because the testing procedure used for determining the added mass is similar to the dynamic determination of the spring constant.

A sample of recorder paper from tests on the 1.5 inch diameter sphere is shown in Fig 4-3. The figure illustrates the procedure for calculating the period of oscillation of the system.

3.1.5 Test Results

The data from tests on the disk is presented in terms of the additional mass, M', in order that results may be compared with those of Ref 1. The working equation used for calculating M' was arrived at by modification of Eqn (4.6) of Progress Report No 20. The modified equation has the form

$$I' = \frac{K}{4\pi^2} (T_W^2 - T_A^2) - I_S. \qquad (4.3)$$

where the subscripts w and A refer to water and air respectively.

Under present testing conditions, the added moment of inertia of the system without models, I_S, was found to be negligible. Also, for the whole system,

$$I' = M' \ell^2 . \qquad (4.4)$$

Then for one model,

$$M' = \frac{I'}{2\ell^2} = \frac{K}{8\pi^2\ell^2}\left(T_W^2 - T_A^2\right). \qquad (4.5)$$

To facilitate the comparison of test results with the results of Ref 2, the data from tests on the cube and sphere models is presented as the dimensionless ratio M'/M_W, where M_W is the mass of the water displaced by the model. These experimental results are presented in Table 4-1, where column 1 gives the characteristic dimension of the model in metric units. Figure 4-4 is a graph comparing data from tests on disks with experimental and theoretical values obtained from Ref 1. This project's test results lie between previously obtained experimental values and the values calculated from available theory. The comparison of this project's experimental results and Lamb's theoretical values for spheres and cubes is presented in Fig 4-5.

Since the project's test results compare well with previous results and available theory, it is felt that the experimental apparatus used and the test procedure developed are suitable for the experimental determination of the apparent mass and apparent moment of inertia of rigid canopy models.

3.1.6 Proposed Work

During the next reporting period, models of circular flat, ribless guide surface, and ribbon parachute canopies will be constructed and tested. Further refinements in the experimental apparatus and technique will be made where necessary.

3.2 Wind Tunnel Investigation of Parachute Models

A second draft of the technical report entitled

"Stablility and Drag of Parachutes with Varying Effective Porosity," has been submitted to the Procuring Agency for approval.

3.3 Theoretical Investigation of the Dynamic Stability of Parachutes

A preliminary technical report of this data has been written and is currently being reviewed.

REFERENCES

1. Yu, Yee Tak: Virtual Masses and Moments of Inertia of Discs and Cylinders in Various Liquids, Journal of Applied Physics, 1942, Volume 13, pp. 66-69.

2. Stelson, J. M. and Mavid, F. T.: Virtual Mass and Acceleration in Fluids, Trans., ASCE, Volume 22, 1957, pp. 518-530.

$$M' = \frac{K}{8\pi^2 L^2}(T_W^2 - T_A^2)$$

MODEL	r or s (cm)	t (cm)	L (cm)	L^2	$\frac{I}{L^3} \times 10^3$	$K \times 10^{-6}$ (dyne-cm)	$\frac{K}{8\pi^2} \times 10^{-6}$	$\frac{K}{8\pi^2 L^2}$	T_W (sec)	T_A (sec)	$T_W^2 - T_A^2 \times 10^2$	M' (gm)	M_W water displaced (gm)	$\frac{C'}{M_W}$
DISK I	1.920	0.356	11.60	134.6	7.429	47.00	59.53	4422.	.1127	.0866	.5207	23.02		
	"	"	"	"	"	"	"	"	.1124	.0867	.5117	22.63		
	"	"	"	"	"	"	"	"	.1127	.0867	.5184	22.92		
DISK II	1.683	0.295	11.49	132.0	7.576	47.00	59.53	4510.	.0926	.0710	.3534	15.94		
	"	"	"	"	"	"	"	"	.0926	.0710	.3534	15.94		
	"	"	"	"	"	"	"	"	.0929	.0710	.3589	16.19		
DISK III	2.500	0.335	12.30	151.3	6.609	47.00	59.53	3934.	.1650	.1201	1.280	50.36		
	"	"	"	"	"	"	"	"	.1650	.1205	1.270	49.98		
	"	"	"	"	"	"	"	"	.1644	.1203	1.256	49.39		
DISK IV	3.176	0.320	12.98	168.5	5.935	47.00	59.53	3533.	.2342	.1622	2.854	100.8		
	"	"	"	"	"	"	"	"	.2353	.1621	2.904	102.6		
	"	"	"	"	"	"	"	"	.2346	.1621	2.876	101.6		
DISK V	3.178	0.312	12.98	168.5	5.935	47.00	59.53	3533.	.1942	.0930	2.906	102.7		
	"	"	"	"	"	"	"	"	.1948	.0930	2.930	103.5		
	"	"	"	"	"	"	"	"	.1935	.0932	2.876	101.6		
CUBE S=.923in=2.34cm	2.344	----	10.85	117.7	8.496	47.21	59.79	5080.	.1536	.1480	.1689	8.580	12.80	.6703
	"	"	"	"	"	"	"	"	.1534	.1480	.1628	8.270	"	.6462
	"	"	"	"	"	"	"	"	.1535	.1481	.1629	8.275	"	.6465
SPHERE D=1.25in=3.18cm	1.588	----	11.26	126.9	7.880	47.25	59.84	4715.	.1733	.1678	.1876	8.845	16.80	.5265
	"	"	"	"	"	"	"	"	.1732	.1678	.1841	8.680	"	.5167
	"	"	"	"	"	"	"	"	.1733	.1678	.1876	8.845	"	.5265
SPHERE D=1.50in=3.81cm	1.905	----	11.58	134.14	7.455	46.48	58.87	4389.	.2349	.2278	.3285	14.42	29.00	.4972
	"	"	"	"	"	"	"	"	.2348	.2278	.3238	14.21	"	.4900
	"	"	"	"	"	"	"	"	.2351	.2278n	.3379	14.83	"	.5114

TABLE 4-1. DATA AND CALCULATIONS FOR M' AND C' OF VARIOUS MODELS

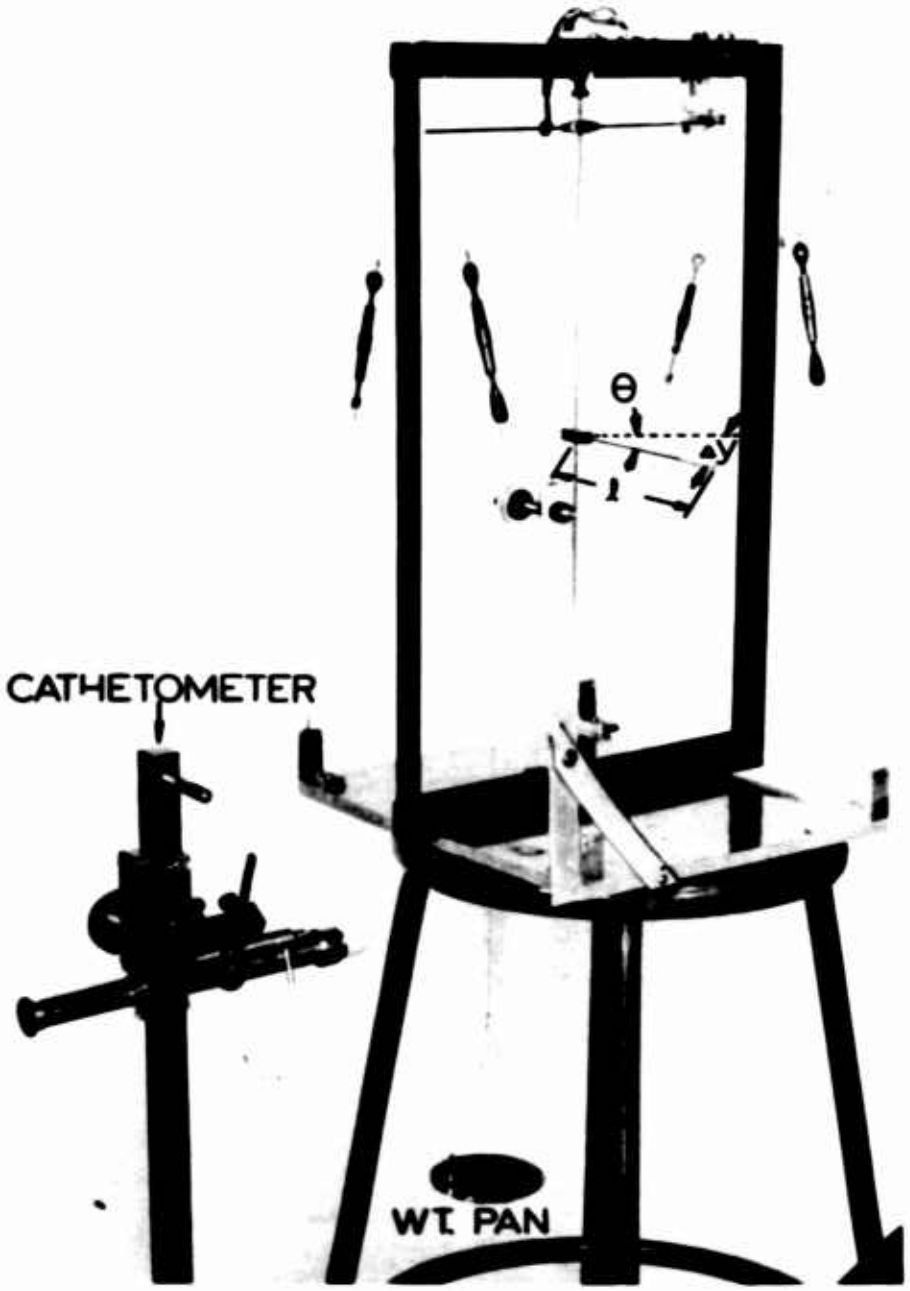

FIG 4-1. EXPERIMENTAL ARRANGEMENT FOR STATIC MEASUREMENT OF SPRING CONSTANT

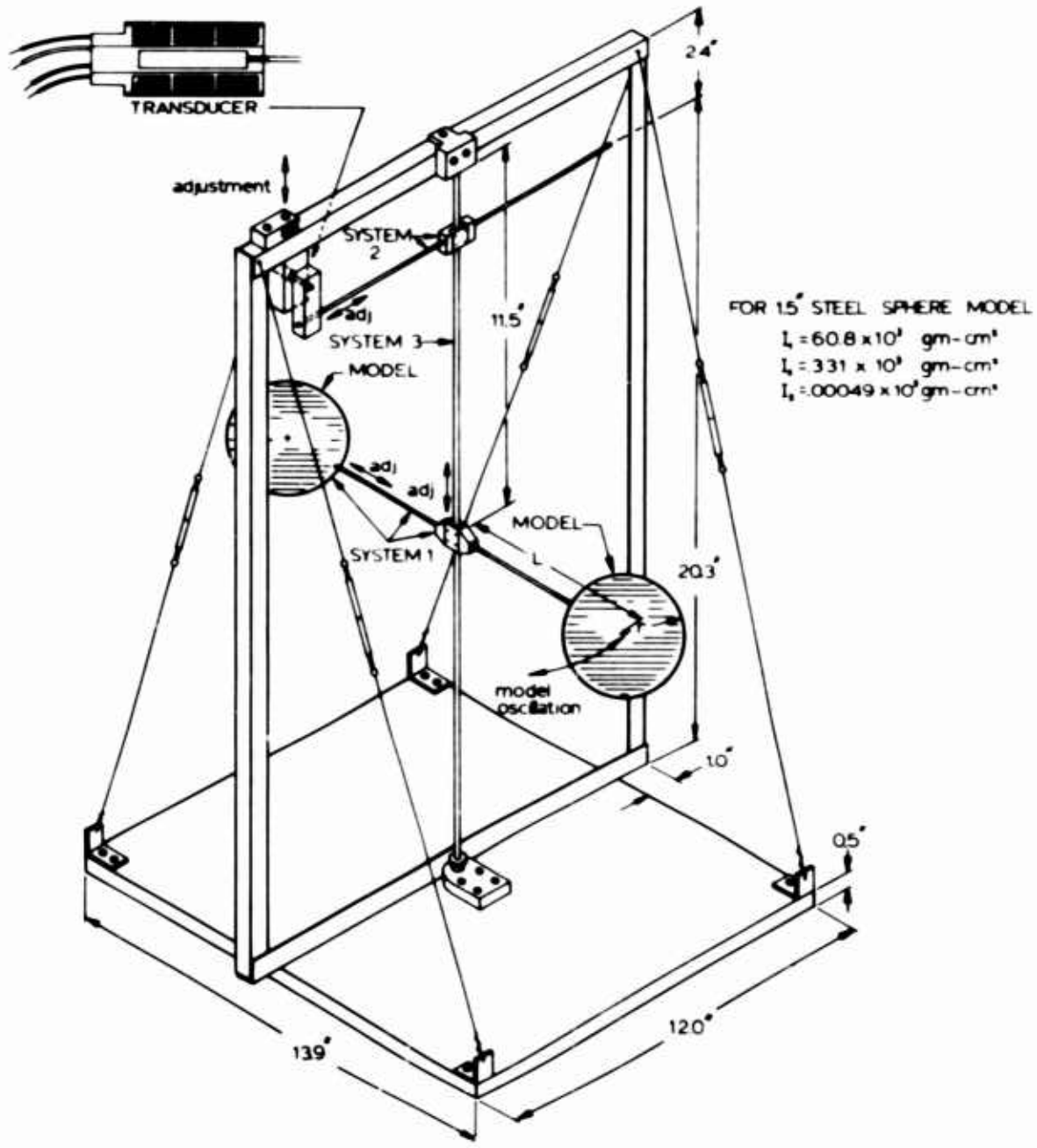

FIG 4-2. SKETCH OF TEST FRAME SHOWING LOCATION OF MODEL AND BREAK DOWN OF SYSTEM FOR MOMENT OF INERTIA CALCULATIONS

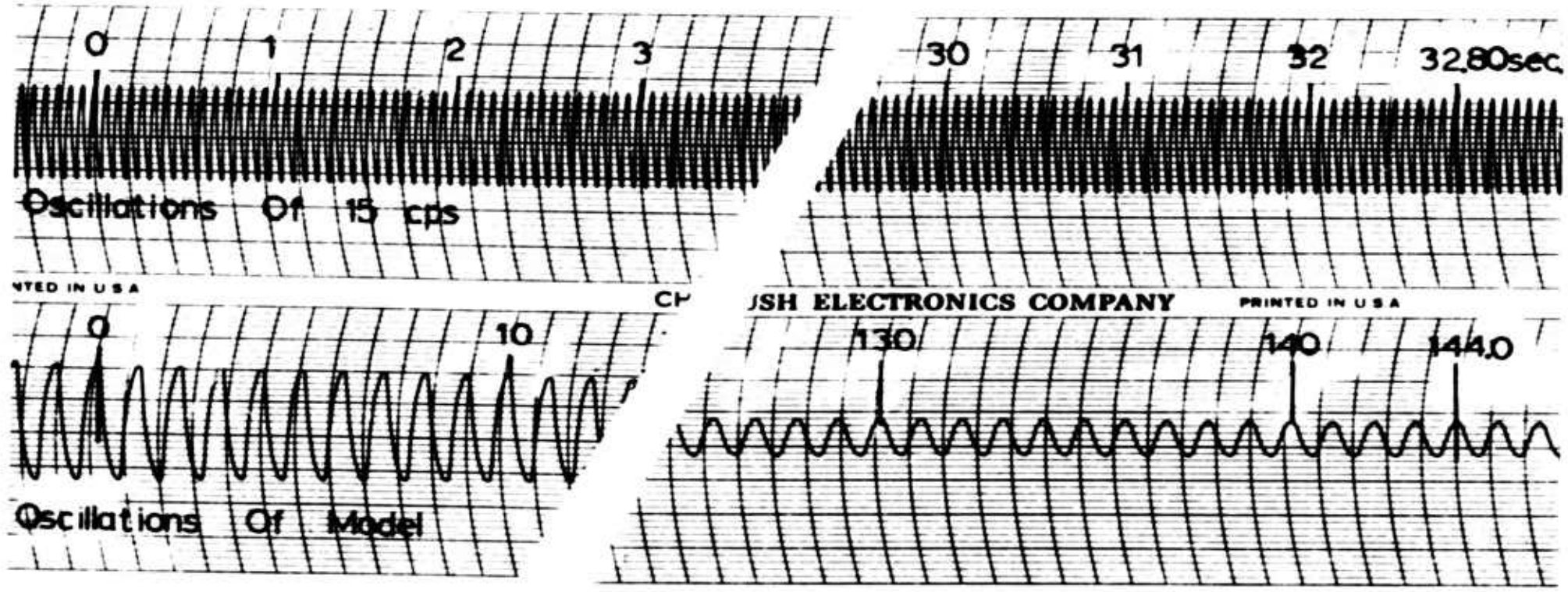

$T = 32.8 \div 144.0 = .2278$ seconds

FIG 4-3. SAMPLE OF DATA ON RECORDING PAPER SHOWING CALCULATION OF PERIOD T OF 1.50 INCH DIAMETER SPHERE

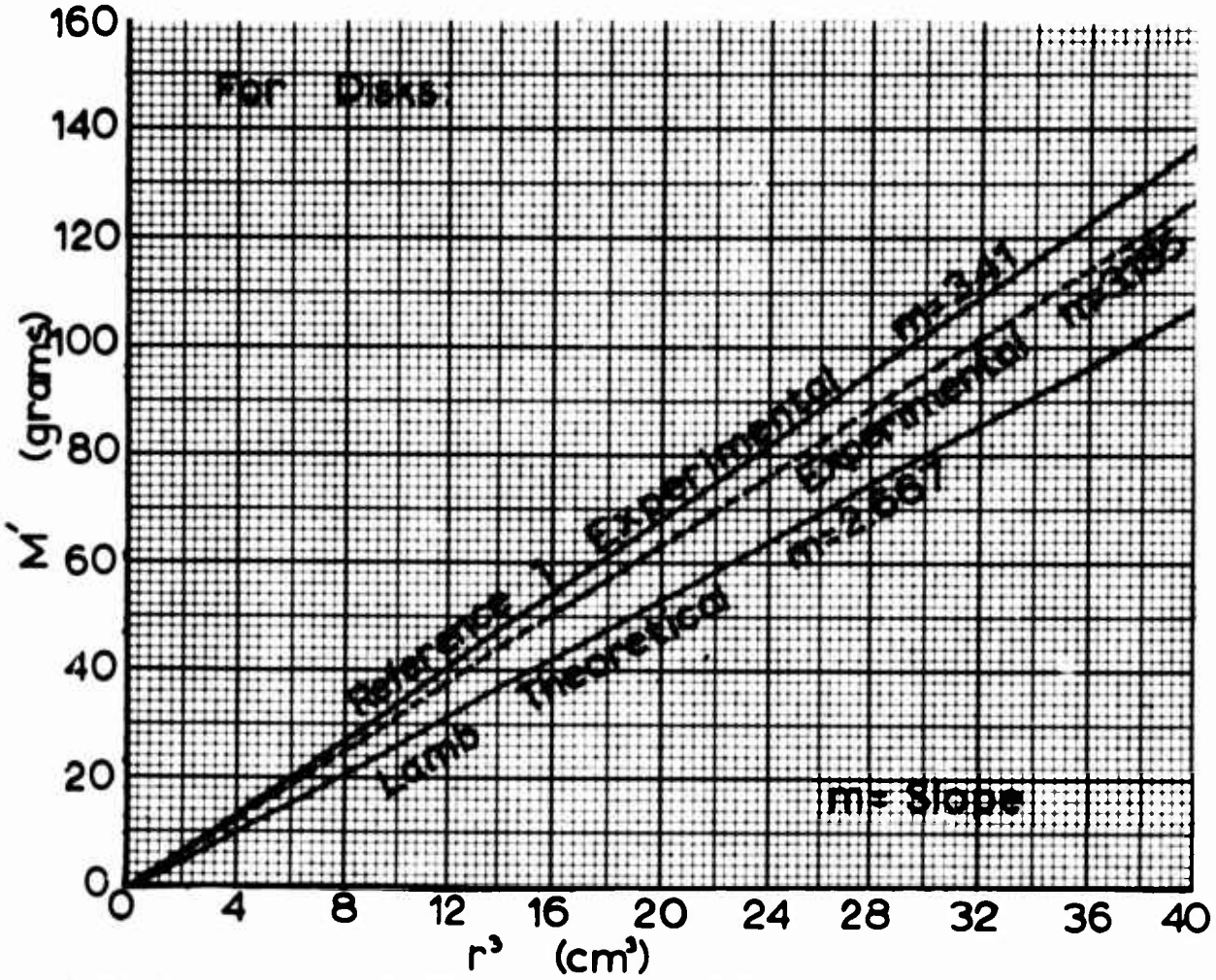

FIG 4-4. ADDED MASS VERSUS RADIUS CUBED

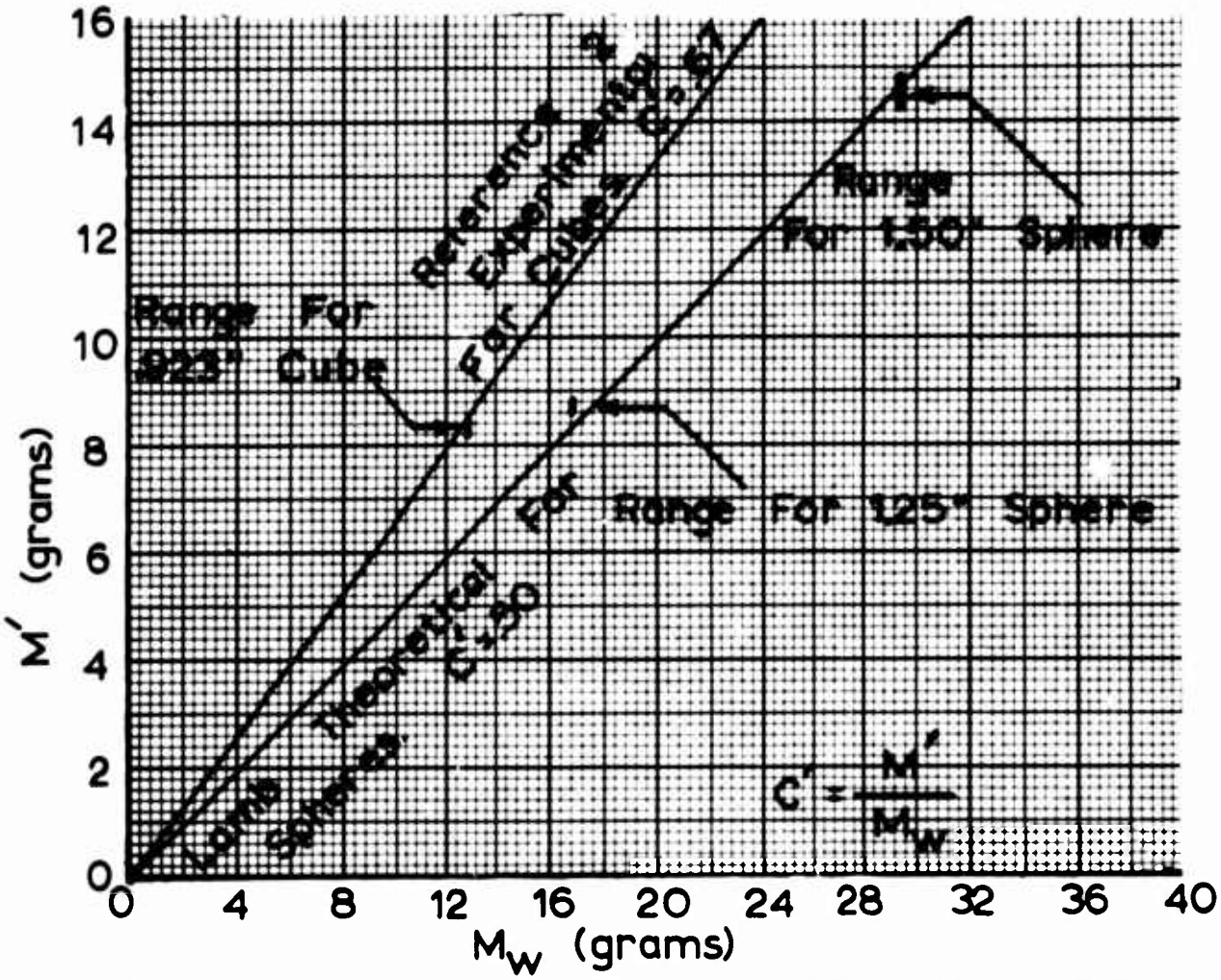

FIG 4-5. ADDED MASS VERSUS DISPLACED MASS

Project No 7

4.0 Theoretical Study of Supersonic Parachute Phenomena

4.1 Introduction

This study has analyzed the behavior of conventional parachutes in supersonic flow in the wind tunnel and by means of the water analogy. Based on this analysis, a supersonic decelerator was conceived which utilizes a pressure reducing "spike" in connection with a solid cloth canopy.

As originally noted in Progress Report No 20, the investigation of the spike concept in combination with a ribbon parachute canopy will be presented under this study. It was previously presented as Project No 10 of Progress Reports Nos 18 and 19.

The work done during this reporting period will be reported in the following phases:

a) Supersonic wind tunnel studies of flexible spiked parachutes
b) Pressure distribution studies on spiked parachutes in supersonic flow
c) Supersonic wind tunnel studies of spiked ribbon parachutes.

4.2 Supersonic Wind Tunnel Studies of Flexible Spiked Parachutes

4.2.1 Past Work

Rigid models of the spiked solid canopy parachute, both with and without suspension lines, have been found stable in wind tunnel tests at Mach numbers of 1.14, 2.0, and

3.0. Test results for configurations with textile canopies were presented in Progress Reports Nos 17, 18, 19, and 20.

Mechanical damage to the model and to the wind tunnel suspension system occurring in the early tests of flexible canopy models prompted the improvement of the suspension line connection, design of a new deployment device, and minor improvements in the parachute model. The new deployment device appeared in Fig 7-2 of Progress Report No 20. Damage to the model was reduced through the use of heavier MIL-C-8021A, Type II nylon cloth (300 lb/in), and by elimination of the wire ring used in the canopy edges. In addition, cones are now molded of low density "Arothane," a product of the Archer-Daniels-Midland Company of Minneapolis, Minnesota. These lighter weight cones have reduced the number of suspension line failures while at the same time improving the dynamic balance of the system as reported in Progress Report No 20.

4.2.2 Continuation

Tests have been continued during the present reporting period on flexible models of the spiked solid canopy parachute. The aim of these tests is to further improve structural reliability and strength, and to establish an optimum geometry for the configuration. Improvements made in the suspension lines, models, and deployment device continue to serve very satisfactorily. Figure 7-1 shows a detailed canopy edge view of how suspension lines are fastened to the canopy fabric.

Continued good test results indicate that the present spiked solid cloth canopy parachute model is very near to an optimum geometric form. During the present reporting period 85% of the wind tunnel tests conducted were completely successful. These results and the valuable information gained from

the limited success of the remaining 15% of the tests firmly indicate the good repeatability of the parachute's performance. A Schlieren photograph of the flexible model during a wind tunnel test is shown in Fig 7-2.

Test measurements to determine the drag of the flexible parachute models were obtained during this reporting period. The drag coefficient, based on total cloth area, was $C_D = 0.335$. While the results from such a very limited investigation are far from conclusive, the drag coefficient obtained is in the general range of the values characteristic of supersonic deceleration devices. These tests incorporated the drag balance arrangement shown in Fig 7-3.

In the latter part of this reporting period, two wind tunnel tests were conducted on a flexible parachute model in combination with an ogive forebody. The ogive has a calibre of 2.5, a fineness ratio of 2.5, and a base diameter D_1 of 1.83 inches. Size and distance relationships between the forebody and the parachute model are $D_1/D_2 = 0.458$ and $L/D_1 = 9.75$, where D_2 is the maximum diameter of the canopy, D_1 the diameter of the forebody, and L is the distance between the leading edge of the canopy and the base of the forebody. The test arrangement used in these wind tunnel tests is shown in Fig 7-4. Further testing will be necessary before any definite results concerning the forebody experiments can be presented.

4.2.3 Proposed Work

Supersonic wind tunnel tests will be continued on the spiked solid cloth canopy models to insure an optimum model geometry. Drag measurements in free stream will be continued in order to obtain more conclusive results. In addition, testing will be conducted to determine the effect of the forebody on the drag of the flexible spiked parachute.

4.3 Pressure Distribution Studies on Spiked Parachutes in Supersonic Flow

Progress Report No 20 presented tabulated results from the pressure distribution studies of rigid models of the spiked solid canopy parachute. Table 7-1 and Fig 7-4 of that report presented the data from Mach 3 tests in terms of pressure coefficients as it is defined in Sec 4.3.3 of Progress Report No 19. No further work in this direction has been undertaken during the present reporting period.

It is proposed that during the next reporting period pressure distribution studies on rigid models of the spiked solid cloth canopy parachute in the wake of a forebody be conducted. This testing, in conjunction with the forebody studies on flexible models of the spiked parachute as noted previously, will make it possible to obtain a parachute design that performs satisfactorily in the wake of a forebody.

In conjunction with the previously described test program, a series of tests are also being conducted at the Naval Ordnance Laboratory at Silver Springs, Maryland. This particular segment of the test program is under the direction of Mr. George Sloan. In these tests, a two inch diameter steel model of the spiked solid canopy parachute is towed behind a heavy forebody which is fired from a cold gas gun. A description of the test facilities in Aerodynamics Range No 1 used for these tests can be found in the Naval Ordnance Laboratory publication, AEROBALLISTIC RESEARCH FACILITIES, NOLR 1233. At the end of this reporting period only preliminary tests had been conducted. Figure 7-5 shows a typical model and forebody with connecting cable.

4.4 Supersonic Wind Tunnel Studies of Spiked Ribbon Parachutes

4.4.1 Introduction

The "spike" concept used successfully in the previously mentioned parachute has been used in conjunction with ribbon parachute canopies. The water analogy tests conducted on this type of configuration, as presented in Progress Report No 18, Project 10, lead to the construction of rigid models of the parachute. Results from tests on rigid models with geometric porosities of 20, 25, and 30 per cent distributed evenly over the canopy were originally presented in Table 7-2 of Progress Report No 20. During this reporting period, tests have been conducted on a rigid model with 40% geometric porosity distributed evenly over the canopy (Fig 7-6).

4.4.2 Tests

The rigid models are tested in a supersonic wind tunnel at Mach 3.0. Figure 7-7 of Progress Report No 20 shows the test arrangement used. During the test runs, visual observation and high speed Schlieren movies are used to determine the stability of the model as the cone and canopy are moved to varying H/D_1 positions, as defined in Fig 7-5 of Progress Report No 20.

The effect of cone size is investigated by using two different cone sizes for each test position. Each cone has a half angle Θ of 34°. For the "small" cone the base diameter d is 37% of the canopy inlet diameter D_1 and the "large" cone has a base diameter that is 47% of the inlet diameter.

4.4.3 Results

The criteria for the degree of stability in the rigid model tests is a combination of model vibration and the shock pattern stability as determined from analysis of the Schlieren

movies. The results of this analysis are presented in Table 7-1. As different model configurations were tested under this project, the following trends, first noted in Progress Report No 20, held true:

a) The overall stability of the flow patterns increased with increasing geometric porosity of the models.
b) As the distance from the cone to the canopy was increased, stability of the flow pattern decreased.

For a third trend that was observed for models of lower geometric porosity, the 40% model displayed a contrary effect. In this case, the model was more stable with a large cone than with a small cone. It was also noted that the "buzzing" effect representative of lower porosity models was absent in tests on the 40% model, indicating that mass was not being spilled over the front of the canopy as it was in the models with lower geometric porosity.

4.4.4 Proposed Work

In view of the above experiments, it is proposed that rigid pressure distribution models of the 40% geometric porosity configuration be constructed. These models will then be tested at the H/D_1 positions that have shown the best results to date. Experiments will also be conducted to investigate the characteristics of higher geometric porosity rigid models.

TEST RUNS FOR MACH NO.= 3.00			
POROSITY %	$\frac{H}{D_1}$	CONE SIZE	STABILITY CHARACTERISTICS
20	0.507*	Large	
	0.615		Violently Unstable
	0.728		" "
	0.838		" "
25	0.507	Small	Unstable
	0.615		"
	0.728		"
	0.507	Large	"
	0.615		"
	0.728		"
	0.838		"
30	0	No Cone	
	0.507	Small	Moderately Stable
	0.615*		
	0.728		Violently Unstable
	0.507	Large	Unstable
	0.615		Violently Unstable
	0.728		Moderately Unstable
	0.838		Unstable
40	0.615	Small	Unstable
	0.728		Moderately Unstable
	0.615	Large	Moderately Stable
	0.728		Stable
	0.838		Moderately Unstable
	0.987		Unstable
DATA NOT USED IS STARRED			

TABLE 7-1. RIGID SPIKED RIBBON PARACHUTE CONFIGURATIONS TESTED

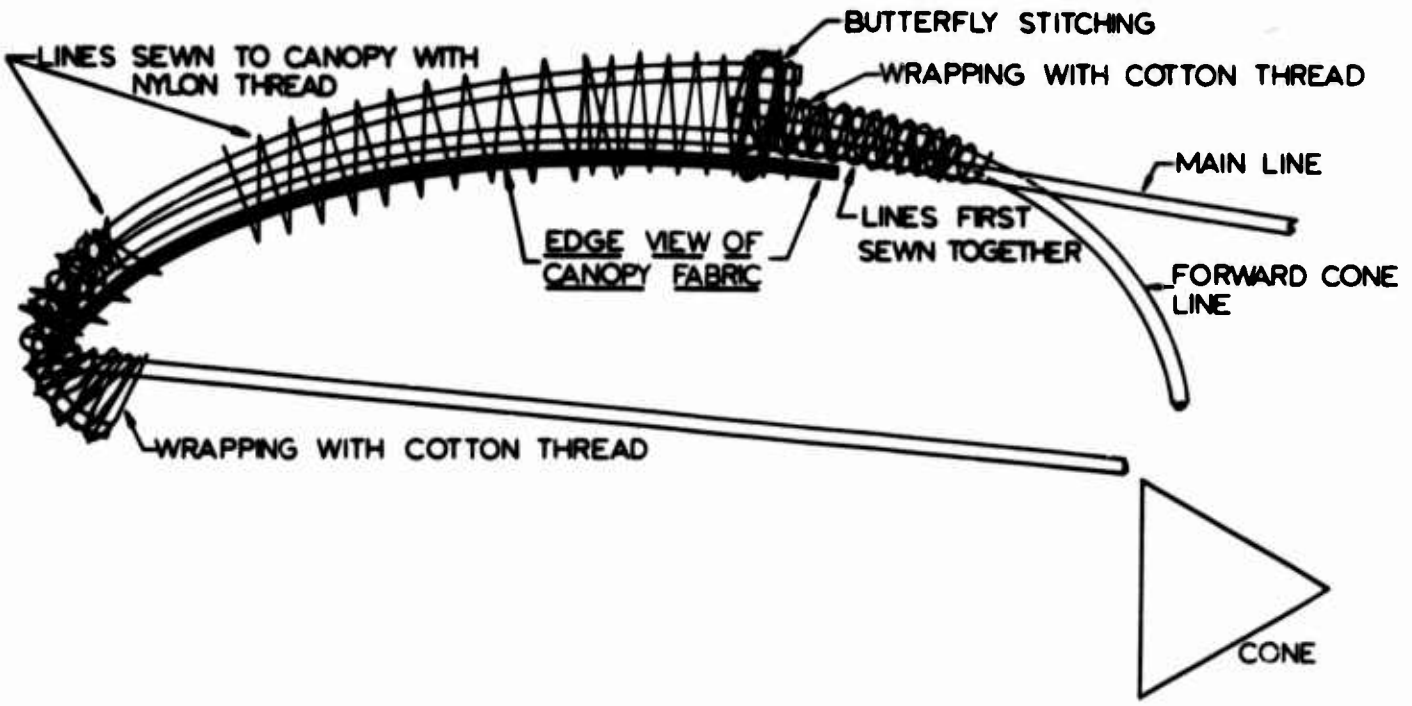

FIG 7-1. DETAIL VIEW OF ATTACHMENT OF SUSPENSION LINES TO CANOPY OF SPIKED PARACHUTE

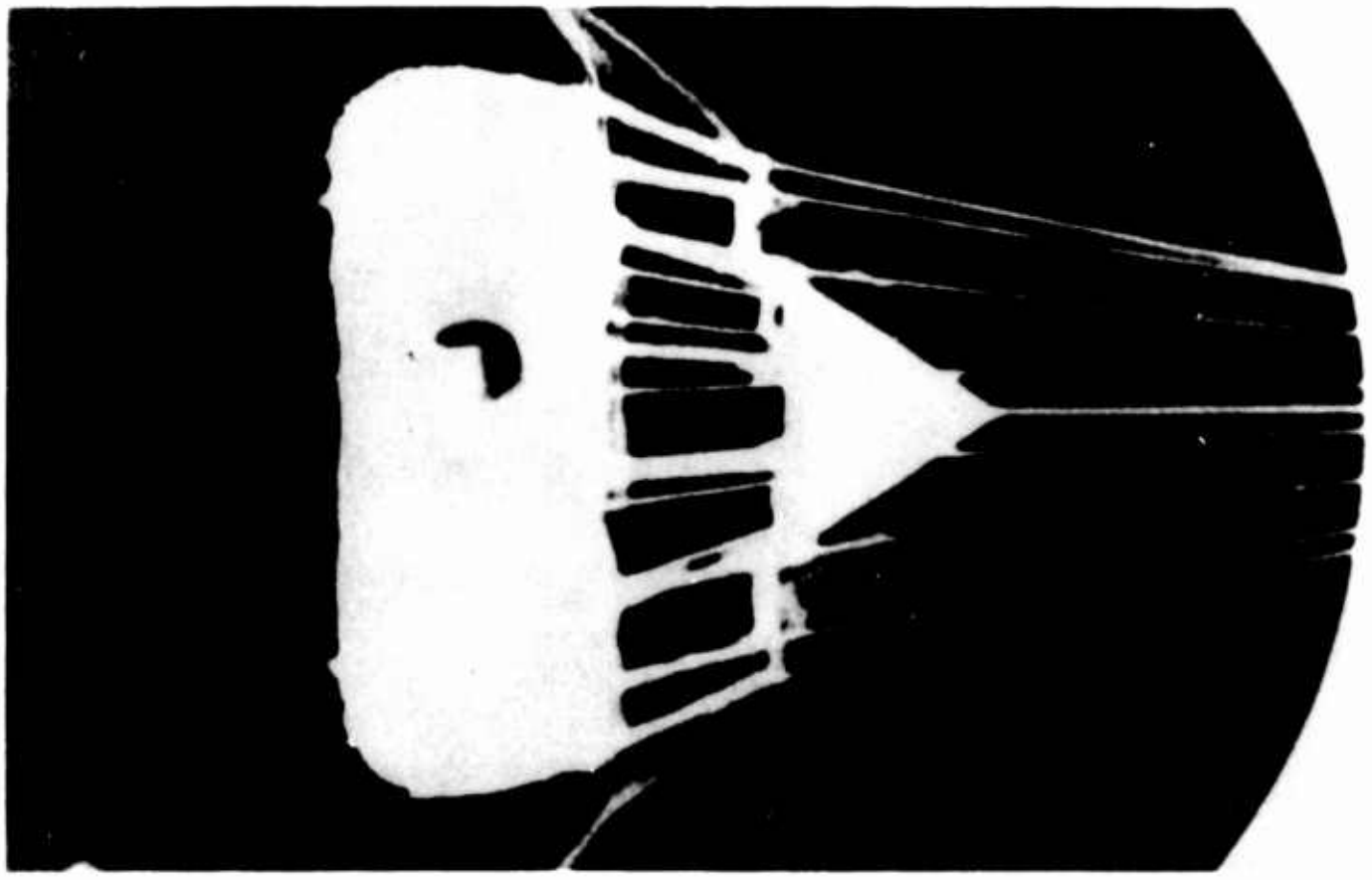

FIG 7-2. FLEXIBLE SPIKED SOLID CLOTH CANOPY PARACHUTE AT MACH 3.0.
($H/D_1 = 0.62$, $D_o/D_1 = 0.90$, $1/D_1 = 0.35$)

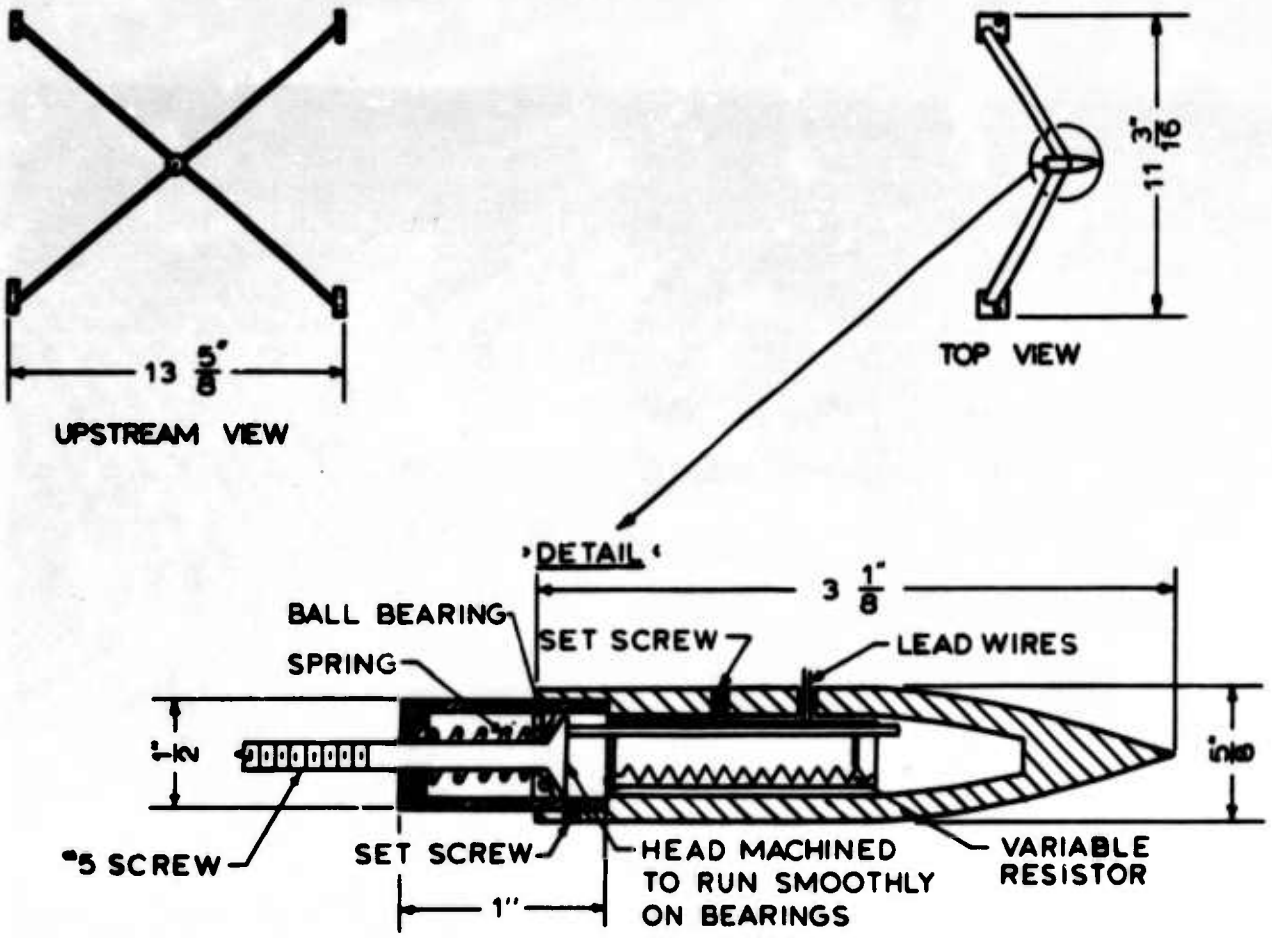

FIG 7-3. WIND TUNNEL SUSPENSION ARRANGEMENT FOR FLEXIBLE SUPERSONIC PARACHUTE MODEL DRAG BALANCE

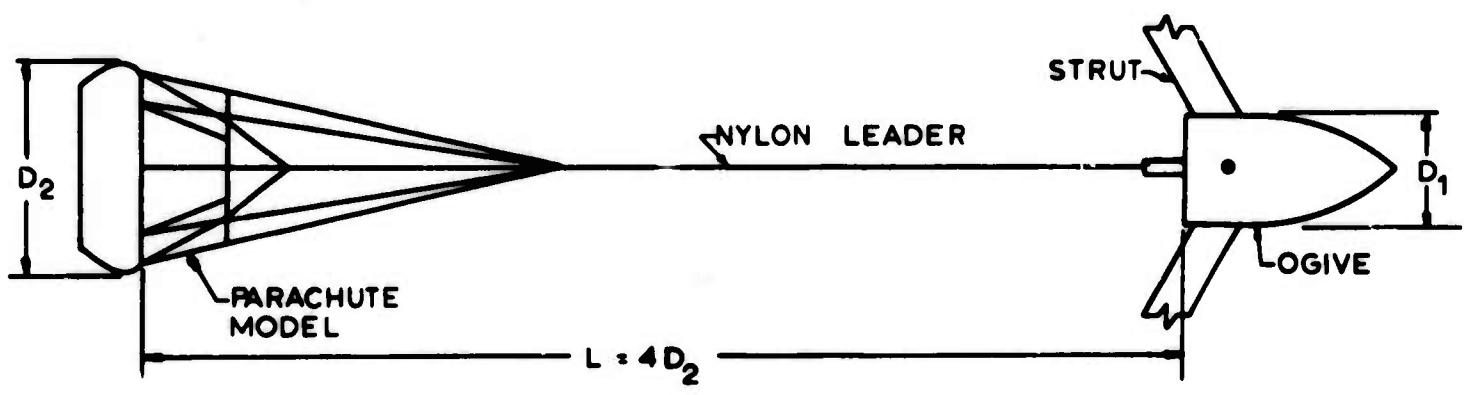

DETAIL OF OGIVE

CALIBER = 2.5
FINENESS RATIO = 2.5

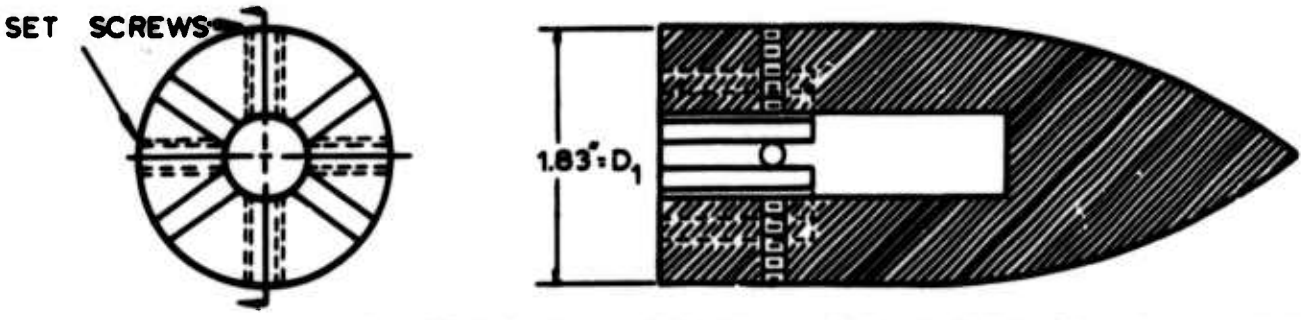

FIG 7-4. WIND TUNNEL TEST ARRANGEMENT FOR FLEXIBLE SUPERSONIC PARACHUTE MODEL WITH FOREBODY

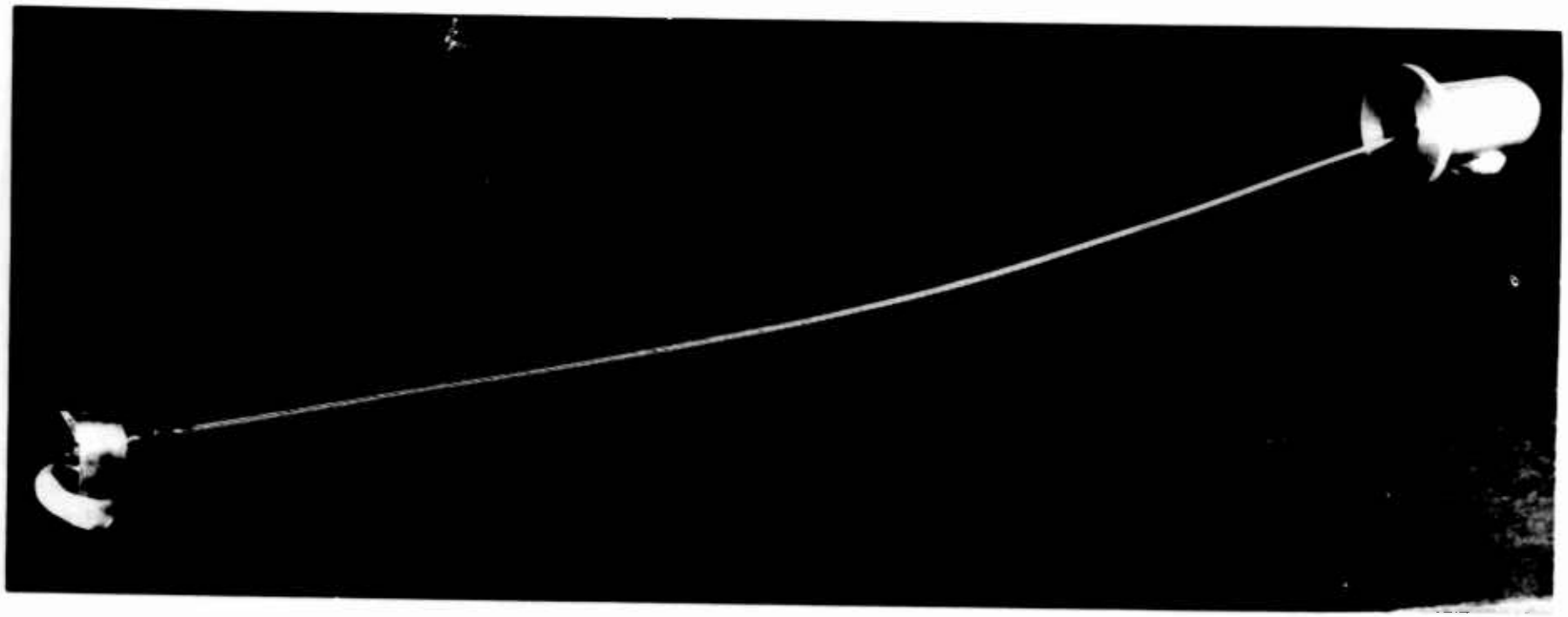

FIG 7-5. BALLISTICS RANGE TEST DEVICE FOR RIGID MODEL OF SPIKED SOLID CANOPY PARACHUTE

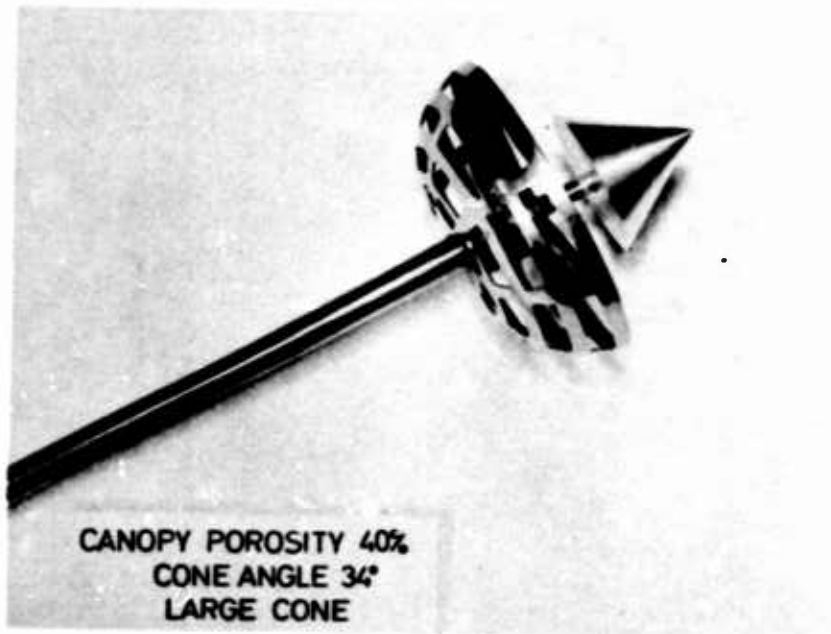

FIG 7-6. RIGID MODEL OF SPIKED RIBBON PARACHUTE

5.0 Theoretical Analysis of the Dynamics of the Opening Parachute

No work concerning this project will be reported during the present reporting period.

Project No 9

6.0 Statistical Analysis of Extraction Time, Deployment Time, Opening Time, and Drag Coefficient for Aerial Delivery Parachutes and Systems

A draft of the technical report entitled, "Analysis of Parachute Deployment of Heavy Cargo" by Helmut G. Heinrich, Ivan R. Russell, and Donald J. Eckstrom has been submitted to the Procuring Agency for review.

7.0 Gliding Aerodynamic Decelerator

7.1 Introduction

The objective of this study is to develop a self-inflating aerodynamic decelerator with a lift to drag ratio of two. With such a lift to drag ratio, a parachute would glide at an angle of 26.5° with the horizon and would have an angle of attack α of 63.5°. Figure 12-1 shows the forces and coordinates for a gliding parachute. Progress Report No 20 presented an account of experimental investigation of gliding characteristics of present aerodynamically unstable parachutes and conventional steerable parachutes. None of the parachutes tested met the necessary glide angle specifications.

Experimental balsa wood and clay models of new configurations constructed during previous reporting periods achieved a glide angle close to that desired. These models as noted in Progress Reports Nos 18 and 19, were improved upon and during the last reporting period a specific configuration was described. Drawings of the solid test models are shown in Figs 12-8 and 12-9 of Progress Report No 20.

7.2 Continuation

A wood and metal form based on a modified 37.5 inch nominal diameter, 10% extended skirt parachute canopy was constructed and is shown in Fig 12-2. With this model it was possible to obtain gore and rib patterns of the proposed gliding parachute.

During the present reporting period the gore and rib patterns were made and a cloth parachute was constructed from

1.1 oz nylon cloth with a nominal porosity of 120 $ft^3/(ft^2\text{-min})$. The design is based on a 10% extended skirt canopy modified with a gliding surface as shown in Figs 12-3 and 12-4. The inflated parachute in the wind tunnel is shown in Fig 12-5.

7.3 Tests

Tests of the cloth gliding parachute were conducted in the open section of the subsonic wind tunnel (Fig 12-6). The model was tested at a flow velocity of approximately 25 ft/sec. A special suspension system was developed which allows for the systematic inflight adjustment of individual suspension line length.

The wind tunnel tests showed the design of the original configuration to be basically sound. By adjustment of the suspension line lengths a stable angle of attack α of 25° ± 3° was achieved, corresponding to a glide angle with the horizon of 65° ± 3° and a lift to drag ratio of 0.47. To achieve test results closer to the desired glide characteristics, this original test model was modified.

A three inch wide strip of cloth was removed from the base of eight of the gores contained in the 10% extended skirt portion of the canopy. Slots were cut from four of the guide surface panels along the line of intersection of the roof and guide surface panels. The modifications allow for greater inlet area at the base of the extended skirt canopy and provide an exhaust jet area at the rear of the glide surface.

The same suspension line system and test arrangement were used in wind tunnel tests of the modified parachute model. Fig 12-7 shows the modified model in the wind tunnel. The maximum stable angle of attack was generally greater than that of the original model. By shortening the forward suspension lines by 0.18 L_o, where L_o is the original line length, a

maximum angle of attack of 35° ± 3° was obtained giving a glide angle with the horizon of 55° ± 3°. In this attitude the parachute was moderately stable. At angles of attack greater than 35° the front portion of the canopy tended to deform and at an angle of attack greater than 45° the canopy collapsed.

Further tests were conducted on the modified model to determine what effect the porosity of the canopy had on test results. In order that the same modified model could be used in these tests, the nominal porosity was reduced by starching the canopy. As is customary, the low porosity model displayed less stability than did the more porous model. In tests, the less porous starched model had a glide angle with the horizon of 50° ± 3°.

7.4 Proposed Work

Further modification and tests will be made on the nylon cloth parachute during the next reporting period. In addition, an investigation will be conducted to determine the relevant characteristics of the A/P 28 S-3 (Air Force Systems Command publication AFFTC-TR-61-37, August, 1961) "HALO" parachute which incorporates a modified MC-1 canopy with a single orifice. Also, other existing parachutes will be studied when models and other pertinent information become available.

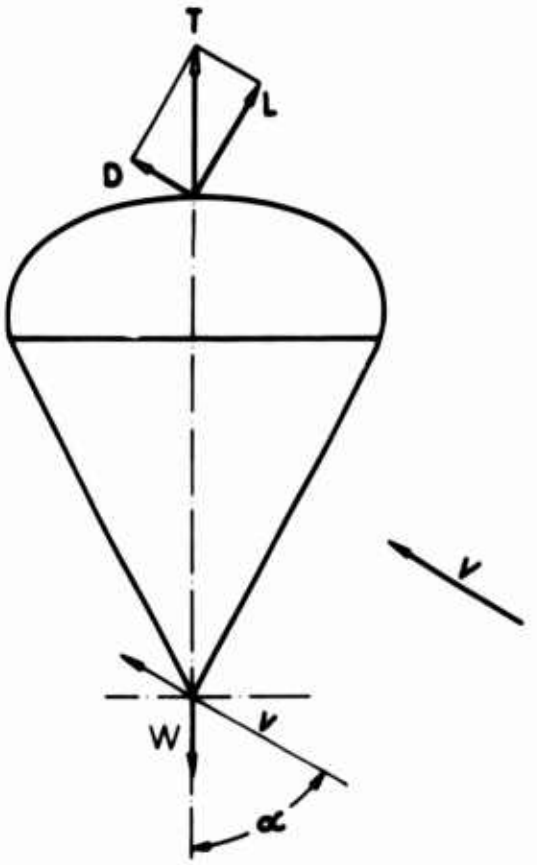

FIG 12-1 FORCES AND COORDINATES FOR A GLIDING PARACHUTE

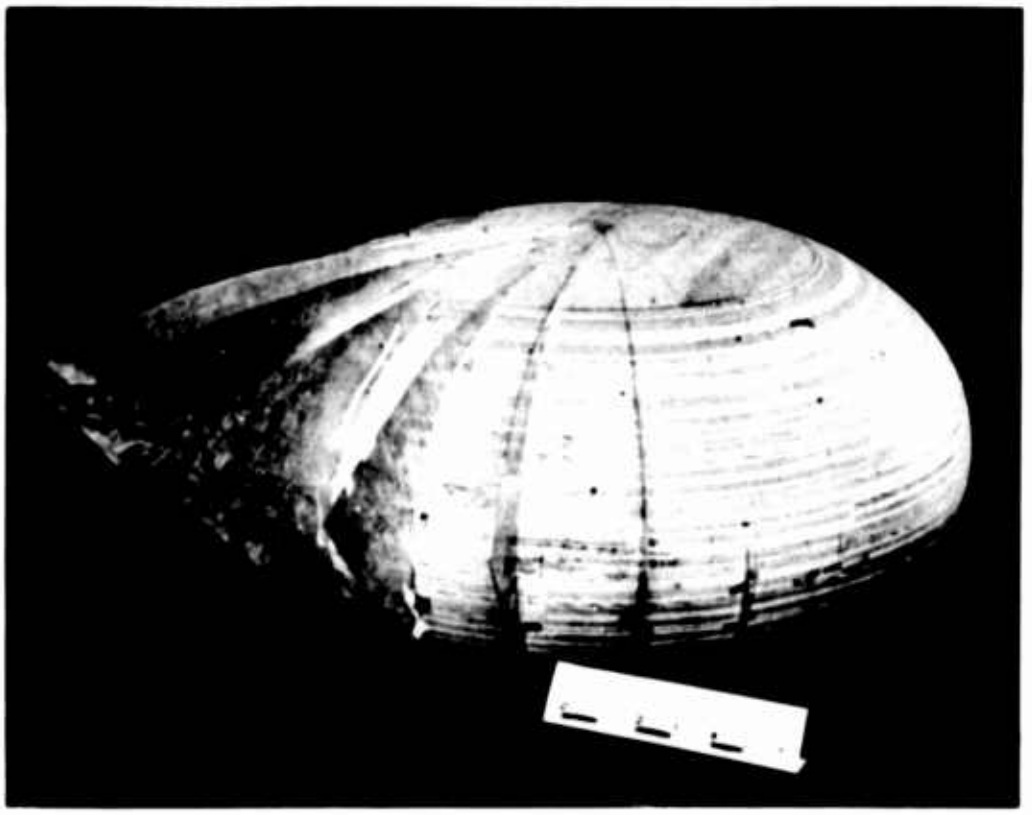

FIG 12-2. MODIFIED 37.5 INCH NOMINAL DIAMETER 10% EXTENDED SKIRT CANOPY FOR OBTAINING GORE AND RIB PATTERN OF GLIDING PARACHUTE

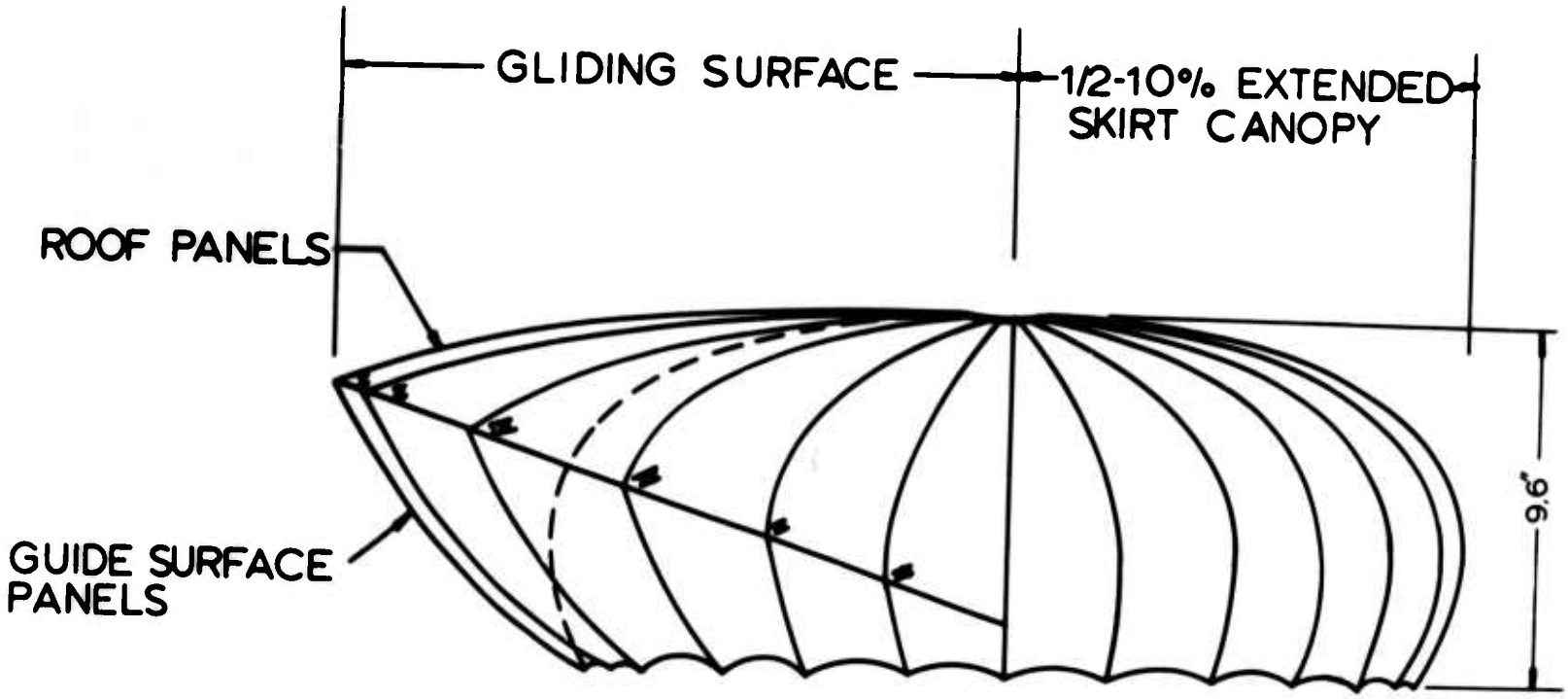

FIG 12-3. GLIDING PARACHUTE (SIDE VIEW)

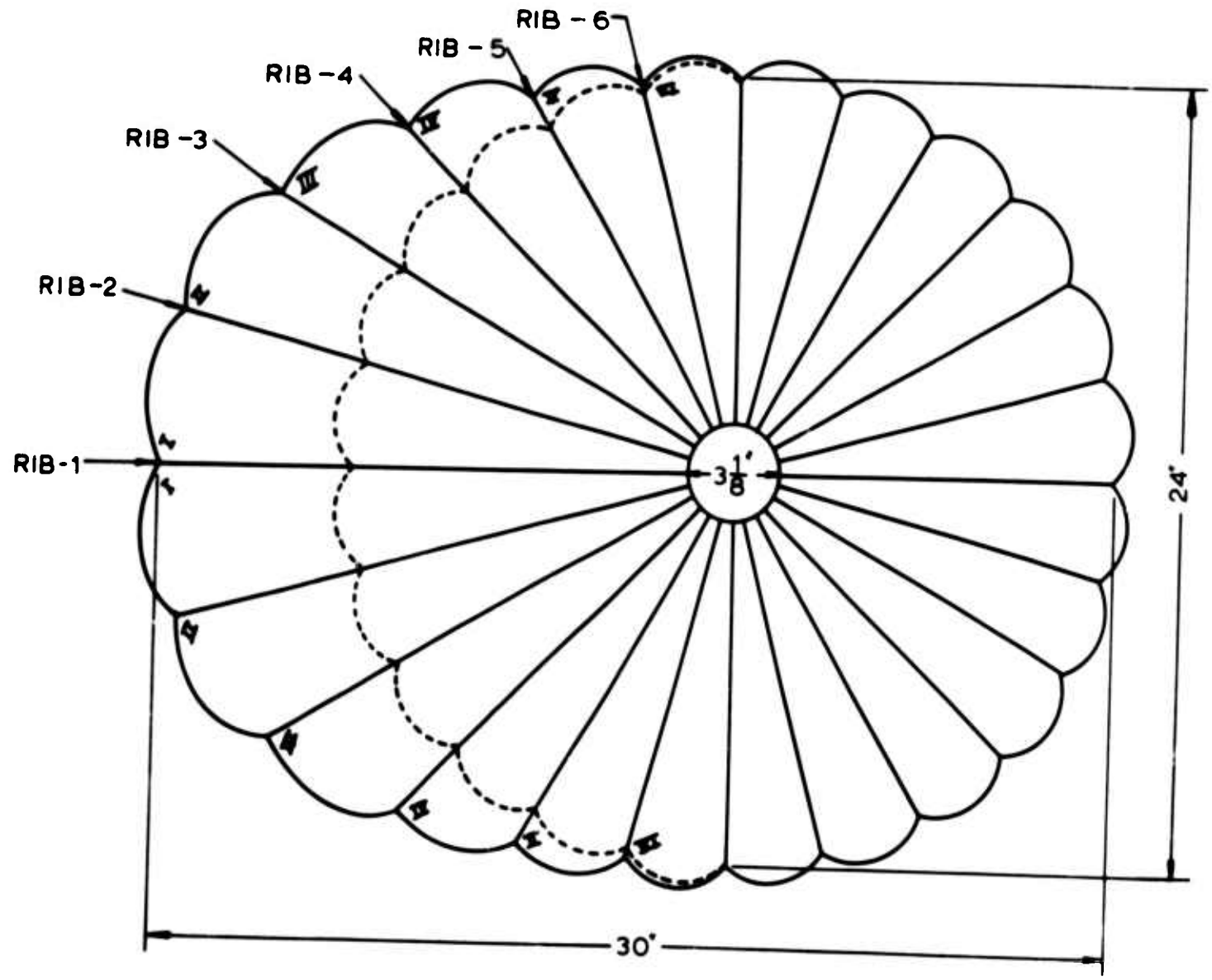

FIG 12-4. GLIDING PARACHUTE (TOP VIEW)

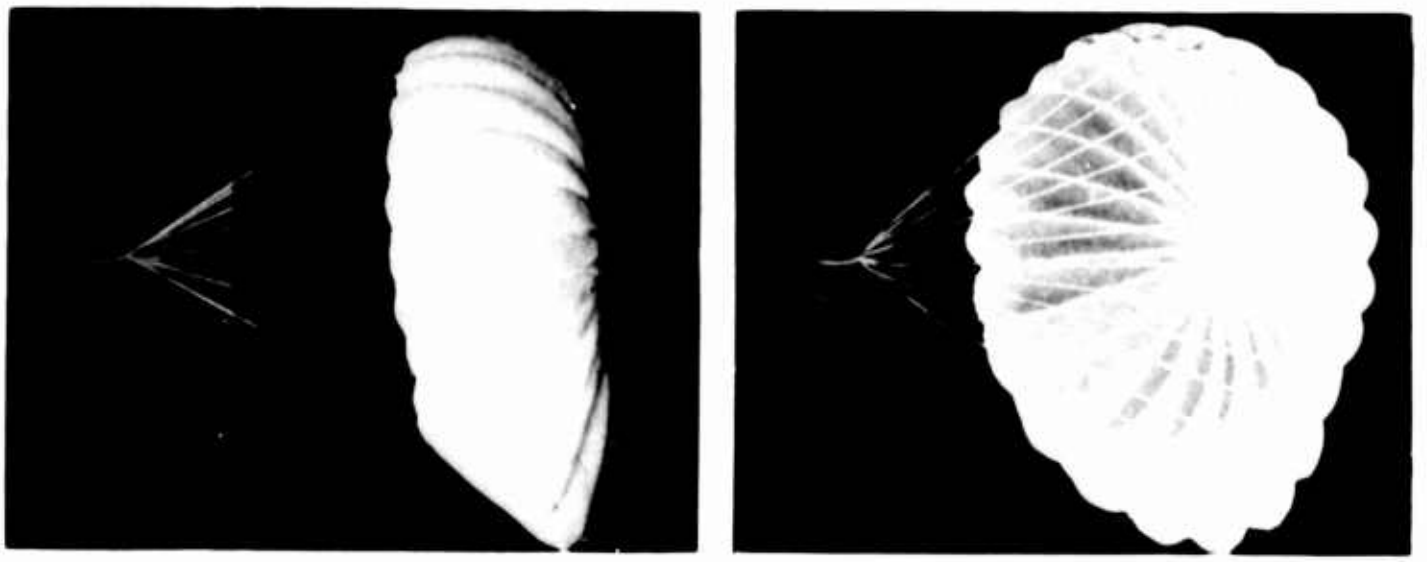

FIG 12-5. GLIDING AERODYNAMIC DECELERATOR IN WIND TUNNEL

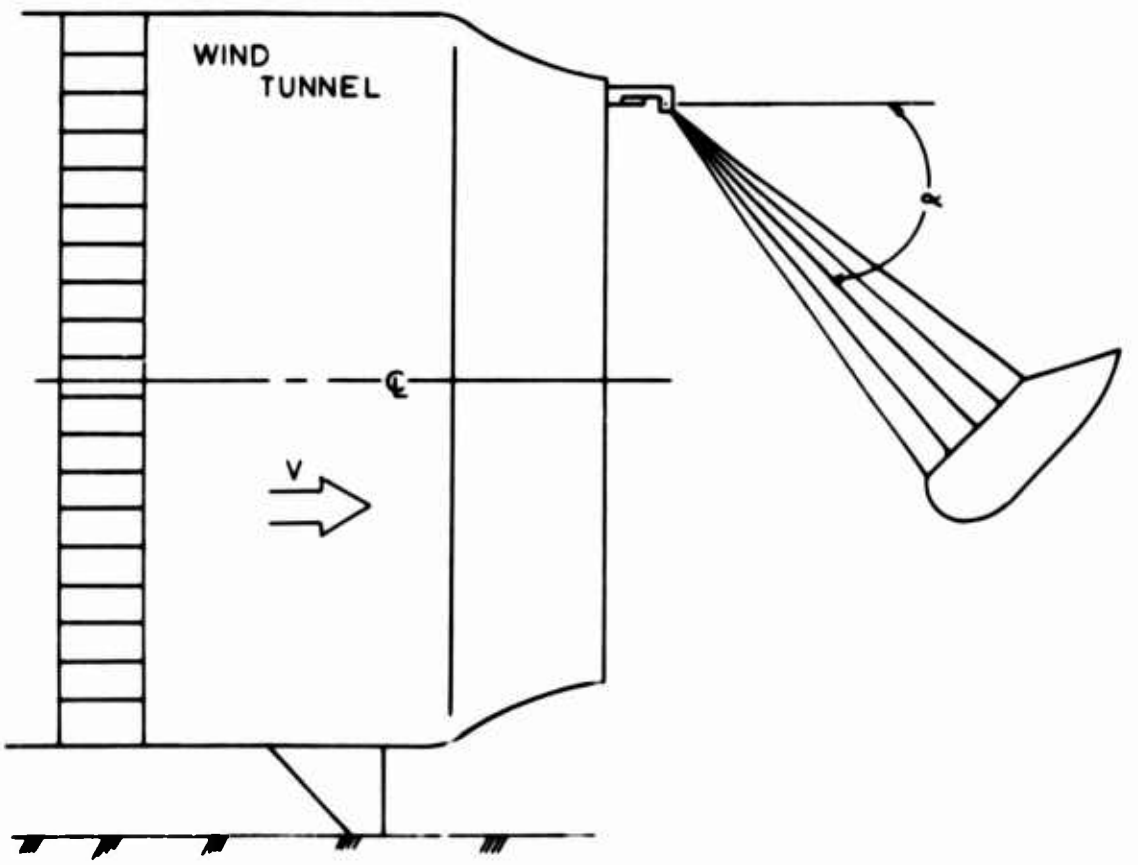

FIG 12-6. SUBSONIC WIND TUNNEL TEST ARRANGEMENT

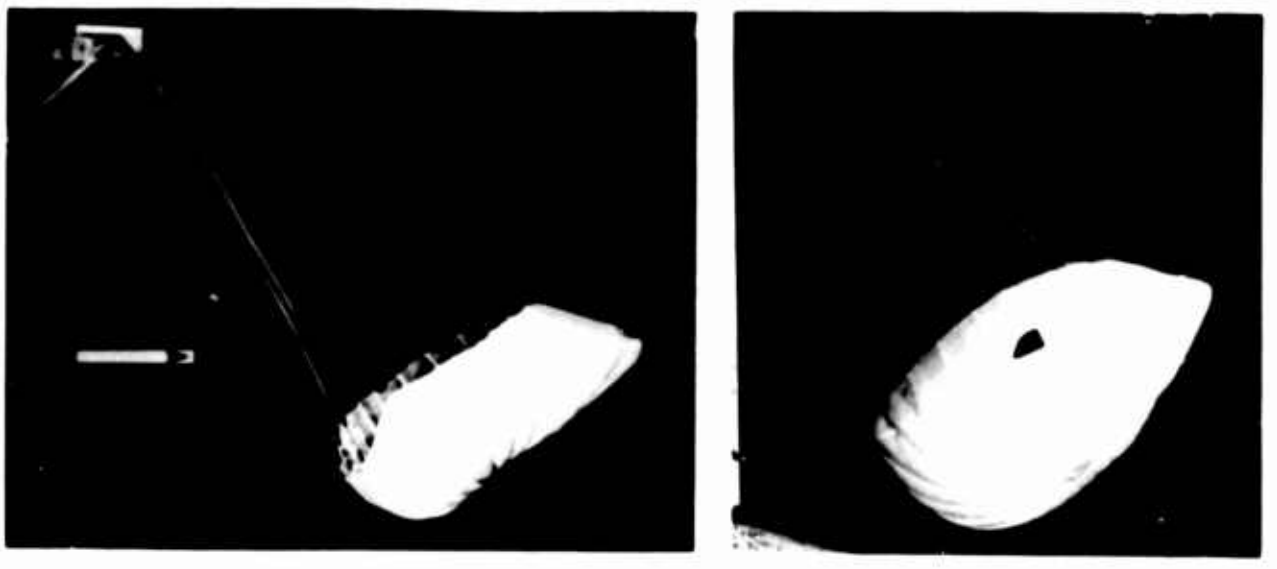

FIG 12-7. MODIFIED GLIDING AERODYNAMIC DECELERATOR IN WIND TUNNEL

8.0 Effective Porosity Studies

8.1 Parachute Cloths

Progress Report No 20, Section 9.1, presented results obtained from tests conducted on specially mounted samples of four different parachute cloths, relating effective porosity, C, to the pressure ratio, $\Delta p/\Delta p_{cr}$, with density ratio, σ, as a parameter. The special mounting was used to eliminate stretching and slipping of the cloth sample in its test frame. Despite the special mountings, previously established trends were followed and these tests served merely as a validation of earlier experiments.

During this reporting period no new results are presented. Further research will remain on a relatively low priority basis.

8.2 Ribbon Grid Configurations

8.2.1 Introduction

During the last reporting period, tests relating effective porosity to pressure ratio with the grid angle θ as a parameter, were conducted on a series of ribbon grid patterns fabricated from steel shim stock. Through the use of this relatively rigid material, some of the factors associated with cloth deformation were eliminated. The tests were conducted on grids with included grid angles θ of 0°, 15°, 45°, 60°, 75°, and 90°. Aside from angle variation, all models were identical in construction, each having a geometric porosity of 25%. The design of a representative grid pattern

is shown in Progress Report No 20, Fig 13-6.

During the present reporting period the data from previously conducted effective porosity tests of 1/4" MIL-R-5608B, Class B nylon ribbon grids has been reduced. By comparing these nylon ribbon grid results with the results from steel ribbon grid tests, conclusions can be drawn concerning the effect of cloth deformation on effective porosity.

8.2.2 Results

The data from the tests of steel and nylon ribbon grids is presented in Figs 13-1 and 13-2. The effective porosity as a function of the pressure ratio with the grid angle θ as a parameter varies in a similar manner for both the nylon grids (Fig 13-2) and the steel grids (Fig 13-1) for $0.03 \leqslant \Delta p/\Delta p_{cr} \leqslant 2.00$, with the effective porosity being generally greater for the nylon grids.

In Figs 13-3 and 13-4 the same data as in Figs 13-1 and 13-2 is plotted, but with the effective porosity as a function of the grid angle θ, $\Delta p/\Delta p_{cr}$ being the parameter. In these two graphs the behavior of the curves for the nylon and for the steel grids shows a marked difference. In this case, for $0° \leqslant \theta \leqslant 90°$, the effective porosity of the steel ribbon grids increases steadily with increasing angle θ (Fig 13-3). Since all of the grids have a geometric porosity of 25% this variation indicates that the discharge coefficient of the grid openings increases as θ increases. A difference is seen in the behavior of the effective porosity versus grid angle curve for the nylon grids (Fig 13-4). For $45° \leqslant \theta \leqslant 90°$ the effective porosity increases as θ increases, while for $0° \leqslant \theta \leqslant 45°$ the effective porosity is larger for smaller angles.

This latter characteristic is explained by

investigation of the deformation of the nylon grids during testing. Figure 13-5 shows photographically this deformation for 30°, 45°, and 90° angle nylon grids. For nylon ribbon grids with $\theta \leq 30°$ there is a particularly large deformation of the grid. This results in a net increase in geometric porosity, thereby explaining the variation shown in the graphs.

F

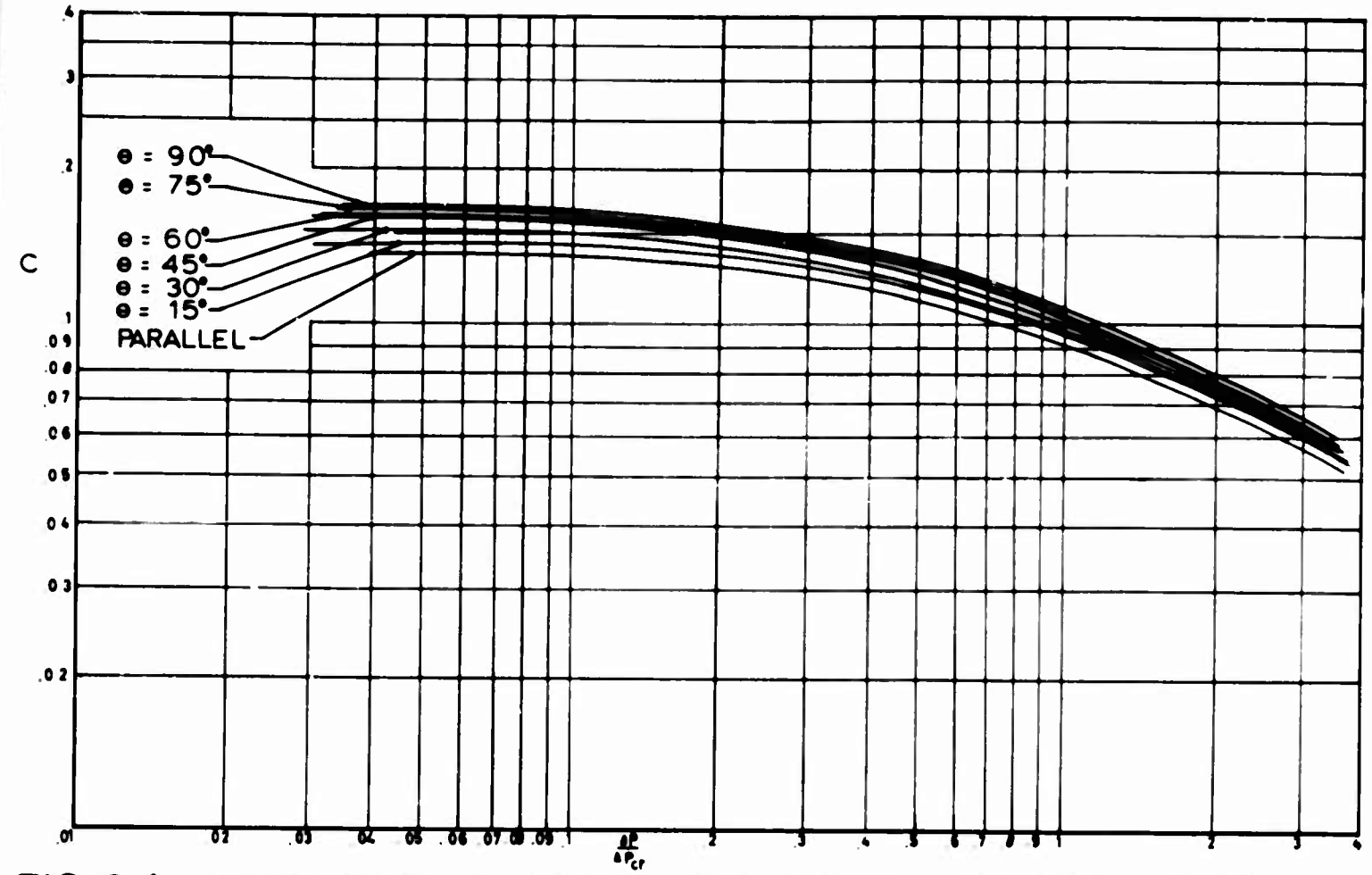

FIG 13-1. EFFECTIVE POROSITY OF STEEL RIBBON GRID CONFIGURATIONS AS A FUNCTION OF DIFFERENTIAL PRESSURE

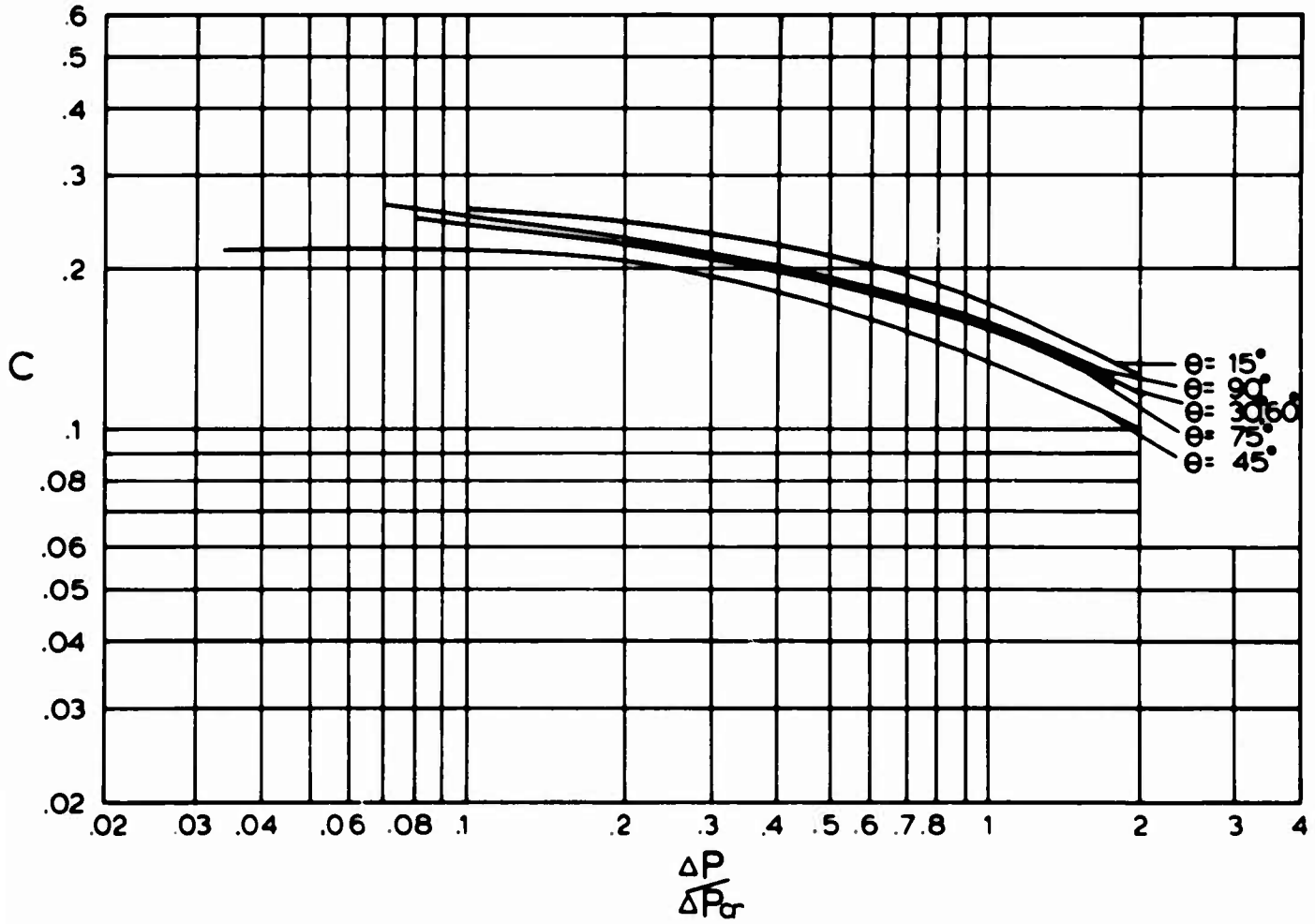

FIG 13-2. EFFECTIVE POROSITY OF NYLON RIBBON GRID CONFIGURATIONS AS A FUNCTION OF DIFFERENTIAL PRESSURE

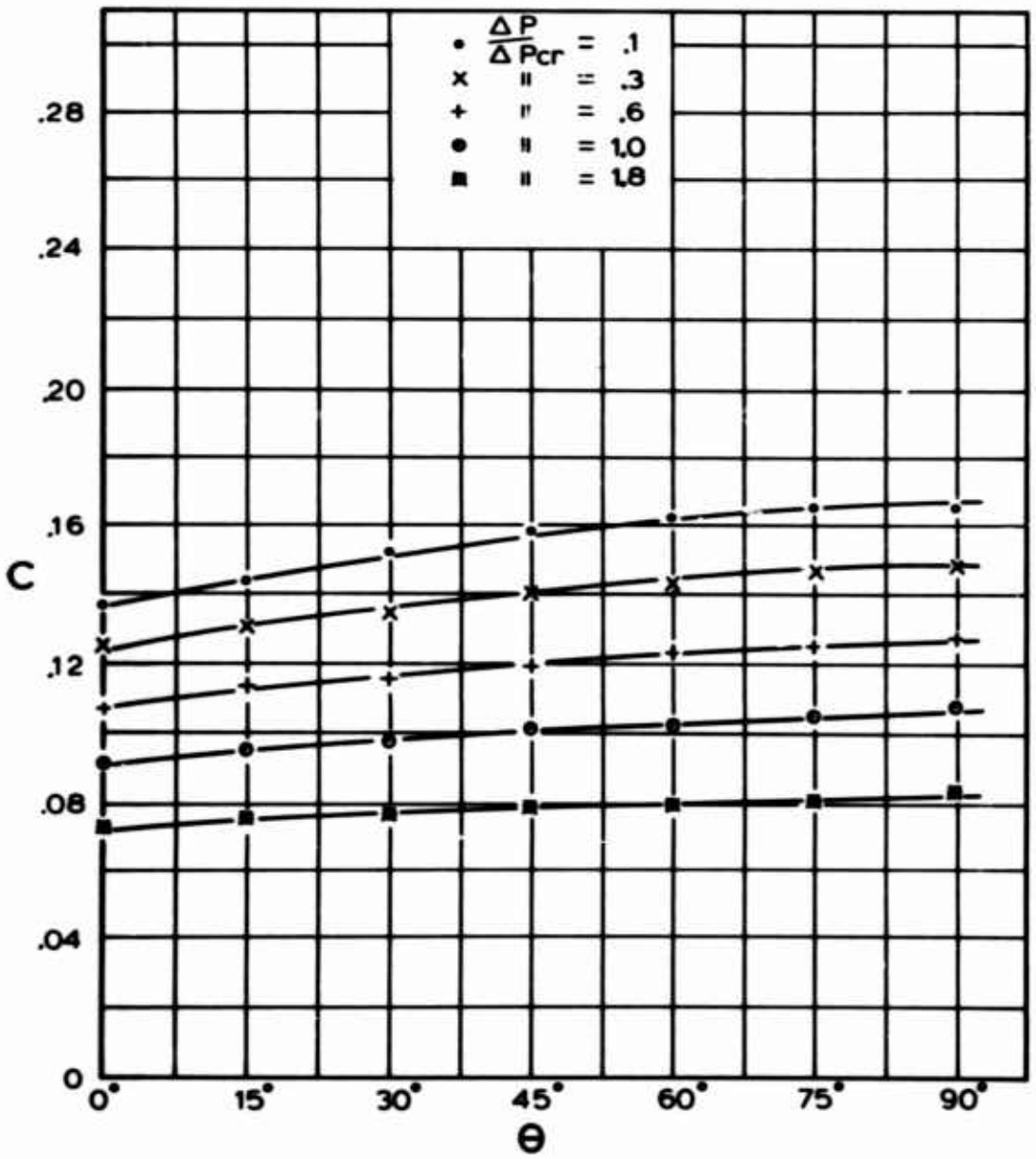

FIG 13-3. EFFECTIVE POROSITY VERSUS GRID ANGLE FOR STEEL RIBBON GRIDS

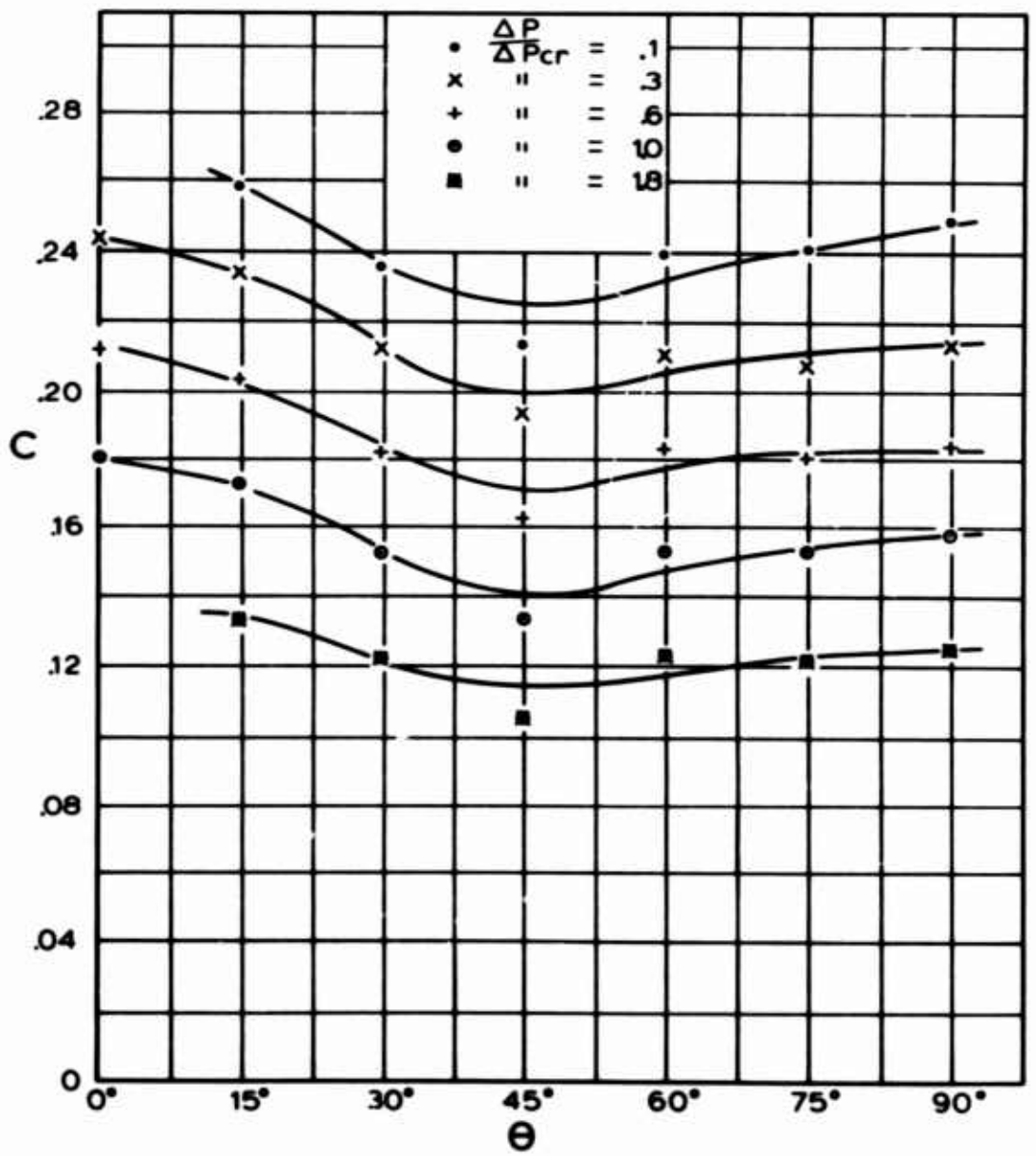

FIG 13-4. EFFECTIVE POROSITY VERSUS GRID ANGLE FOR NYLON RIBBON GRIDS

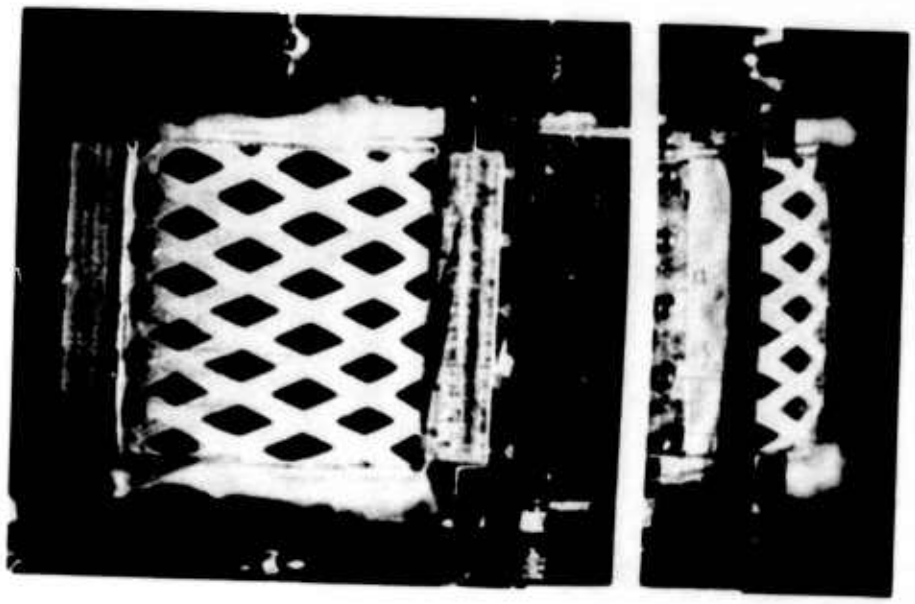

$\Theta = 30°$

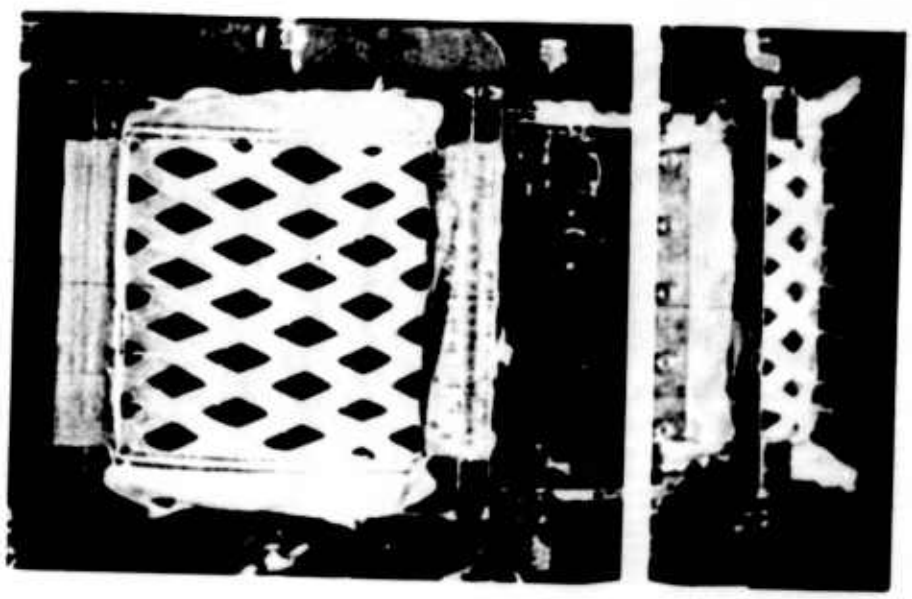

$\Theta = 45°$

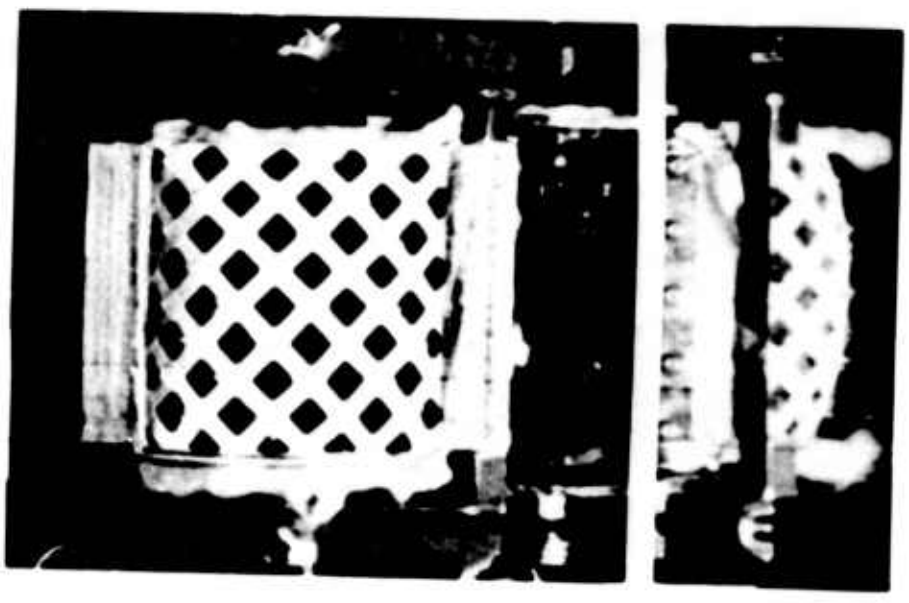

$\Theta = 90°$

FIG 13-5. DEFORMATION OF NYLON RIBBON GRIDS AT $\Delta p/\Delta p_{cr} = 1.0$

9.0 Study of Flow Patterns of Aerodynamic Decelerators by Means of the Surface Wave Analogy

9.1 Introduction

Progress Report No 20 reported the final alignment of the water channel and guide rails, the completion of a shadowgraph and a Schlieren system for detailed flow observation, work concerning the design of special water depth probes, and construction of a model of the supersonic parachute configuration proposed in Project No 7. Also described was a special dye technique for obtaining the water depth profile around a model.

9.2 Present Work

9.2.1 Test Section Depth Survey

Before conducting any quantitative tests, a depth survey of the channel test section area was carried out to determine the tolerance margins of depth measurements. For this purpose the depth probes described in the last progress report were used. With the channel floor set horizontally in both the longitudinal and transverse directions, the water depth in the test section area was found to be within $\pm$ 0.003 inch from the reference value.

9.2.2 Channel Slope

The flow rate in the channel is a function of the water depth and channel slope in the flow direction. The commonly accepted Manning's formula for open channel flow

(Ref 1) was employed to determine the channel slope necessary to produce a given Froude number (Fr). Hence the velocity corresponding to different water depths is determined by,

$$V = \frac{1.49}{n} R_h^{2/3} S^{1/2} \qquad (10.1)$$

where V = water velocity in feet per second
R_h = hydraulic radius in feet; this is the ratio of flow cross-sectional area to the wetted perimeter
S = slope of the channel bed
n = roughness coefficient.

From Ref 2, a value of n = 0.008 was used for the smooth glass.

In the hydraulic flow, the Froude number (Fr) simulates the Mach number (M) of the aerodynamic flow. The quantitative tests reported here were for a Froude number Fr = 2.

9.2.3 Instrumentation

A special nozzle depth gage to enable a quick setting of the opening of the variable nozzle to the desired free stream water depth was constructed. It consists of a plexiglass wedge with a rise of 1 inch over a length of 10 inches and is graduated along the length in 0.1 inch divisions, corresponding to a 0.01 inch rise.

It was observed that the plastic Fresnel lenses of the Shadowgraph and Schlieren systems tended to warp in their original mounting rings resulting in minor distortions and a poor field image. This defect was remedied by remounting each Fresnel lens between two sheets of single weight glass.

A large piece of clear plastic, covering the field of view of the 14 inch diameter lens, was ruled off in 1/2 inch squares and attached to the glass under the test section area, thereby providing a reference grid which aids in the initial

positioning of the model, defines clearly the probe positions in the flow field, and helps interpret the shadowgraph and Schlieren images.

Some preliminary tests conducted during the previous reporting period with a water pressure probe consisting essentially of an impact or pitot tube connected to a micromanometer showed the necessity for minimizing the size of the probe and a careful choice of its dimensions. A recently developed pressure sensitive paint (Celab Pressure Sensitive Paint # 9-A) appeared to hold great promise for use as a simple transducing element for hydrostatic and total pressure probes. Preliminary tests with this paint were carried out to evaluate its general operating characteristics such as sensitivity, repeatability, and drift. Gages have been constructed on pieces of plastic 0.015 inch thick. Unfortunately, all gages constructed so far have shown a marked zero drift and it appears that the design of a satisfactory pressure transducer of this type for water channel application may require rather extensive development work.

9.2.4 Calculation of Simulated Pressure Distribution from Water Depth Measurements

9.2.4.1 Summary of Analogical Quantities

The theoretical basis of the analogy and the assumptions underlying it are well known and have been presented in Refs 2 and 3. It is convenient here to summarize the analytical quantities:

Gas Flow	Water Flow
Two dimensional, compressible gas with $\gamma = \frac{C_p}{C_v} = 2$	Liquid flow with free surface in gravity field
Velocity ratio, $\left(\frac{V_2}{V_1}\right)_a$	Velocity ratio, $\left(\frac{V_2}{V_1}\right)_w$

Density ratio, $\frac{\rho_2}{\rho_1}$	Water depth ratio, $\frac{d_2}{d_1}$
Temperature ratio, $\frac{T_2}{T_1}$	Water depth ratio, $\frac{d_2}{d_1}$
Pressure ratio, $\frac{P_2}{P_1}$	(Water depth ratio)^2, $\left(\frac{d_2}{d_1}\right)^2$
Velocity of sound, $a = \sqrt{\frac{\gamma p}{\rho}}$	Velocity of surface wave propagation, $c = \sqrt{gd}$
Mach number, $M = \frac{V_a}{a}$	Froude number, $Fr = \frac{V_w}{c}$
Shock wave	Hydraulic jump.

For flows involving shocks the analogy is imperfect for two main reasons:

a) For air, $\gamma = 1.4$, whereas the analogy assumes a hypothetical value of $\gamma = 2$

b) The change in internal energy for air is not equivalent to that for water.

In a simple quantitative application of the analogy, one may derive the air density, temperature and pressure distributions directly from the water depth distribution using in each case the correspondence indicated. It will then be found that varying degrees of agreement will result and that the best agreement obtained is that between the depth ratio and the density ratio.

9.2.4.2 Modification of the Direct Analogy

A modification of the direct analogy, originally proposed in Ref 2, produces greatly improved numerical results. The basis of this modification is the use of the depth ratio to determine the analogous density ratio only. All the other

necessary aerodynamic quantities are calculated from the density ratio by means of well known aerodynamic relations. In this way, the good agreement between air density ratio and water depth ratio is more fully exploited.

In all the numerical applications reported here, the modified analogy was used.

9.2.4.3 Experimental Procedure

Since no direct water velocity measurements can yet be made, owing to the lack of suitable total pressure probes, the simulated flow Mach number was obtained by means of wave angle measurements using a symmetrical diamond airfoil with a wedge angle of 18° at both leading and trailing edges.

The channel flow was adjusted to the necessary conditions for simulating a Mach 2 flow by adjusting the nozzle flap to the desired opening height by means of the nozzle depth gage, setting the longitudinal channel slope to the required value as calculated from Eqn 10.1 , and by adjusting the pump discharge by means of the Walworth gate valve until the oblique shock angle coming off the leading edge of the diamond airfoil corresponded to the value for Mach 2.

The model was then placed in the test section, carefully aligned with respect to the reference grid, and water depth measurements were taken at all grid points in the area of interest and also at points of intersection of the reference grid and the model surface as close to the model as the probes allowed. In order to minimize individual differences of interpretation, all depth readings of a given test were made by the same operator. However, tests of the same model by different individuals produced substantially the same results. The measurements of water depth on the model itself were obtained by means of the Eosin dye technique described in Progress Report No 20, and,

in this case, a correction factor for the meniscus was determined experimentally using the same model with placid water of known depth. The correction factor thus established reduced the indicated height by 0.08 inch for the flat or gently curved surfaces and 0.04 inch for the corners.

9.2.4.4 Data Reduction Procedure

1) The values of ρ_∞/ρ_T, P_∞/P_T, and q_∞/P_T corresponding to the desired flow Mach number are taken from standard compressible flow tables such as Ref 4. Subscripts ∞ and T indicate the free stream and total conditions respectively.
2) From the experimental value of the local depth d and the free stream depth d_∞, the dimensionless water depth ratio d/d_∞ is calculated and interpreted as the air density ratio ρ/ρ_∞.
3) The value of ρ/ρ_T is calculated by means of the simple relation:

$$\rho/\rho_T = \rho/\rho_\infty \times \rho_\infty/\rho_T. \qquad (10.2)$$

4) Using Ref 4, any aerodynamic property corresponding to ρ/ρ_T such as P/P_T, T/T_T or local Mach number can be obtained.
5) The local pressure coefficient can then be obtained by means of the relation:

$$C_p = \frac{P - P_\infty}{q_\infty} = \left(\frac{P}{P_T} - \frac{P_\infty}{P_T}\right) \frac{P_T}{q_\infty} . \qquad (10.3)$$

9.2.5 Experimental Results

9.2.5.1 Diamond Airfoil Tests

The main object of testing this model was to develop the experimental and data reduction procedures and to compare the experimental results with those of accepted aerodynamic theories.

Table 14-1 gives the experimental data and calculated results for the diamond airfoil model at Mach 2.

Figure 14-1 provides a comparison between the pressure coefficients obtained experimentally and the values calculated theoretically. There is a satisfactory agreement except at the corners of the model where the analogy indicates a rounded, more gradual change of pressure instead of the abrupt, step function change predicted by theory.

9.2.5.2 Test with Model of Proposed Supersonic Parachute

The main geometric characteristics of this model are given in Fig 14-2A and illustrated in the accompanying photographic view (Fig 14-2B).

Depth probings were taken at all the reference grid points and also at points close to the model surface both inside and outside the canopy. The experimental and data reduction procedures outlined previously were followed and the pressure coefficients were calculated. Shadowgraph and Schlieren pictures were taken. Figure 14-3 shows the point designation system and the calculated contour lines of constant pressure (isobars). Figure 14-4 is a shadowgraph of the flow on which the contour lines of Fig 14-3 have been superimposed. Figure 14-5 is a Schlieren image of the same flow with the calculated constant pressure lines also superimposed. It is interesting to note the generally good correspondence between the contour lines and the Schlieren image. It should be noted that Fig 14-5 was obtained by enlargement from a small part of a 35 mm negative; a relatively long exposure time of 1/2 sec was used to minimize high frequency random changes. With modifications in the photographic

technique and simple optical refinements, it is anticipated that much improved shadowgraph and Schlieren images will be obtained.

9.2.6 Other Experiments with the Analogy

9.2.6.1 The Starting Flow of the Supersonic Parachute

While investigating the supersonic parachute configuration by means of the Schlieren system, certain interesting flow characteristics were observed during the starting phase; they are illustrated in Figs 14-6 A, B, and C. When the water flow initially passes over the symmetrical wedge forming the spike, a typical wave pattern consisting of an oblique shock at the nose and a Prandtl-Meyer expansion fan at each wedge corner is established. The presence of the canopy creates a back pressure behind the spike and generates a compression wave which travels upstream. This wave is clearly shown in Fig 14-6A. As this wave travels upstream, it acts on the expansion waves coming off the wedge corners (Fig 14-6B), eventually eliminating these expansion waves and, in their place, oblique shocks develop; in stable configurations, these waves pass ahead of the canopy leading edges (Fig 14-6 C). These oblique shocks may be considered as resulting from the stagnant wake behind the wedge forming a virtual extension of the wedge profile.

9.2.6.2 Effect of a Primary Body on the Performance of the Supersonic Parachute

It is well known that, under certain operating conditions, the presence of a primary body may have a marked influence on the performance of trailing deceleration devices.

During the present reporting period, a preliminary investigation of the effect of primary body wake on the supersonic parachute was initiated. For this purpose, a two dimensional model of an ogive cylinder was used. The main geometric characteristics of the configuration tested are shown in Fig 14-7A. Figure 14-7B is a Schlieren photograph of the wave pattern of the supersonic parachute model at M = 2 without a primary body. Figure 14-7C shows the wave pattern of the same model behind a primary body with $D_1/D_2 = 11/16$ and $L/D_1 = 5.3$. It is apparent in this case that the presence of the primary body wake causes detachment of the shock wave at the spike nose and creates irregularities in the flow with a consequent loss of stability.

9.3 Proposed Work

The usefulness and versatility of the newly developed stationary model water channel facility is adequately illustrated by the examples presented in this reporting period, particularly when considering the quantitative pressure distribution experiments. Further development and refinement of instrumentation and experimental techniques will be introduced whenever the need arises. A new light source, using a carbon arc has been acquired and is expected to greatly improve the shadowgraph and Schlieren images, allowing for movie camera recording of unsteady phenomena. Attention will be devoted to the design and construction of miniature total pressure probes to enable detailed velocity surveys and complete channel calibration.

In conjunction with such developments and refinements, further investigations with the proposed supersonic parachute configuration, both with and without primary bodies will be conducted.

The water channel as presently developed is also available for other investigations that may be required in connection with the total contract effort.

REFERENCES

1. Olson, R. M.: Essentials of Engineering Fluid Mechanics, Chapter 12, p. 290, International Textbook Company, Scranton, Pennsylvania, 1961.

2. Ippen, A. T., and Harleman, D. R. F.: Studies on the Validity of the Hydraulic Analogy of Supersonic Flow, Parts I and II, AF TR 5985, May, 1950, revised January, 1951.

3. Heinrich, H. G. and Ibrahim, S. K.: Application of the Water Surface Wave Analogy in Visualizing the Wave Pattern of a Number of Primary and Secondary Body Combinations in Supersonic Flow, WADC TR 59-457, September, 1959.

4. Ames Research Staff: Equations, Tables, and Charts for Compressible Flow, NACA TR 1135, 1953.

TEST CONDITIONS

FROUDE NUMBER: Fr = 2.0

FREE STREAM WATER DEPTH: d_∞ = .304 in

FROM NACA TR 1135 FOR $M_\infty = 2$

ρ_∞/ρ_T = .230 P_∞/P_T = .128 q_∞/P_T = .358

STA-TION	d (in)	$d_{(ave)}$ (in)	d/d_∞ (= ρ/ρ_∞)	ρ/ρ_T	P/P_T NACA TR 1135	$\frac{P}{P_T} - \frac{P_\infty}{P_T}$	C_P
0 L	0.334						
		0.332	1.09	0.251	0.145	0.017	0.048
0 R	0.330						
1 L	0.552						
		0.542	1.78	0.409	0.284	0.156	0.436
1 R	0.532						
2 L	0.523						
		0.506	1.66	0.382	0.261	0.133	0.372
2 R	0.492						
3 L	0.492						
		0.484	1.59	0.366	0.246	0.118	0.330
3 R	0.476						
4 L	0.499						
		0.488	1.60	0.368	0.246	0.118	0.330
4 R	0.478						
5 L	0.426						
		0.423	1.39	0.320	0.203	0.075	0.210
5 R	0.420						
6 L	0.204						
		0.207	0.68	0.156	0.074	-0.054	-0.151
6 R	0.210						
7 L	0.196						
		0.196	0.64	0.147	0.068	-0.060	-0.168
7 R	0.197						
8 L	0.199						
		0.202	0.66	0.152	0.072	-0.056	-0.156
8 R	0.204						
9 L	0.205						
		0.201	0.66	0.152	0.072	-0.056	-0.156
9 R	0.197						
10 L	0.239						
		0.232	0.76	0.175	0.087	-0.041	-0.114
10 R	0.224						

TABLE 14-1. EXPERIMENTAL DATA AND RESULTS FOR DIAMOND AIRFOIL MODEL

POSITION NOTATION { S — AT CONE SURFACE; iS — INSIDE OF CANOPY SURFACE; oS — OUTSIDE OF CANOPY SURFACE

Station X,Y	d depth (in)	C_p
-2 A	.289	.00
-2 C	.287	.00
-2 E	.288	.00
-2 G	.286	.00
-1 A	.309	.03
-1 B	.308	.03
-1 C	.296	.00
-1 E	.290	.00
-1 G	.286	.00
0 A	.359	.11
0 B	.350	.11
0 C	.331	.08
0 D	.318	.06
0 E	.310	.03
0 F	.300	.03
0 G	.293	.00
0 I	.290	.00
0 K	.290	.00
0 M	.285	.00
0 O	.285	.00
1 S	.639	.73
1 B	.578	.59
1 C	.438	.28
1 D	.408	.22
1 E	.371	.14
1 F	.337	.08
1 G	.317	.06
1 H	.301	.03
1 I	.295	.00
1 K	.287	.00
1 M	.283	.00
1 O	.280	.03
2 S	.671	.81
2 B	.669	.81
2 C	.652	.75
2 D	.612	.67
2 E	.484	.39
2 F	.428	.25
2 G	.380	.17
2 H	.334	.08
2 I	.315	.06
2 J	.296	.00
2 K	.285	.00
2 M	.317	.17
2 O	.279	.03
3 S	.590	.50
3 C	.572	.59
3 D	.615	.67
3 E	.639	.73
3 F	.641	.73
3 G	.581	.59
3 H	.492	.39
3 I	.420	.25
3 J	.354	.11
3 K	.315	.06
3 L	.302	.03
3 M	.290	.00
3 O	.282	-.03
4 S	.531	.47
4 C	.504	.41
4 D	.491	.39
4 E	.491	.39
4 F	.515	.45
4 G	.564	.56
4 H	.607	.64
4 I	.606	.64
4 J	.502	.42
4 K	.434	.28
4 L	.380	.17
4 M	.327	.06
4 N	.309	.03
4 O	.293	.00
5 S	.554	.53
5 D	.482	.36
5 E	.453	.31
5 F	.449	.31
5 G	.470	.36
5 H	.513	.45
5 I	.569	.56
5 J	.605	.64
5 K	.601	.64
5 L	.541	.50
5 M	.460	.34
5 N	.377	.17
5 O	.338	.08
6 R	.560	.56
6 B	.559	.56
6 C	.559	.56
6 D	.569	.56
6 E	.552	.53
6 F	.494	.14
6 G	.451	.31
6 H	.435	.28
6 I	.439	.28
6 J	.461	.34
6 K	.524	.47
6 K	.524	.47
6 L	.576	.59
6 M	.591	.61
6 N	.551	.53
6 O	.466	.34
7 R	.561	.56
7 B	.563	.56
7 C	.562	.56
7 D	.569	.56
7 E	.585	.59
7 F	.584	.59
7 G	.530	.47
7 H	.490	.39
7 I	.438	.28
7 J	.422	.25
7 K	.431	.25
7 L	.461	.34
7 M	.520	.45
7 N	.576	.59
7 O	.560	.56
8 R	.566	.56
8 B	.570	.56
8 C	.571	.59
8 D	.578	.59
8 E	.579	.59
8 F	.611	.67
8 G	.639	.73
8 H	.637	.73
8 I	.559	.56
8 J	.488	.39
8 K	.432	.28
8 L	.411	.22

(Continued)

Station X,Y	d depth (in)	C_p
8 M	.417	.25
8 N	.417	.25
8 O	.456	.31
9 R	.582	.59
9 B	.582	.59
9 C	.583	.59
9 D	.582	.59
9 E	.574	.59
9 F	.557	.53
9 G	.548	.53
9 H	.560	.56
9 I	.560	.56
9 J	.588	.61
9 K	.610	.67
9 L	.546	.53
9 M	.470	.36
9 N	.413	.22
9 O	.401	.20
10 R	.584	.59
10 B	.584	.59
10 C	.582	.59
10 D	.582	.59
10 E	.581	.59
10 F	.582	.59
10 G	.566	.56
10 H	.655	.78
10 oS	.505	.42
10 I	.483	.36
10 J	.464	.34
10 K	.500	.42
10 L	.530	.47
10 M	.568	.56
10 N	.527	.47
10 O	.460	.34
11 F	.615	.67
11 G	.657	.78
11 H	.727	.95
11 iS	.758	1.03
11 oS	.405	.22
11 J	.425	.25
11 K	.422	.25
11 L	.427	.25
11 M	.453	.31
11 N	.521	.45
11 O	.552	.53
12 R	.589	.61
12 B	.589	.61
12 C	.586	.61
12 D	.585	.61
12 E	.598	.64
12 F	.629	.70
12 G	.688	.84
12 H	.700	.89
12 iS	.765	1.03
12 oS	.401	.20
12 J	.401	.20
12 K	.396	.20
12 L	.384	.17
12 M	.379	.17
12 N	.403	.20
12 O	.447	.31
13 R	.596	.61
13 B	.591	.61
13 C	.589	.61
13 D	.589	.61
13 E	.602	.64
13 F	.617	.67
13 G	.651	.75
13 H	.700	.87
13 I	.755	1.03
13 oS	.298	.06
13 J	.307	.06
13 K	.390	.20
13 L	.388	.17
13 M	.371	.14
13 N	.360	.14
13 O	.375	.17
14 R	.601	.64
14 B	.600	.64
14 C	.598	.64
14 D	.598	.64
14 E	.607	.64
14 F	.617	.67
14 G	.696	.87
14 H	.723	.92
14 iS	.784	1.09
14 oS	.227	-.11
14 J	.247	-.08
14 K	.306	.03
14 L	.372	.14
14 M	.372	.14
14 N	.360	.14
14 O	.351	.11
15 R	.614	.67
15 B	.6.4	.67
15 C	.607	.64
15 D	.608	.67
15 E	.662	.78
15 F	.694	.87
15 G	.713	.92
15 H	.761	1.03
15 iS	.840	1.26
15 oS	.145	-.22
15 J	.206	-.14
15 K	.261	.06
15 L	.316	.06
15 M	.364	.14
15 N	.379	.17
15 O	.368	.14
16 R	.621	.70
16 B	.621	.70
16 C	.621	.70
16 D	.621	.70
16 F	.670	.81
16 G	.749	1.01
16 H	.815	1.17
16 iS	.836	1.23
16 oS	.090	-.31
16 I	.112	-.28
16 J	.180	-.17
16 K	.240	-.08
16 L	.273	-.03
16 M	.317	.06
16 N	.361	.14
16 O	.376	.17
17 R	.638	.73
17 B	.638	.73
17 C	.638	.73

(Continued)

Station X, Y	d depth (in)	C_p
17 D	.625	.70
17 E	.625	.70
17 F	.710	.89
17 iS	.818	1.17
17 oS	.102	-.28
17 H	.069	-.31
17 I	.107	-.28
17 J	.169	-.20
17 K	.224	-.11
17 L	.255	-.06
17 M	.289	.00
17 N	.317	.06
17 O	.353	.11
18 R	.612	.67
18 B	.621	.70
18 C	.632	.70
18 D	.632	.70
18 E	.725	.95
18 oS	.137	-.22
18 F	.127	-.25
18 G	.102	-.28
18 H	.063	-.31
18 I	.103	-.28
18 J	.147	-.22
18 K	.196	-.14
18 L	.236	-.08
18 M	.259	-.06
18 N	.290	.00
18 O	.331	.06
19 R	.588	.61
19 B	.572	.59
19 C	.491	.39
19 D	.201	-.14
19 E	.133	-.25
19 F	.126	-.25
19 G	.117	-.25
19 H	.080	-.31
19 I	.097	-.28
19 J	.140	-.22
19 K	.154	-.17
19 L	.221	-.11
19 M	.243	-.08
19 N	.208	-.03
19 O	.298	.03
20 R	.501	.42
20 B	.493	.39
20 C	.365	.14
20 D	.099	-.28
20 E	.042	-.34
20 F	.100	-.28
20 G	.070	-.31
20 H	.063	-.31
20 I	.099	-.28
20 J	.133	-.25
20 K	.170	-.20
20 L	.205	-.14
20 M	.235	-.08
20 N	.256	-.06
20 O	.279	-.03
21 R	.435	.28
21 B	.393	.20
21 C	.341	.08
21 D	.143	-.22
21 E	.061	-.34
21 F	.120	-.25
21 G	.097	-.28
21 H	.074	-.31
21 I	.100	-.28
21 J	.130	-.25
21 K	.168	-.20
21 L	.196	-.14
21 M	.224	-.11
21 N	.246	-.08
21 O	.267	-.03
22 R	.364	.14
22 B	.345	.11
22 C	.300	.03
22 D	.207	-.14
22 E	.126	-.25
22 F	.130	-.25
22 G	.113	-.25
22 H	.077	-.31
22 I	.104	-.28
22 J	.130	-.25
22 K	.160	-.20
22 L	.185	-.17
22 M	.215	-.11
22 N	.240	-.08
22 O	.260	-.06
23 R	.306	.03
23 B	.284	.00
23 C	.253	-.06
23 D	.227	-.11
23 E	.179	-.17
23 F	.216	-.11
23 G	.139	-.22
23 H	.097	-.28
23 I	.108	-.28
23 J	.138	-.25
23 K	.154	-.22
23 L	.182	-.17
23 M	.206	-.14
23 N	.228	-.11
23 O	.249	-.06
24 R	.276	-.03
24 B	.263	-.06
24 C	.236	-.08
24 D	.205	-.14
24 E	.173	-.20
24 F	.239	-.08
24 G	.181	-.17
24 H	.145	-.25
24 I	.109	-.28
24 J	.126	-.20
24 K	.154	-.22
24 L	.172	-.20
24 M	.193	-.17
24 N	.219	-.11
24 O	.238	-.08

TABLE 14-2. EXPERIMENTAL WATER DEPTH d AND CALCULATED PRESSURE COEFFICIENT C_p FOR THE SPIKED SUPERSONIC PARACHUTE MODEL AT M=2

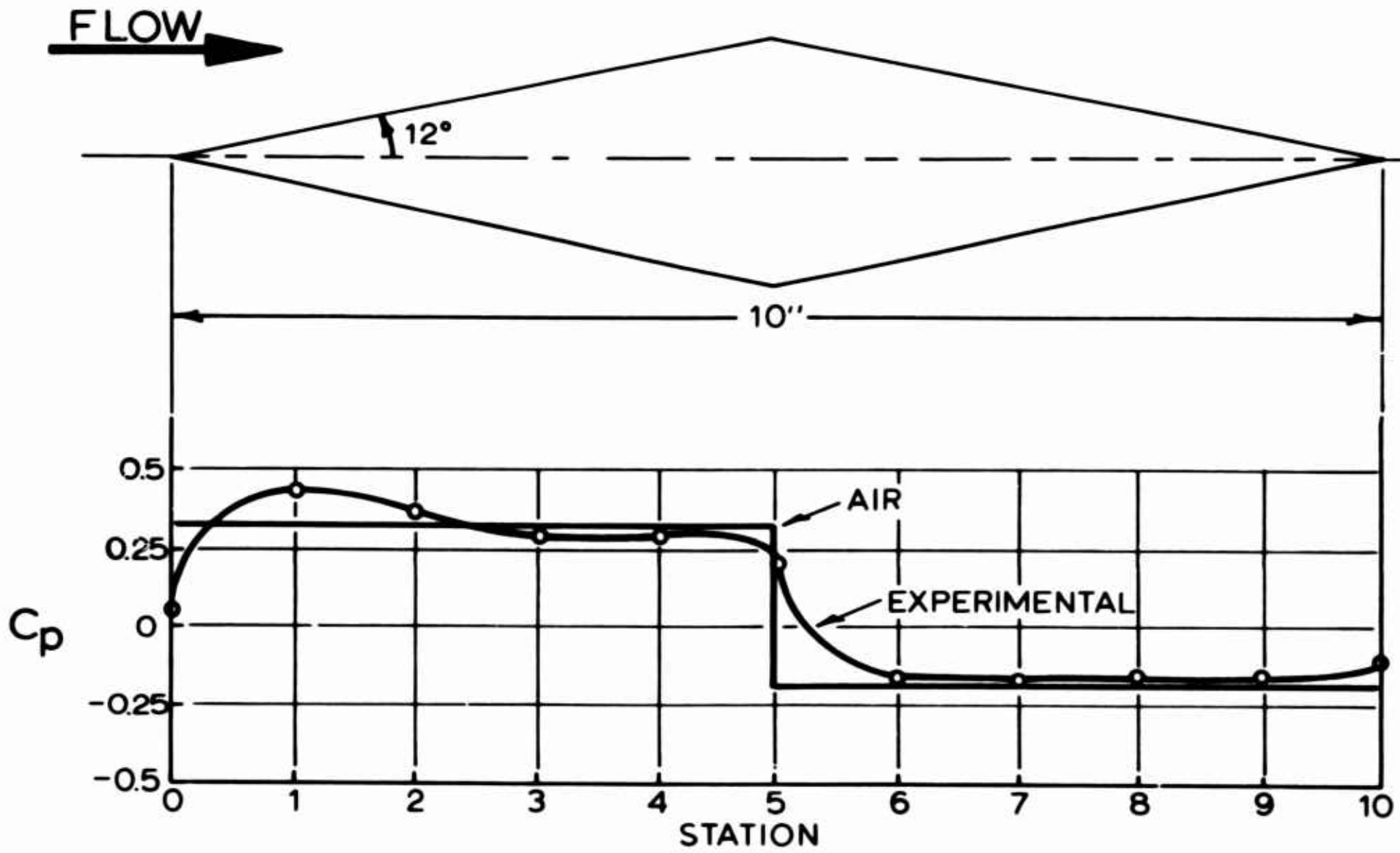

FIG 14-1. COMPARISON OF EXPERIMENTAL PRESSURE COEFFICIENTS WITH THEORETICAL VALUES FOR A SYMMETRICAL DIAMOND AIRFOIL AT M=2

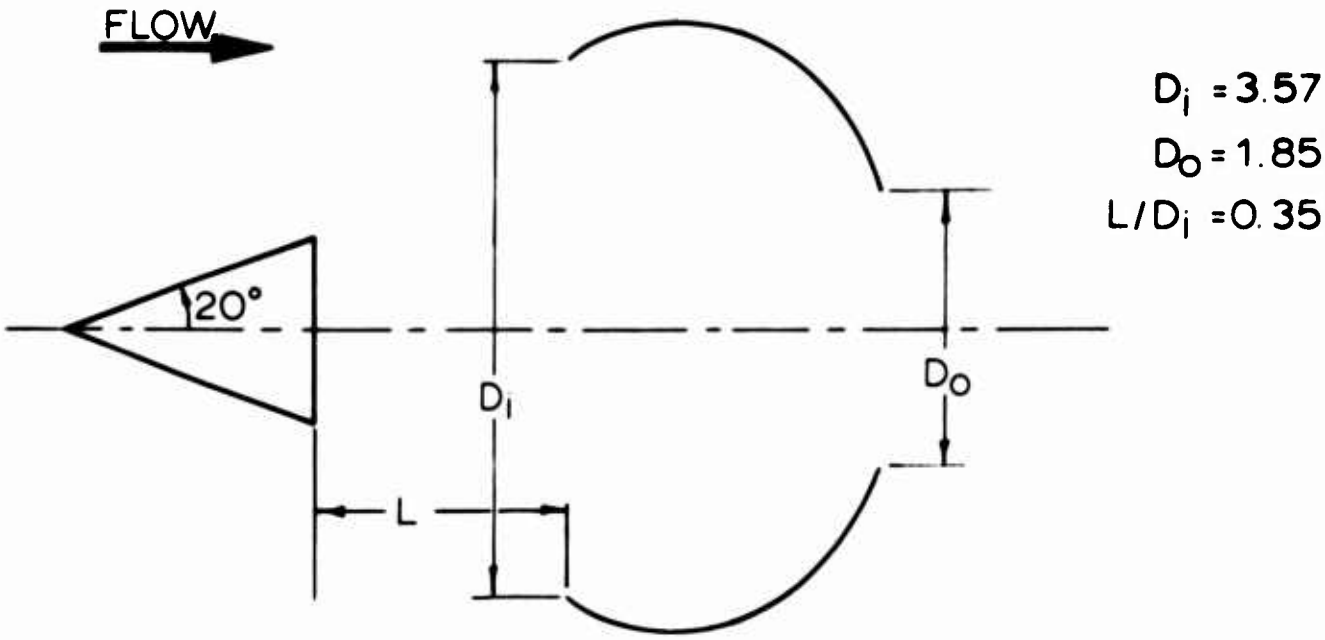

A) GENERAL ARRANGEMENT AND DIMENSIONS

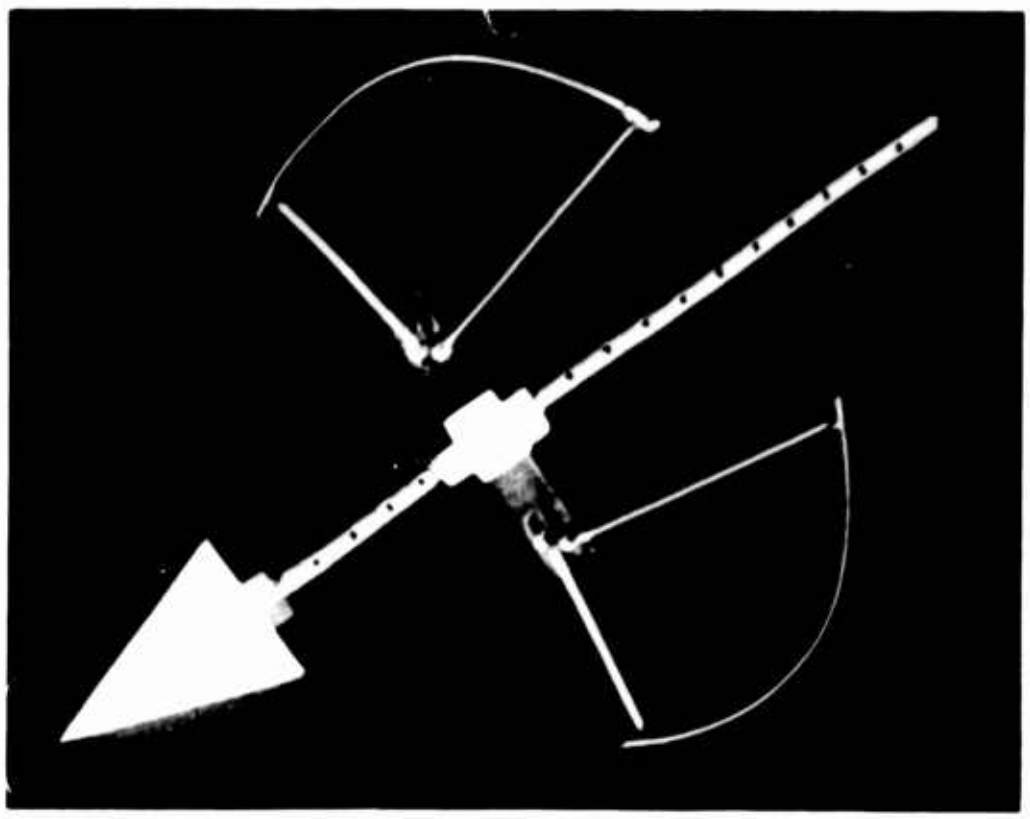

B) PHOTOGRAPH OF WATER CHANNEL MODEL

FIG 14-2. SPIKED SUPERSONIC PARACHUTE CONFIGURATION

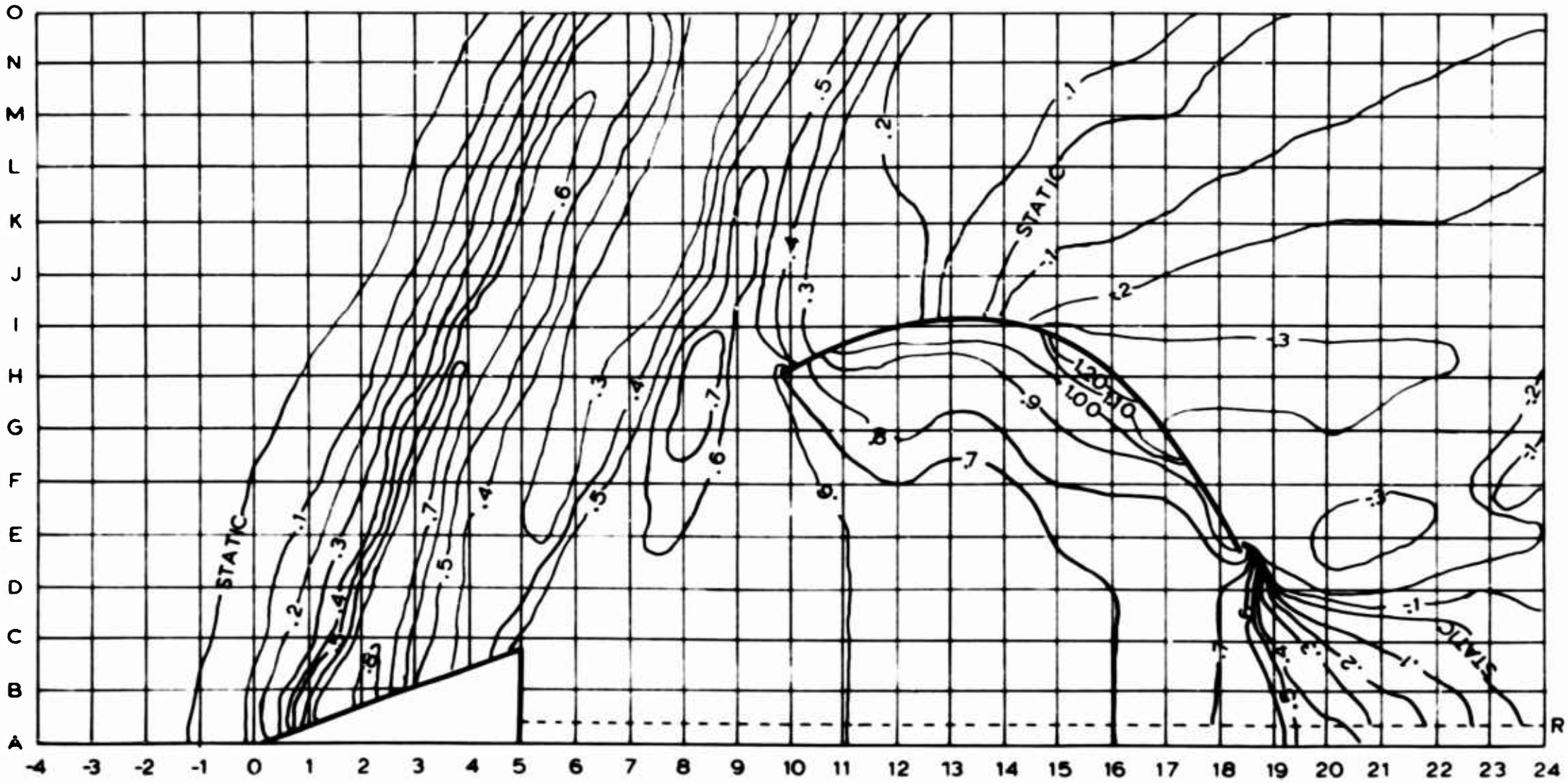

FIG 14-3. REFERENCE GRID AND PRESSURE COEFFICIENT CONTOUR MAP FOR THE SPIKED PARACHUTE CONFIGURATION AT M=2

FIG 14-4. SHADOWGRAPH OF HALF TEST SECTION WITH SUPERPOSED PRESSURE COEFFICIENT CONTOUR LINES FOR SPIKED PARACHUTE CONFIGURATION AT M = 2

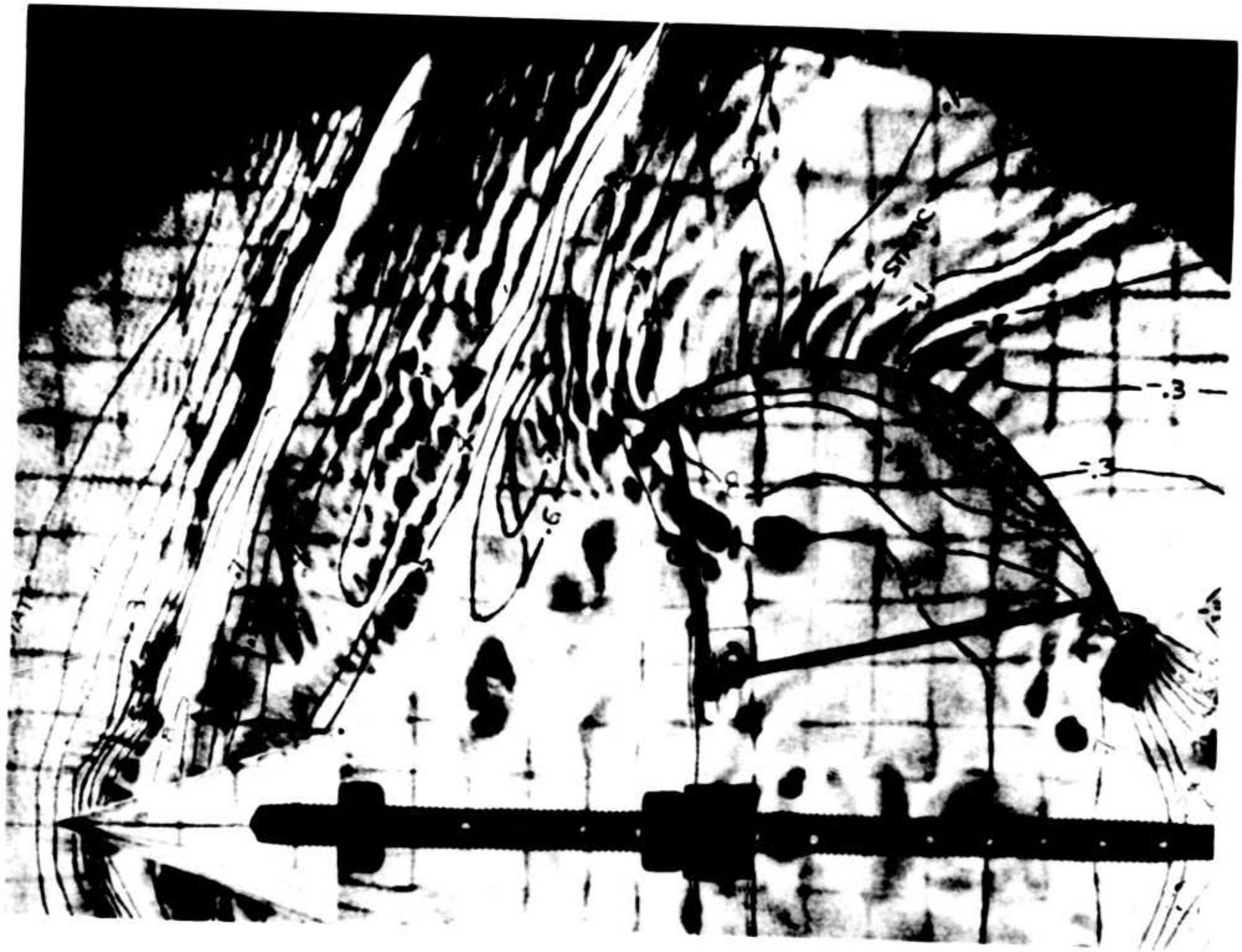

FIG 14-5. SCHLIEREN PHOTOGRAPH OF HALF TEST SECTION WITH SUPERPOSED PRESSURE COEFFICIENT CONTOUR LINES FOR SPIKED PARACHUTE CONFIGURATION AT M = 2

A) INITIAL STAGE - NOTE PRANDTL-MEYER EXPANSION AT CORNERS OF SPIKE WEDGE

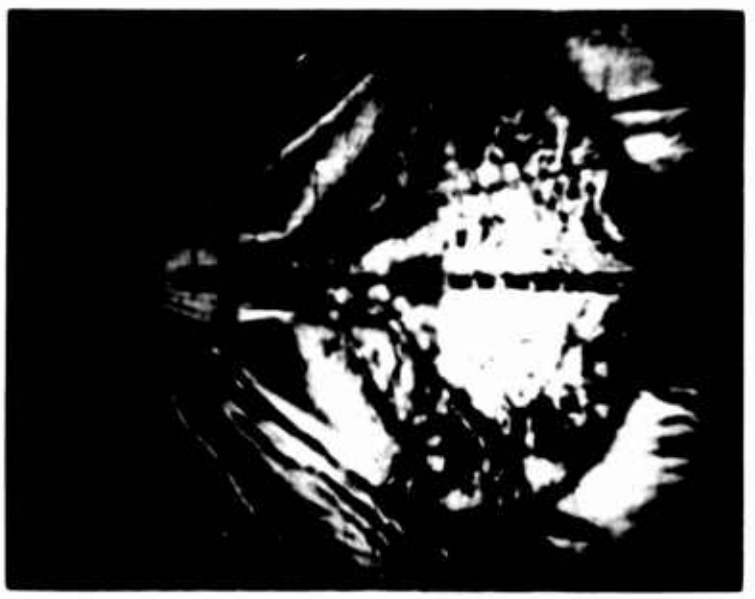

B) INTERMEDIATE STAGE - EXPANSION FAN STILL PRESENT

C) FINAL STAGE - STABLE FLOW PATTERN ESTABLISHED, EXPANSION FAN NOW REPLACED BY SHOCK WAVE

FIG 14-6. STARTING FLOW FOR SPIKED PARACHUTE CONFIGURATION AT M = 2

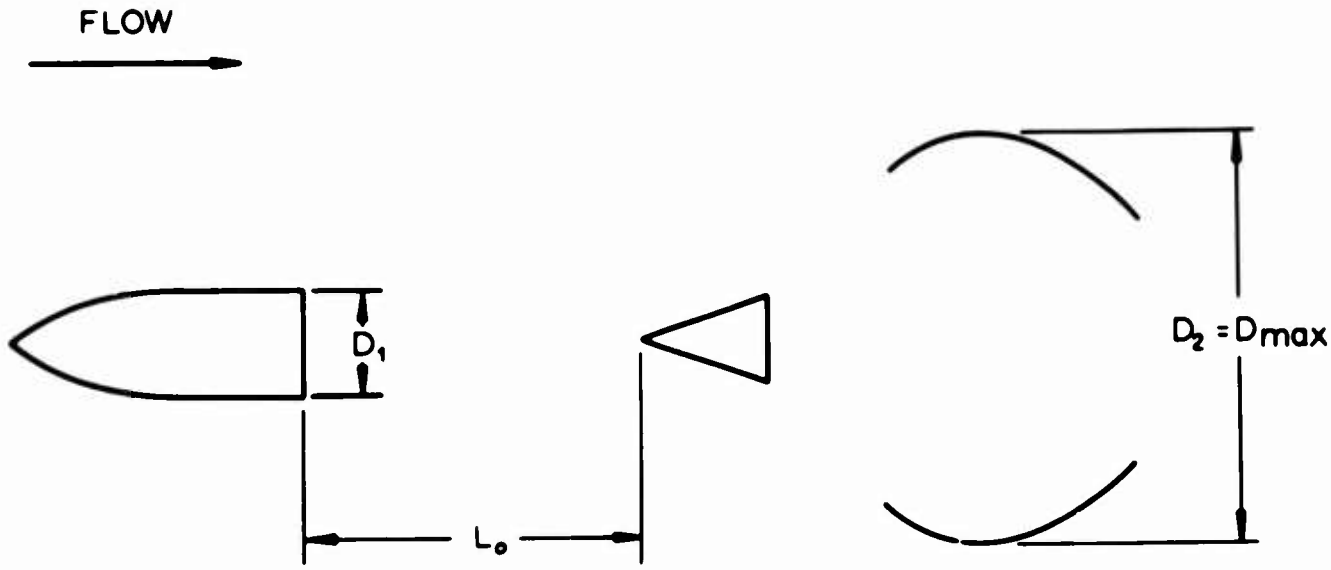

A) GENERAL ARRANGEMENT

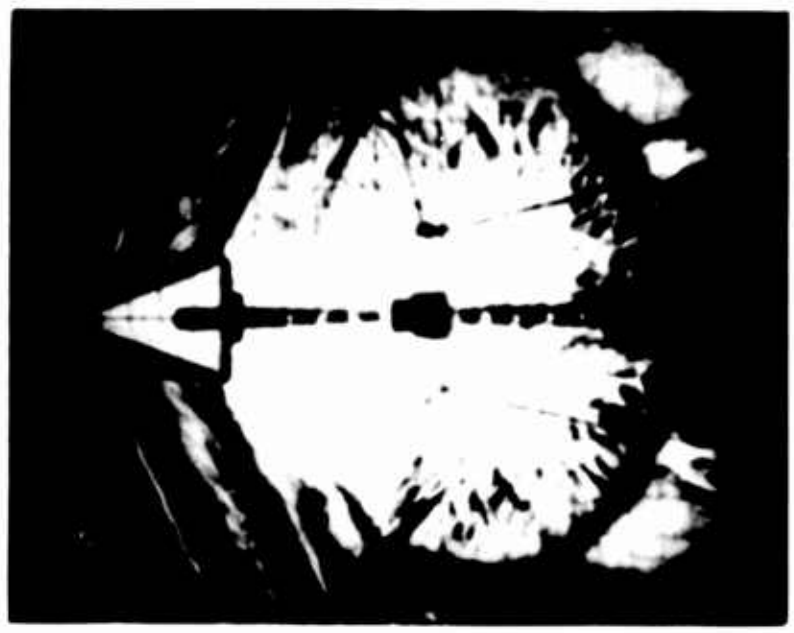

B) FLOW PATTERN WITH NO PRIMARY BODY

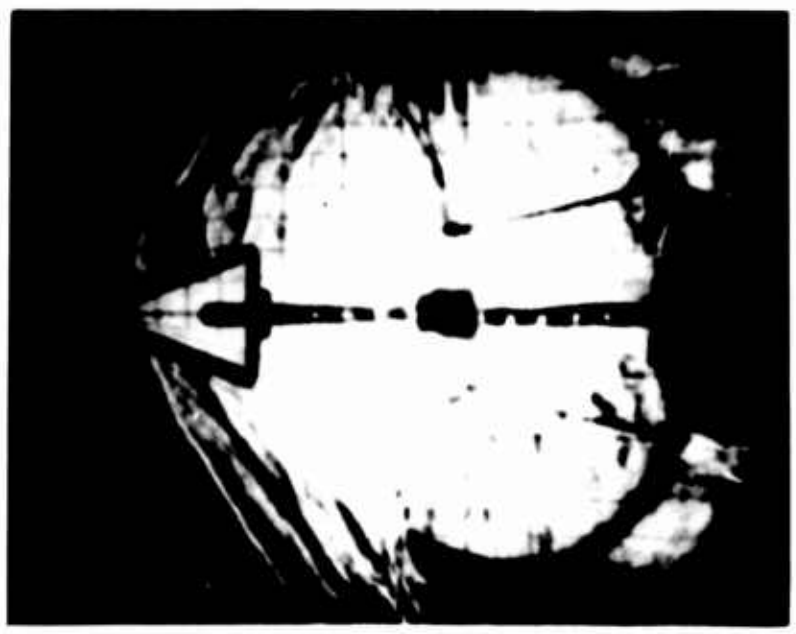

C) FLOW PATTERN WITH PRIMARY BODY: $D_1/D_2 = 11/16; L_o/D = 5.3$

FIG 14-7. EFFECT OF PRIMARY BODY ON WAVE PATTERN OF SPIKED PARACHUTE

Project No 16

10.0 Stress Analysis of the T-10 Troop Parachute

Progress Report No 18 presented an analytical method for obtaining the stress distribution over a fully inflated canopy in steady descent.

Efforts have now been directed at extending the basic theory to the more complex case of finding the stress over an opening canopy. It is hoped that when this method is completely developed, the fully opened canopy can be treated as a special case under this more general theory. Certain simplifications appear possible in the theory as thus far developed and these will be incorporated in the general development. Preliminary results of these new efforts should be available during the next reporting period.

APPENDIX

The authors of this report who are listed on the front page wish to acknowledge the accomplishments and assistance of the following personnel:

Clerical Staff:

E. Zembergs, Sr. Engineering Assistant
Beverly M. Broers, Secretary

Graduate Students:

R. O. Bailey, Research Assistant
D. J. Eckstrom, Research Assistant
S. R. Hess, Research Assistant
E. M. Linhart, Research Assistant
D. J. Monson, Research Assistant
L. W. Rust, Research Fellow

Undergraduate Students:

R. E. Albrecht, Engineering Assistant
J. R. Baker, Engineering Assistant
J. W. Bushard, Engineering Assistant
J. M. Carlson, Engineering Assistant
D. F. Coleman, Engineering Assistant
D. D. Evenson, Engineering Assistant
D. K. Florman, Engineering Assistant
R. W. Friestad, Engineering Assistant
K. J. Goar, Engineering Assistant
L. G. Jacobson, Engineering Assistant
L. R. Jamison, Engineering Assistant
J. M. Johnson, Engineering Assistant
H. R. Kokal, Engineering Assistant
H. M. Lippa, Engineering Assistant
D. A. MacLean, Engineering Assistant
M. J. Martin, Engineering Assistant
D. E. McGee, Engineering Assistant
T. C. Nietz, Engineering Assistant
E. H. Nierengarten, Engineering Assistant
D. R. Nordwall, Engineering Assistant
R. A. Noreen, Engineering Assistant
D. L. Pekarek, Engineering Assistant
S. T. Schwartz, Engineering Assistant
R. O. Strom, Engineering Assistant
L. M. Timmons, Engineering Assistant
B. J. Williams, Engineering Assistant

Machine Shop Personnel:

J. Taube, Laboratory Machinist
P. A. Huehnert, Wind Tunnel Mechanic